2015

Evaluation and optimization of photovoltaic cells comprised from benzodifuran and benzobisoxazole based polymers

Monique Donica Ewan
Iowa State University

Evaluation and optimization of photovoltaic cells comprised from benzodifuran and benzobisoxazole based polymers

by

Monique D. Ewan

A dissertation submitted to the graduate faculty

in partial fulfillment of the requirements for the degree of

DOCTOR OF PHILOSOPHY

Major: Chemistry (*Materials Chemistry*)

Program of Study Committee:

Malika Jeffries-EL, Co-Major Professor
Sumit Chaudhary, Co-Major Professor
Javier Vela
Arthur Winter
Joseph Shinar

Iowa State University

Ames, Iowa

2015

TABLE OF CONTENTS

CHAPTER 1

INTRODUCTION

1.1 Outline of the Dissertation

This dissertation summarizes the work of the author, Monique D. Ewan, in the Jeffries-EL research group from 2010-2015. The main objective of the research has been two-fold: to develop novel materials for organic semiconductors, and to fabricate organic semiconducting devices.

Chapter 1 provides an outline of this dissertation as well as an overall introduction to the topics covered in this dissertation. Firstly, there will be an introduction to organic solar cells, followed by a discussion on the theory behind organic semiconductors and the requirements for polymers tailored for organic solar cells

Chapter 2 is based on published works (*Polymer Chemistry* **2013,** 1, 5329-5336) and (*Chemical Communications* **2012,** 48, 8919-8921). All polymers were synthesized and characterized by Dr. Brandon Kobilka. The solar cells were fabricated and characterized by the author, Monique D. Ewan. SCLC mobility measurements and AFM images were also obtained by the author.

Chapter 3 is based on a series of polymers synthesized and characterized by Monique D Ewan. The benzodifuran monomer was synthesized by Dr. Brandon M. Kobilka. Solar cells were fabricated and characterized by Monique D. Ewan.

Chapter 4 is based on published work (*Journal of Polymer Science A* **2015,** 53, 1533-1540). The polymers were synthesized and characterized by Dr. Achala Bhuwalka. The solar cells were fabricated and characterized by the author, Monique D. Ewan. SCLC

mobility measurements were performed by Monique D. Ewan and Dr. Moneim Elshobaki. AFM measurements were taken by Dr. Moneim Elshobaki.

Chapter 5 is based on published work in the (*Journal of Polymer Science A* *10.1002/pola.27793, 2015)*. The solar cells were fabricated and characterized by the author, Monique D. Ewan. The polymers were synthesized and characterized by Dr. Achala Bhuwalka. SCLC mobility measurements were performed by Monique D. Ewan and Dr. Moneim Elshobaki. AFM measurements were taken by Dr. Moneim Elshobaki.

Chapter 6 concludes the dissertation with a summary of the described research, as well as, any recommendations on future directions that should be investigated.

1.2 Organic solar cells (OSCs)

In the United States, and the world at large, fossil fuels are the prominent energy source. Although readily available now, the reserves of energy are finite and dwindling. Furthermore, burning fossil fuels accelerates the release of CO_2 into the atmosphere, which has been shown to be a leading cause in global climate change[1-3]. Consequently, there is an eminent need for the development of energy sources that are both renewable and environmentally responsible. Solar energy is one of the cleanest energy sources available today. The global energy requirement by 2050 is projected to be ~ 30 TW. The sun provides approximately 120,000 TW of energy annually i.e. more sunlight energy strikes the earth in 1 hour than all the energy consumed worldwide in an entire year[4]. In principle covering 25, 921 km^2 (about the size of the state of New Hampshire) of land in Nevada with solar cells that have at least 15% efficient could power the entire United States (Figure 1-1)[5].

Figure 1-1. Area (in red) covered with 15% efficient solar cells could provide a a years woth of electricity for the US

The most efficient solar cells, to date, are based on silicon[6]. Unfortunately, their fabrication requires elaborate processing conditions resulting in high processing costs[7]. Additionally, improvements upon the traditional silicon solar cell require the incorporation of rare, expensive elements such as indium and toxic elements such as germanium[8]. As a result these types of devices are not a practical, long-term option. Conversely, organic solar cells (OSCs) represent a low cost alternative. They have lower fabrication cost as a 10% OSC is expected to cost \$50/m^2 as opposed to \$350/m^2 for inorganic solar cells[9]. This is because OSCs can be solution processed with high fabrication speeds. They can also perform better at lower light levels and can be made on flexible substrates[10] Currently, there are several reports on OSCs

with power conversion efficiencies between 7-9%[11-14]. There have even been a few examples of higher efficiencies[15, 16]. There is still, however, room for improvement. This can be achieved through device engineering as well as the development of new materials[11, 17, 18].

1.2.1 Operating Principles

1.2.1a Exciton Generation, Diffusion and Dissociation

When a solar cell is exposed to light from the visible spectrum, a photon is absorbed. An electron from an electron donating, or p-type, material gets excited from its highest occupied molecular orbital (HOMO) to its lowest unoccupied molecular orbital (LUMO) (Figure 1-2a). At this point, it forms a bound electron – hole pair called an exciton[19] with a binding energy of 0.1 – 1.4 eV [20]. The newly formed exciton migrates to the heterojunction or interface of the p-type and n-type materials (Figure 1-2b). Here, the n-type material is the electron acceptor. Once at the heterojunction, the exciton separates as the electron migrates to the LUMO of the acceptor material. The hole remains on the HOMO of the donor (Figure 1-2c). This process is called exciton dissociation and is only energetically favorable if the difference between the HOMO of the donor and LUMO of the acceptor is lower than the exciton binding energy[21].

This charge transfer process occurs at a relatively fast timescale of ~45 fs [22] which is much faster than the timescale of its competing process of exciton recombination (1 ns) [23]. Therefore, exciton dissociation is more likely to occur at a more efficient rate. After exciton dissociation, there is a critical distance along the heterojunction called the exciton diffusion length (10-20 nm) [24-29]. If the exciton has to go further than this distance, it will recombine. This results in a lower exciton dissociation efficiency[21]. Consequently, the active layers have to be kept sufficiently thin to ensure good phase separation between the donor and acceptor materials.

1.2.1b Carrier Transport and Collection

After dissociation, the electron-hole charge pair, called a geminate pair, is still coulombically bound and needs to be so that the charges can be collected at their respective electrodes.

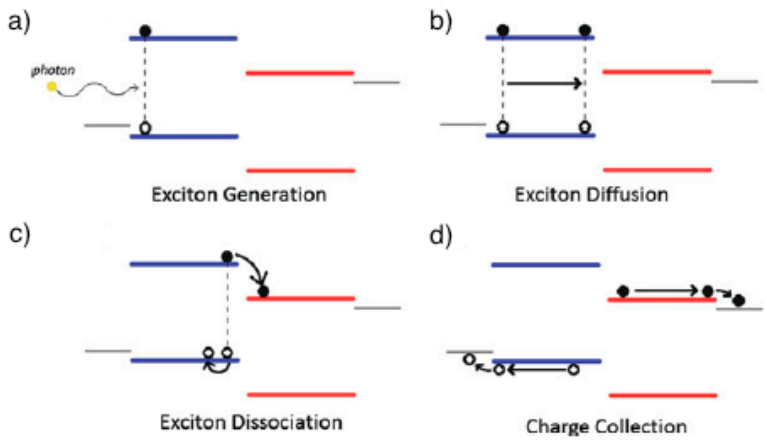

Figure 1-2. Charge separation and transfer within an organic solar cell. Adapted from Ref. 21.

The driving forces for charge collection include drift and diffusion currents. The drift current relates to the carrier movement along the potential gradient in the solar cell. This potential gradient is determined by the choice of electrodes within the solar cell. A high work function anode (-4.7 eV), such as indium tin oxide (ITO), and a low work function metal cathode (-4.3 eV), such as aluminum, are usually used. The difference between the work function of the electrodes creates a built-in electric field within the solar cell. The application of an external bias results in the modification of the internal electric field and a change in the drift current. The carriers end up drifting along the internal electric field towards their respective electrodes (Figure 1-2d).

The diffusion current involves the diffusion of carriers along their carrier concentration current in the solar cell. When the geminate pairs are generated at the heterojunction, there is large concentration of holes and electrons. The carriers will diffuse from where they are strongly concentrated and hence diffuse away from the heterojunction. The diffusion current is dominant when the internal electric field is modified to nearly zero by the applied bias. The drift current is dominant when the internal electric field is large.

Efficient charge extraction occurs within the solar cell when the work function of the anode matchers the work function of the p-type material and the work function of the cathode matches the LUMO of the n-type material; i.e., when there is ohmic contact. Various interlayers can be used to electrode work functions and the p-type material HOMO and the LUMO of the n-type material. Interlayers that are commonly used include hole transport layers and electron transport layers.

1.2.2 Anode Interlayers

Anode interlayers or hole transporting layers (HTLs) are used to improve contact property between ITO and the organic layer. They also increase the work function of ITO for more efficient hole transporting and collecting[30, 31]. Traditionally, poly(3,4-ethylenedioxythiophene) – polystyrene (PEDOT:PSS) has been used as a HTL, it planarizes the ITO surfaces spikes[32-34], ensures ohmic contact[35], increases the open circuit voltage[34] and enhances hole collection[36]. Unfortunately, PEDOT:PSS is acidic in nature and it corrodes the ITO[37-40]. This causes a decrease in the chemical stability of the ITO: PEDOT:PSS interface[41]. One approach for combating this problem is spincoating a thin layer of ethylene glycol over the

PEDOT: PSS layer[42, 43]. Alternative other HTLs that have been used including semiconducting oxides such as molybdenum oxide (MoO_3)[44, 45], carbon nanotubes[46, 47] and organic materials such as the blend: poly[9,9-dioctylfluorene-co-N-[4-(3-methylpropyl)]-diphenyl-amine] (TFB): 4,4'-bis[(p-trichlorosilylpropylphenyl)-phenylamino]biphenyl ($TPDSi_2$)[48].

1.2.3 Cathode Interlayers

Cathode interlayers or electron transporting layers (ETLs) are used to improve the stability of devices using aluminum as the cathode. When aluminum is deposited onto the device, it is thermally evaporated. During thermal evaporation, the hot Al atoms can diffuse into the organic layer. This results in chemical reactions at the metal/organic interface. Additionally, Al-C bond formation at the metal/organic interface will undoubtedly interfere with and break the π-conjugated system of the organic layer. Cathode interlayers materials include: metals, such as calcium, inorganic compounds such as lithium fluoride (LiF)[49-51] and water or alcohol soluble polymers[52] such as poly[(9,9-bis(3′-(N,N-dimethylamino)propyl)-2,7-fluorene)-*alt*-2,7-(9,9-dioctylfluorene)] (PFN)[53].

1.2.4 P-type Materials

P-type materials serve as the electron donors in the organic solar cell. They are organic semiconductors that come in the form of small molecules or polymers[54]. Examples include the polymers polythieno[3,4-*b*]-thiophene-*co*-benzodithiophene (PTB7)[55], poly[N-9"-hepta-decanyl-2,7-carbazole-alt-5,5-(4',7'-di-2-thienyl-2',1',3'-benzothiadiazole) (PCDTBT)[56] and the small molecule 5,5-bis((4-(7-hexylthiophen-2-yl)thiophen-2-yl)-[1,2,5]thiadiazolo[3,4-c]pyridine)-3,3-di-2-ethylhexylsilylene-2,2-bithiophene ($DTS(PTTh_2)_2$[57] (Figure 1-3). Active layer donor materials will be covered in more detail further in this chapter.

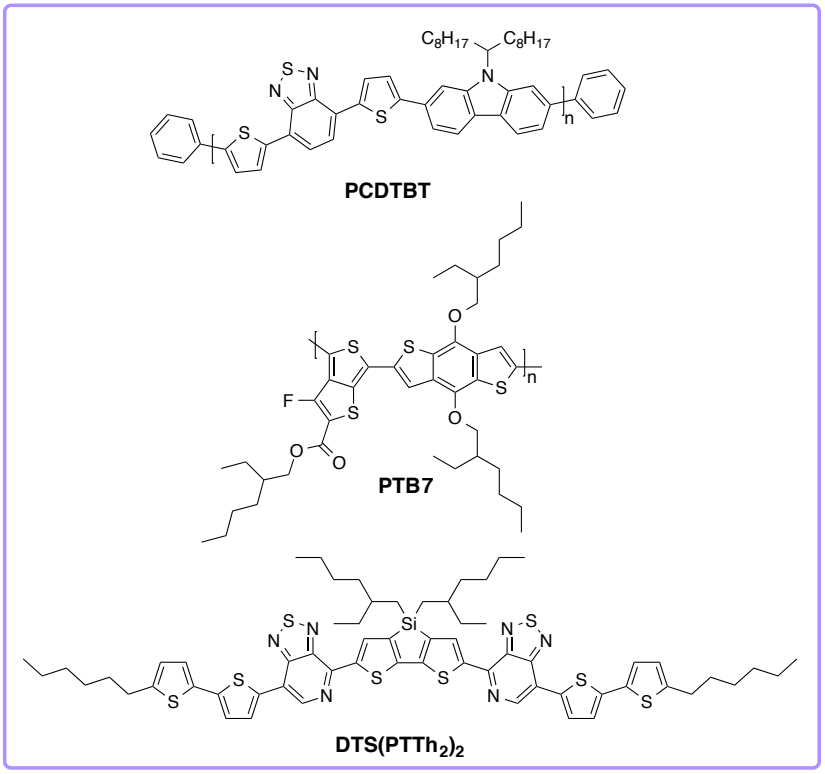

Figure 1-3. Molecular structures of common p-type active layer materials

1.2.5 N-type Materials

In addition to the selection of interlayers the choice of n-type material is also important. In early works, C_{60} fullerene was used as it was observed that there was photoinduced electron transfer in blends of conjugated polymers and the fullerene derivative[58]. C_{60} derivatives have a low-lying HOMO relative to p-type materials, which makes them great electron acceptors[59]. They also have high electron mobilities in OFETs, which is desired for good charge transport for an n-type material[60, 61]. Fullerenes are able to accept six electrons; due to their triply degenerate LUMOs. Electron transfer for fullerenes takes place at 45 fs [62], which is significantly faster than

back electron transfer or the radiative decay that occurs through photoluminescence. Thus they are able to provide a kinetic driving force for efficient charge separation[23].

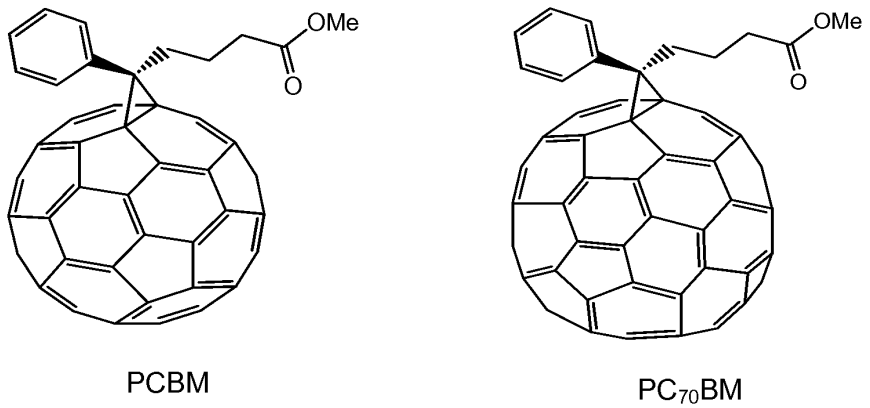

Figure 1-4. Molecular structures of [6,6']-phenyl-C_{61}-butyric acid methyl ester (PCBM) and [6,6']-phenyl-C_{71}-butyric acid methyl ester ($PC_{71}BM$)

P-type materials often suffer from photooxidation of their excited states. Fullerenes can address this problem by rapidly quenching the excited state[63, 64]. Unfortunately, C_{60} has poor solubility in organic solvents. To address this issue, the functionalized derivative $PC_{61}BM$ was created[61] (Figure 1-4). In recent years the use of another fullerene derivative, $PC_{71}BM$ has been more prevalent as this derivative is able to absorb more light in the UV-Vis spectrum[65-67] (Figure 1-5). This increase in absorbed light results in a higher J_{SC} value.

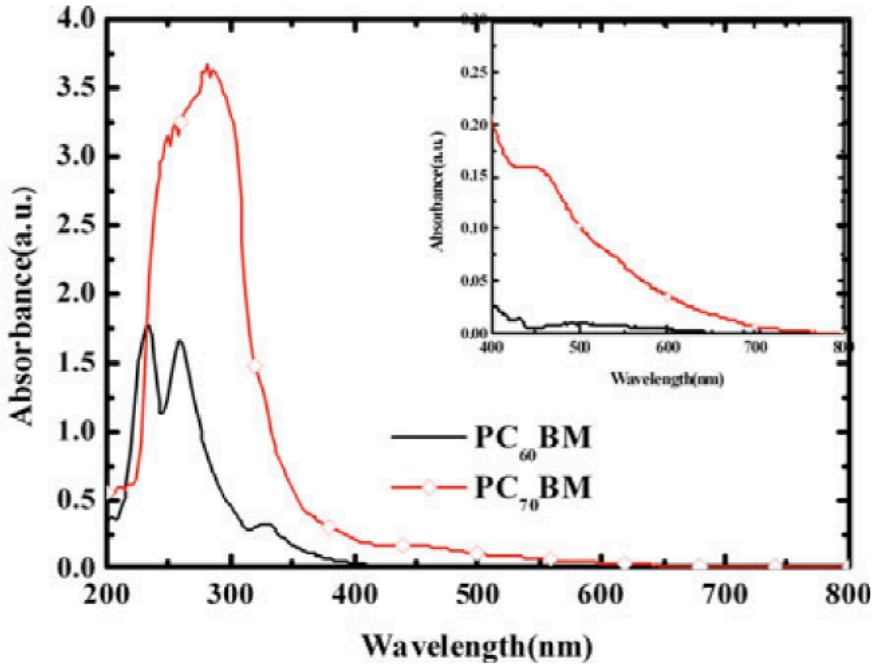

Figure 1-5. UV-Vis absorption spectra of $PC_{60}BM$ and $PC_{70}BM$. Adapted from Reference 21.

1.2.6 Bilayer vs Bulk Heterojunction Architecture

The bilayer structure, created by Tang *et al*, is composed of a junction that uses two organic materials with properly aligned energy levels[68] (Figure 1-6). Here, the acceptor layer is deposited onto a layer of the donor material. In the bilayer architecture, the p-type and n-type materials contact the anode and cathode selectively. The layers of donor and acceptor need to be sufficiently thick for optimal light absorption. Due to the short exciton diffusion lengths, there is often a lot of exciton recombination associated with this structure as the active layers were to thick[69] and separated excitons would have to go past this distance.

In order to combat this problem, the bulk heterojunction structure was developed by Heeger *et al*[70]. The bulk heterojunction architecture, while similar in structure to the bilayer structure, has one key difference: the p and n-type materials are intermixed and deposited as one layer resulting in a bicontinuous and interpenetrating network (Figure 1-6). This ensures that

phase separation is more likely to be within the exciton diffusion length and this results in more efficient exciton dissociation[71]. Bulk heterojunctions are generally achieved by the co-deposition of donor and acceptor or by spincasting solutions of donor/acceptor blends[17].

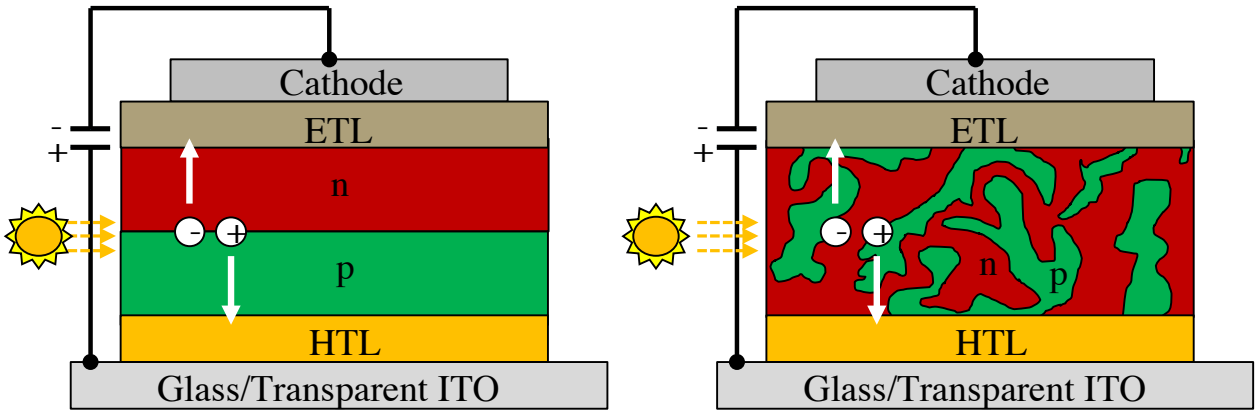

Figure 1-6. Showing difference in structure between the bilayer architecture and the bulk heterojunction architecture.

1.2.7 Solar Cell Characterization

Solar cells are characterized by their power conversion efficiencies, which are calculated by the following equation[72]:

$$PCE = \frac{V_{OC}\, J_{SC} FF}{P_{in}}$$

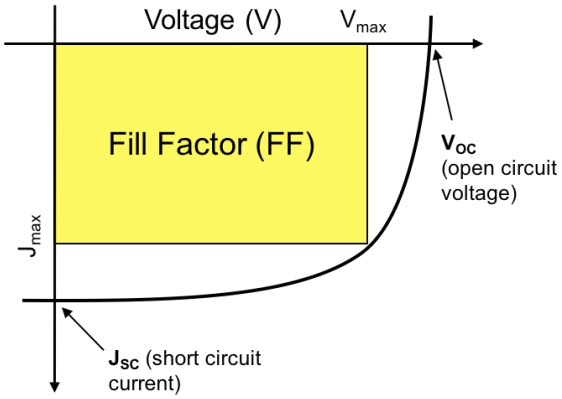

Figure 1-7. Current density vs voltage plot characteristic of a solar cell device. Reprinted with permission from Ref. (72). Copyright (2013), Wiley-VCH.

The open circuit voltage (V_{OC}) is the voltage at zero current density (Figure 1-7) and is dependent on difference in the work function of the metal contacts. The V_{OC} is usually dependent on the HOMO-LUMO difference between the donor and acceptor if there is ohmic contact being formed[22].

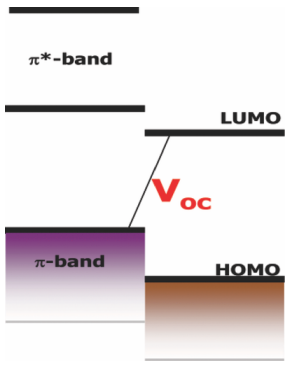

Figure 1-8. Diagram showing the origin of the open-circuit voltage in the BHJ solar cell. Reprinted with permission from Ref. (72). Copyright (2013), Wiley-VCH.

The short circuit current density (J_{SC}) is the current density when the voltage is zero (Figure 1-7). It represents the number of charge carriers that are generated and collected by the electrodes in the solar cell. The J_{SC} becomes markedly better with conditions such as a small band gap of donor materials, high absorption coefficients, smaller phase separations between donor and acceptor blends and high charge carrier mobilities.

The fill factor (FF) (Figure 1-7) describes the dependence of the current output on the internal field of the device and is determined by the charge carriers reaching the electrodes[22]. FF is defined by the equation: $J_{mpp}V_{mpp}/J_{SC}V_{OC}$, where J_{mpp} and V_{mpp} are the current density and voltage at the maximum power input[73] (Figure 1-7). The FF is characterized by series resistance (R_S) and shunt resistance (R_{SH}), whereby an ideal device seeks to have a smaller R_S and larger R_{SH}. Both R_s and R_{SH} are greatly influenced by the morphology of the polymer/fullerene blend.

The J-V characteristics and the power conversion efficiency are not enough to quantify the performance of the solar cell. To further quantify the performance, the optical factors need to

be investigated in detail. This is done by measuring the incident photon to electron conversion efficiency (ICPE). The ICPE measures the amount of absorbed photons that are converted to charge carriers and end up getting collected at electrodes in the solar cell. It is equivalent to the external quantum efficiency (EQE). Trends in the EQE should be proportional to trends in the J_{SC}.

1.2.8 Solar Cell Optimization

In order to properly optimize solar cells of a given polymer, certain parameters have to be varied. These include the concentration of the active layer blend, the speed use to spin coat for active layer blend, the choice of the fullerene derivative as well as the hole transporting layer used. The concentration of the active layer blend affects the thickness of the resulting film, with More concentrated solutions result in thicker films. Reducing the spin coating speeds during the deposition of the active layer blends also result in thicker films. This is beneficial as thicker films increase light absorption, however thicker films have lower mobilities and impeded charge transport[74-76]. Generally, for polymer solar cells, a thickness of ~ 100 nm is desired[75]. This gives the best balance of optimal J_{SC} values as well as optimal mobilities and charge transport in the film. The hole transporting layer can be selected based on the energy levels of the anode used and the donor material. Ideal energy level alignments result in ohmic contact.

Additionally, solvent additives can be used in the active layer blend solutions. Solvent additives elongate the drying process and promote crystallinity in the active layer[77-79]. They improve on the polymer: PCBM interpenetrating network through a better mixing of the blend components (Figures 1-9, 1-10). Commonly used additives include: 1,8-diiodooctane (DIO)[80, 81], 1,8-octanedithiol (ODT)[82, 83] and 1-chloronaphthalene (CN)[77, 84, 85].

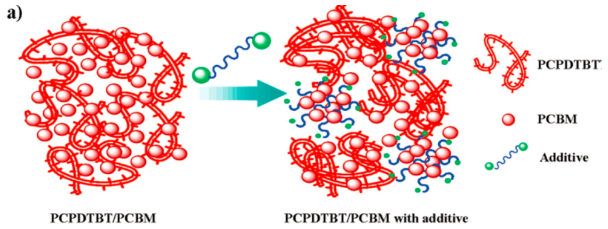

Figure 1-9. Schematic showing the role of the solvent additive in the self-assembly of the bulk heterojunction blend materials. Reprinted with permission from Ref. (80). Copyright (2008), American Chemical Society.

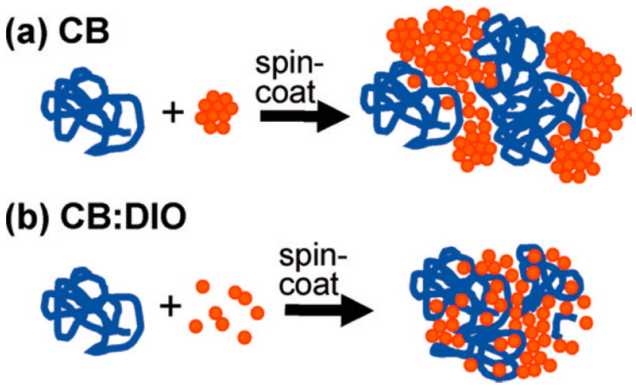

Figure 1-10. Schematic showing the effect of the solvent additive, DIO. Reprinted with permission from Ref. (14). Copyright (2011), American Chemical Society

1.3 Organic semiconductors

Organic semiconductors are unsaturated molecules consisting of alternating double-single (conjugated) bonds. A basic example of an organic semiconducting polymer is trans-polyacetylene. Trans-polyacetylene has a quasi- one-dimensional structure that is held together by trigonal planar σ-orbitals in the polymer backbone. Only three of the carbon electrons participate in the σ backbone. The remaining electron is perpendicular to the trigonal plane in the p_z orbital. All these remaining *pz* ortbital electrons from adjacent carbons overlap to form the π system[86]. This π system is a delocalized electron cloud with periodic alternating density. The polymer has two equivalent structures with the same ground state energies. This is referred to as

the degenerate ground state. The system of π electrons is delocalized along the carbon chain. This, along with weaker inter chain interactions gives polyacetylene its quasi-1D structure.

The alternating double and single bonds found within the polymer, if they were the same length, would consist of π electron bands that are half-filled with electrons by Pauli's principle. This implies that the polymer would be a metal. Peierls, however, predicted that this was not true[87]. The structure has instability due to lattice vibrations. This results in a dimerization of the backbone into longer single bonds and shorter double bonds[87]. X-ray diffraction and nuclear magnetic resonance can be used to measure the difference in the bond lengths at approximately 1.45 Å and 1.35 Å [88]. This reaction is spontaneous and results in a reduction of the crystalline symmetry and subsequent minimization of the ground state energy of the occupied band. Throughout this time, the potential energy of the dimerized polymer chain is increased. This leads to an equilibrium state, where the total energy of the polymer chain is lowered. There is a change in the electron density during an allowed $\pi \rightarrow \pi^*$ transition. This change is an asymmetric change in the dipole moment and a reduction in the bond strength[86].

Peierls' distortion predictions elucidated the development of two molecular bands; the π-band originating from the HOMO and the π*-band originating form the LUMO[89, 90]. These bands have a non-zero energy gap between them, which is referred to as the band gap. The HOMO and LUMO bands are analogous to the valence and conduction bands in inorganic semiconductors; where the valence band is filled with electrons and the conduction band is usually free of electrons. The HOMO and LUMO represent the energy bands that correspond to the various hybridization between the bonding and antibonding π-electrons[86, 91] (Figure 1-11). As the level of conjugation in the polymer increases, the band gap decreases until the effective conjugation

length is reached. At this point, the electronic properties of the materials do not change, even if more repeat, conjugated units are added.

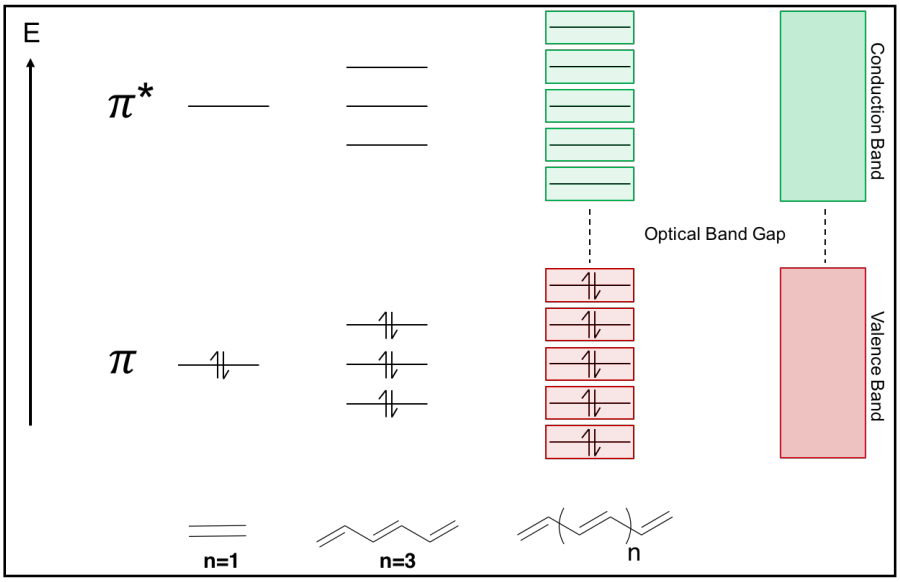

Figure 1-11. The Evolution of conjugated polymer band structures from molecular orbitals

1.3.1 Rational Design of Conjugated Polymers

The design of a conjugated polymer can be divided into three major components: the conjugated backbone, the side chains and the substituents (Figure 1-12)[92].

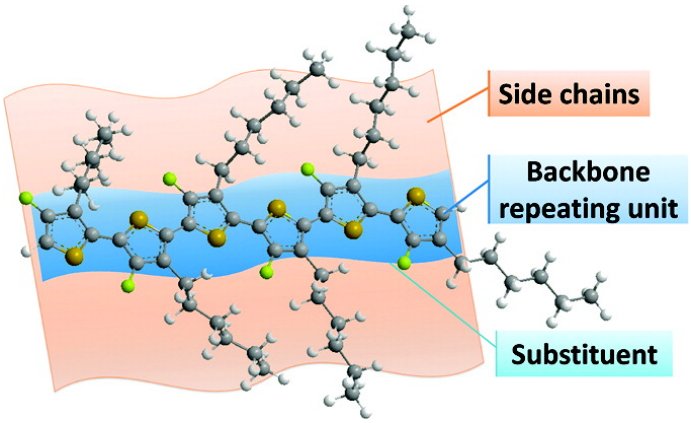

Figure 1-12. The main components of the conjugated semiconducting polymer. Reprinted with permission from Ref. (92). Copyright (2011), American Chemical Society.

The most vital component is the conjugated backbone as it influences the physical properties of the polymer, which are related to solar cell performance. It determines the polymer bandgap, energy levels and intermolecular interactions[93].

Two important solar cell efficiency characteristics, the open circuit voltage (V_{OC}) and short-circuit current density (J_{SC}), are closely related to the polymer's electronic properties. Most of the energy form the solar spectrum (~70%) is found between 380 nm and 900 nm[94] (Figure 1-13). As a result, one of the important requirements for conjugated polymers is the ability to absorb light within this region. This ultimately leads to a polymer bandgap of 1.4-1.5 eV,[95, 96] which would enable to polymer to have a broad and strong absorption range. This is the first prerequisite for achieving high J_{SC} values[93].

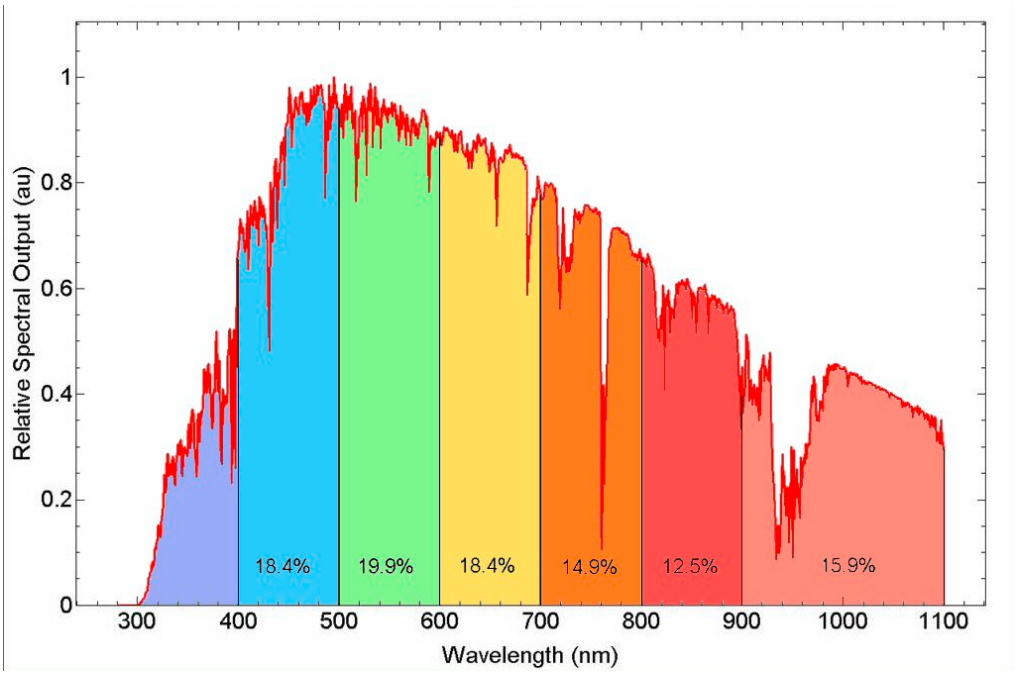

Figure 1-13. Standard AM 1.5 Solar Spectrum

The V_{OC} is directly related to the energy difference between the HOMO of the donor conjugated polymer and the LUMO of the accepter (typically PCBM a fullerene derivative) molecule in the solar cell. There is also a minimum difference of 0.3 eV for the LUMOs of the polymer and acceptor; the exciton driving force, required to dissociate the exciton from a conjugated polymer[97]. PCBM has a LUMO of -4.3 eV. Based on the afore-mentioned information, an ideal conjugated polymer would have a low-lying HOMO of around -5.4 eV to ensure a high V_{OC}.

Early organic solar cells employed the use of the homopolymers, such as poly-3-hexylthiophene (P3HT)[98, 99], as the material for the conjugated polymer backbone (Figure 1-14). The repeat unit of a homopolymer consists of a single aromatic unit or fused aromatic units. The physical properties of these polymers were largely determined by the properties of the constituting aromatic unit(s). As a result, most homopolymers, like P3HT, have large bandgaps

over 1.9 eV[92, 100]. This led to future research that concentrated on designing conjugated polymers with narrow bandgaps.

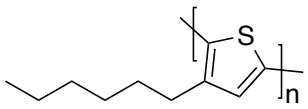

Figure 1-14. Molecular structure of P3HT

1.3.1a Design of polymer backbone

The most established method to narrow the bandgap of a conjugated polymer has been to increase the quinoid structure in the polymer backbone[93]. Conjugated polymers, in their ground states, have two degenerate resonance forms: an aromatic form and a quinoid form[101]. In the aromatic form, the aromaticity of the thiophene units within the polymer is maintained by the confinement of π-electrons within the molecule (Figure 1-14)[102]. In the quinoid form the π-electrons are distributed throughout the polymer backbone by simultaneously changing double bonds to single bonds and single bonds to double bonds. The aromatic form has lower ground state energy relative to the quinoid form[103].For structures with aromatic rings, the band gap does not decrease as a function of decreasing bond length but, rather, as a function of the increasing quinoid character[104]. Polymers with a greater tendency to form a quinoid structure have lower bandgap energies due to their higher ground state energies[105] . The quinoid form also promotes planarity within the polymer because π-electrons are delocalized more effectively along the polymer backbone[103]. One method to increase the quinoid character within a polymer involves the incorporation of thiophene units, which are fused to other aromatic units such as benzene. Benzene has a higher resonance energy and therefore, in these fused systems, thiophene is likely to adopt the quinoid form so that the benzene ring can maintain its aromatic form (Figure 1-15).

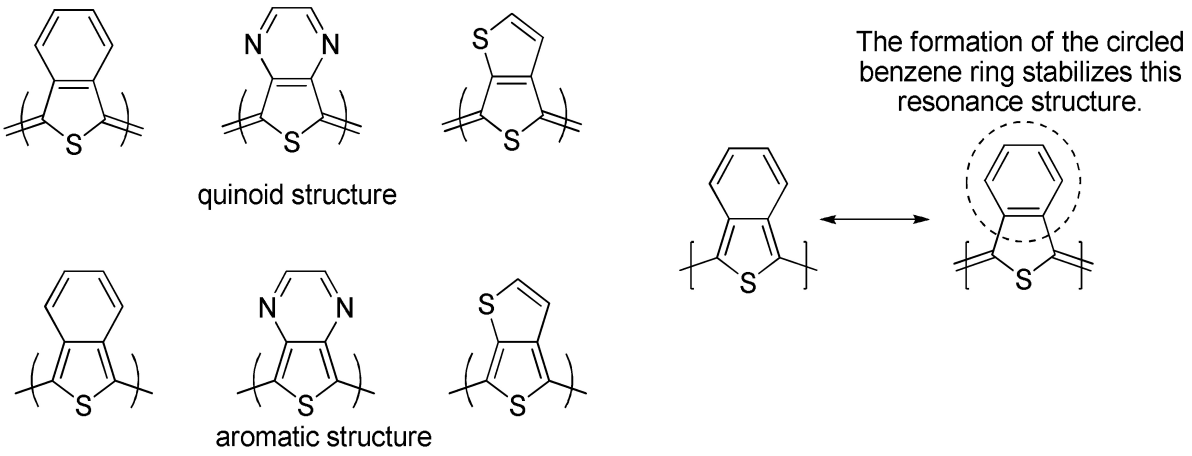

Figure 1-15. Aromatic and quinoid forms of (a) poly(benzo[c]thiophene), (b) polythirnro[3,4-b]pyrazine and (c)poly9thieno[3,4-b]-thiophene). Reprinted with permission from Ref. (102). Copyright (2010), American Chemical Society.

Another way to promote quinoid character in a polymer is to incorporate the use of donor-acceptor polymers, which have been widely implemented through the intramolecular charge transfer (ICT) approach[106-111]. Here, through orbital mixing, the HOMO and LUMO of the conjugated polymer are controlled by its subsequent donor and acceptor monomer units (Figure 1-16). The donor monomer units are electron – rich units and the acceptor units are electron-deficient units. The driving force of the push and pull of electron density between the electron donating units and the electron accepting units favors the polymer's quinoid resonance form[112]. Consequently, the band gap if the copolymers decrease as the π-electrons can be delocalized more effectively.

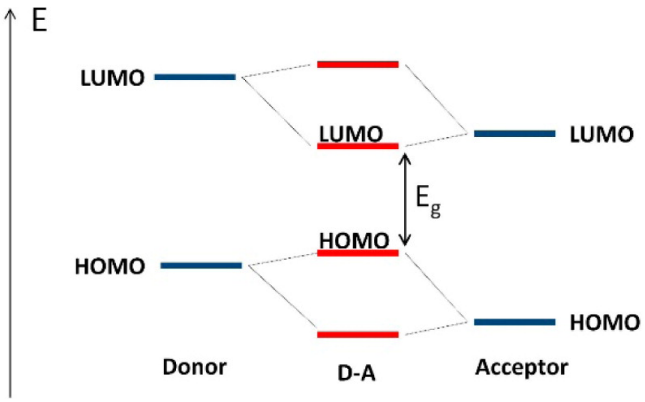

Figure 1-16. Molecular orbital theory explanation for band gap reduction in a D-A copolymer. Reprinted with permission from Ref (112). Copyright (2015), American Chemical Society

1.3.1a-1 Donors

Donors are chosen based on electron richness. Constituents with fused rings are commonly used as the arrangement of aromatic rings can lead to an increase on the charge mobility as well as tuning of the energy levels. Donor moieties are often designed with fused three ring and ladder type structures, [113-116] which ensures that the structure of the donor is planar with and extended π systems. This is beneficial as planar structures add rigidity to the polymer backbone and facilitate better hole mobilities and π- π stacking. In fused systems, replacing center carbon atoms with Si results in better stacking along the polymer backbone (Figure 1-17). While the HOMO levels remain the same, it is the largeness of the Si, relative to C, and the longer C-Si bond that results in this improvement in the molecular packing and therefore, charge transport[117, 118]. Figure 1-18 summarizes electron donors based on their relative donating strength[92].

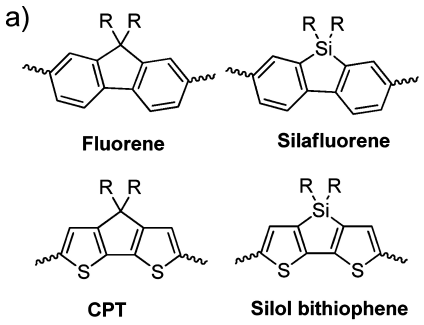

Figure 1-17

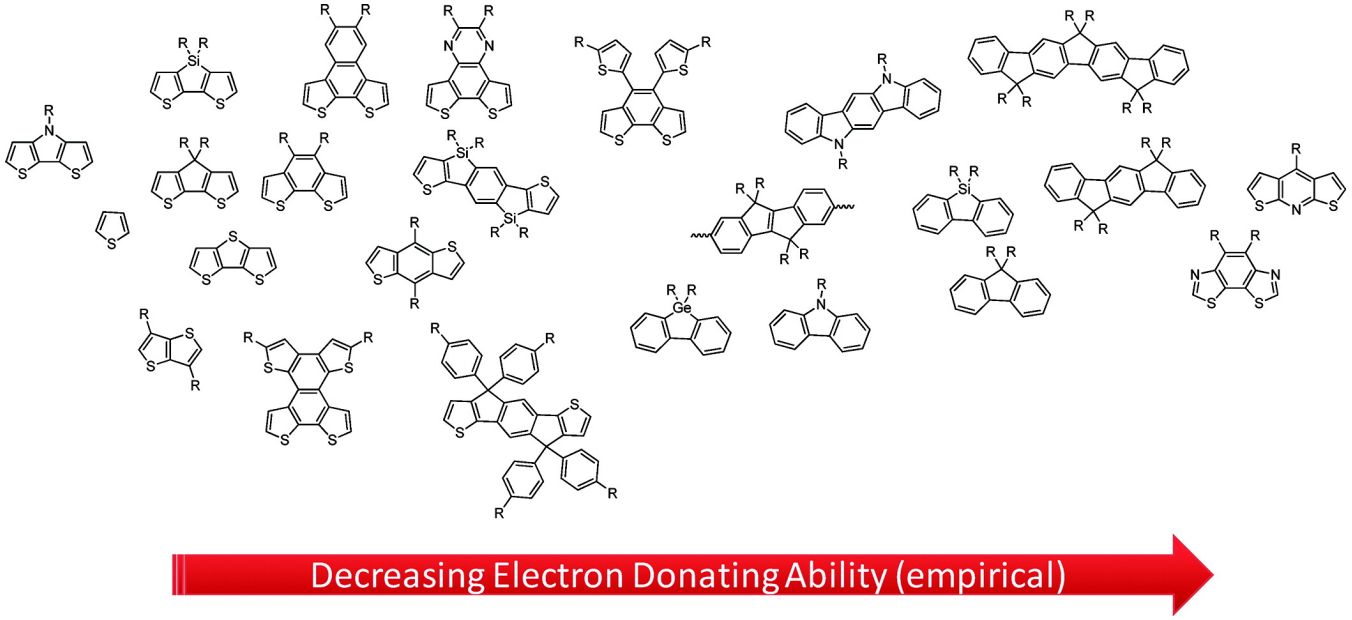

Figure 1-18. Empirical char shoring relative the relative electron-donating ability of various donor units. Reprinted with permission from Ref. (92). Copyright (2012), American Chemical Society.

1.3.1a-2 Electron acceptors for D-A polymers

It is desirable that electron acceptors have excellent electron mobilities, broad absorption spectra, and properly matched energy levels with its copolymerized donor. Electron acceptors typically are made from moieties with high electron affinities and include electron-withdrawing substituents, such as amides, imides and thiadiazoles[92]. Planar structures are also desirable as they promote electron delocalization and enhance intramolecular interactions[119, 120]. While there are a plethora of electron donors available, there are far fewer electron acceptors[121]. This is a

testament of the challenge to synthesize an acceptor that is simultaneously strongly electron deficient as well as stable. Figure 1-19 summarizes some of the most commonly used strong electron acceptors[92].

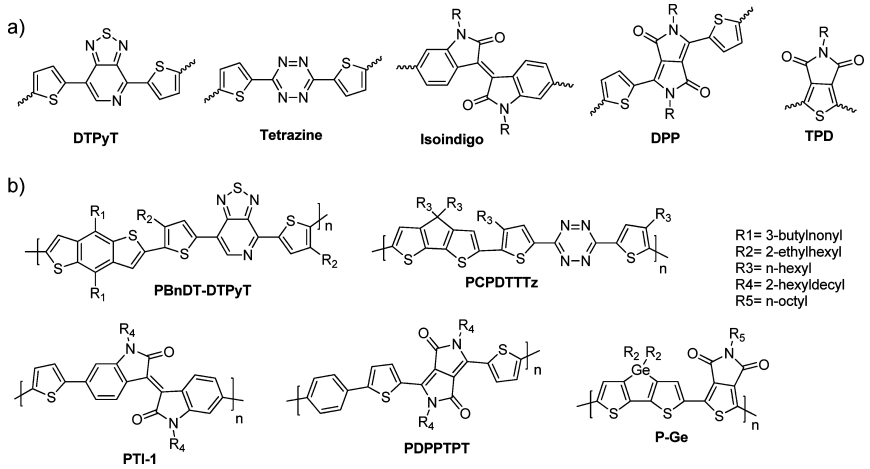

Figure 1-19. Molecular structures of selected strong electron acceptors. Reprinted with permission from Ref. (92). Copyright (2012), American Chemical Society

1.3.1b Weak Donor – Strong Acceptor Polymers

While the use of donor – acceptor polymers is a good way to ensure polymers with narrow bandgaps, it often results in higher HOMO levels and ultimately lower V_{OC} values. To simultaneously decrease the bandgap and lower the HOMO level, weak donor – strong acceptor systems have been studied[122]. The weak donor ensures that the polymer has a lower HOMO level. The strong acceptor reduces the bandgap through ICT (Figure 1-20).

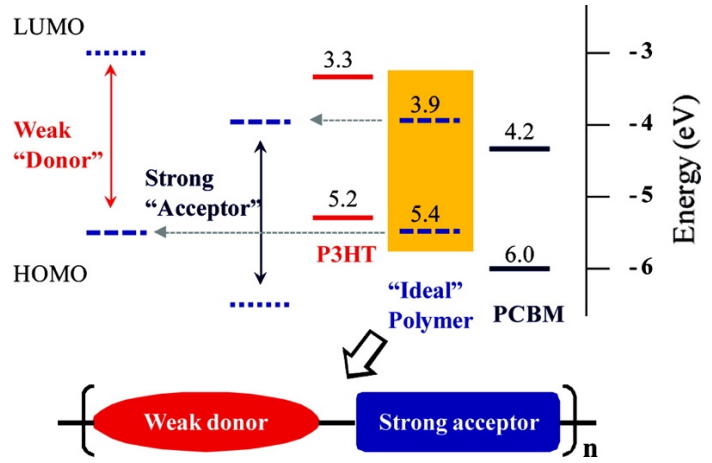

Figure 1-20. Band diagram showing the energy levels of an ideal conjugated polymer relative to PCBM. Reprinted with permission from Ref. (122) . Copyright (2010) American Chemical Society.

1.3.2 Substituents

In order to better fine-tune the energy levels and bandgaps, substituents can be used on the main polymer backbone. They can also affect the molecular interactions with in the polymer, as well as the film morphology. Electron – donating substituents such as methoxy (-OCH_3) raises the HOMO level, electron – withdrawing substituents such as cyano (-CN) have more of an impact on the LUMO level[123-125]. A commonly used substituent is the fluorine atom, which is the smallest electron – withdrawing group with a van der Waals radius of 1.35 Å. Fluorinated molecules exhibit good oxidative and thermal stabilities[126]. They also have a great influence on inter- and intramolecular interactions through C-F---H, and F---S interactions[127, 128]. Fluorine substitution results in approximately the same bandgap values, but a reduction in both the HOMO and LUMO levels[129]. Its presence on the backbone can increase the hole mobility[110, 130]. In the solar cell it allows the polymer to be more miscible with PCBM, which would allow for improved exciton dissociation[110, 131, 132].

1.3.3 Solubilizing side chains

Once the polymer energy levels have been engineered, solubilizing side chains are implemented to allow solution processability[93]. If conjugated polymers were synthesized without solubilizing chains, then their extended π-π systems would lead to insoluble aggregates that would not be solution processable. The addition of solubilizing chains assists in the attainment of higher molecular weight in the polymers. Higher molecular weights translate to better film quality in the active layer of the solar cell, which relates directly to better charge transport, and therefore better solar cell efficiencies. Higher molecular weight polymers are also more thermally stable than low molecular weight oligomers.

The addition of bulky alkyl side chains, where there once was a tiny hydrogen atom, results in considerable steric hindrance between the aromatic units in the polymer[133]. This leads to an increase in the bandgap. In order to combat bandgap enlargements, a good comprise of alkyl chain size and shape needs to be found. Longer alkyl chains result in larger dihedral angles for bonds between aromatic units[133] (Figure 1-21 and Table 1). Small angles are indicative of more complete conjugation. Alternatively, large dihedral angles suggest a disruption in the conjugation of the aromatic units in the polymer. It is this disruption that results in bandgap enlargement and a subsequent blue-shifting of the polymer absorption[133-135].

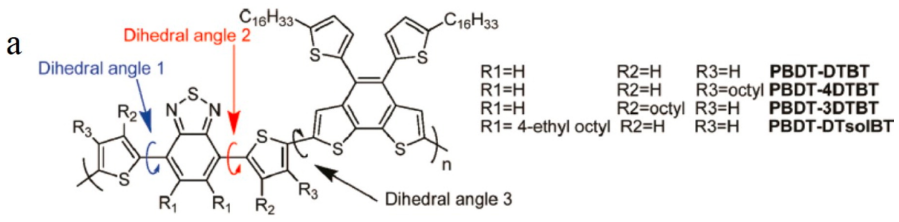

Figure 1-21. Molecular structures of four polymers based on the PBDT-DTBT backbone, showing different dihedral angles. Reprinted with permission from Ref. (133). Copyright (2010), American Chemical Society.

Table 1-1. Calculated dihedral angles of the polymers from Figure 1-20. Reprinted with permission from Ref. (133). Copyright (2010), American Chemical Society.

polymer	dihedral angle 1 (deg)	dihedral angle 2 (deg)	dihedral angle 3 (deg)
PBDT−DTBT	4.1	10.9	14.1
PBDT−4DTBT	5.2	14.3	30.2
PBDT−3DTBT	50.7	36.2	17.7
PBDT−DTsolBT	58.0	55.2	19.9

Unbranched or straight alkyl chains promote better intermolecular interactions within the polymer relative to branched chains. Additionally, polymers with unbranched chains exhibit enhanced molecular packing,[130] which results in a redshift in the absorption spectrum of the polymers. As a result, there is usually a marked improvement in the J_{SC} value relative to that of the same polymers with branched chains. Although short, straight chain alkyl side chains are the best choice molecular packing, they are not the most effective means to achieve optimal solution processability[136, 137]. Branched, alkyl chains promote better intermixing between the polymer and the PCBM in the active layer of the solar cell. This often results in higher V_{OC} values. The challenge, in the design of conjugated polymers, has been to strike a delicate balance between V_{OC} and J_{SC} and it has been shown that a good compromise has been to use short, branched alkyl chains (Figure 1-22). Additionally, positioning the side chains so that there is as little steric hindrance as possible within the molecule helps with better intermolecular interactions and packing.

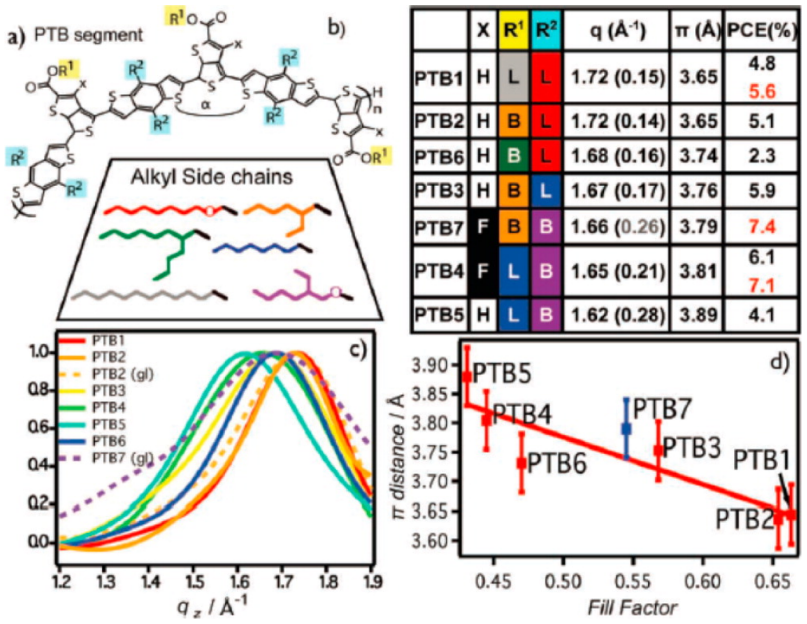

	X	R¹	R²	q (Å⁻¹)	π (Å)	PCE(%)
PTB1	H	L	L	1.72 (0.15)	3.65	4.8 5.6
PTB2	H	B	L	1.72 (0.14)	3.65	5.1
PTB6	H	B	L	1.68 (0.16)	3.74	2.3
PTB3	H	B	L	1.67 (0.17)	3.76	5.9
PTB7	F	B	B	1.66 (0.26)	3.79	7.4
PTB4	F	L	B	1.65 (0.21)	3.81	6.1 7.1
PTB5	H	L	B	1.62 (0.28)	3.89	4.1

Figure 1-22. Solar cell performances of polymers made with various combinations of solubilizing chains. Reprinted with permission.

1.3.4 Heteroatom substitution and effects

The use of heteroatoms is prevalent in all low bandgap polymers used in OPV applications. These heteroatoms, when used in polymers, can affect the electron density and conjugation lengths and resulting molecules differ from the originals. This allows for the fine-tuning of the polymer properties. When selenophene replaces thiophene, the selenium-based analogues have lower bandgaps and increased hole mobilities[138-140]. This is due to stronger interchain interactions from the more polarizable selenium atoms, which result in a stabilization of the HOMO[141]. This often results in an improvement in the PCE. Another example includes replacing the central carbons in PCDTBT with silicon (Figure 1-23). The silicon-containing polymer had better interchain ordering and the J_{SC} was greatly improved relative to the carbon analogue. The length of the C-Si bond (1.89 Å) is significantly larger than the C-C bond (1.53 Å)

and this reduced the steric hindrance from bulky side chains and structures change from amorphous to crystalline with the substitution of silicon[118, 142].

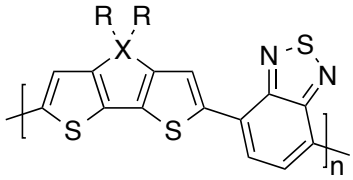

P1: X = C, R = n-dodecyl
P2: X = Si, R = n-dodecyl
P3 :X=Si, R=2-ethylhexyl

Figure 1-23. Examples of heteroatom substitution of silicon for carbon in PCDTBT

In conclusion, the design of the organic solar cell and the organic semiconducting polymer are both important. It is through the marriage of the optimization of the solar cells and fine-tuning of the organic semiconducting electronics that we able to obtain optimal organic solar cell performances.

1.4 REFERENCES

1. Marland, G.; Boden, T. A.; Andres, R. J.; Brenkert, A. L.; Johnston, C. A., *Trends: A compendium of data on global change* **2003**, 34-43.
2. Vitousek, P. M., *Ecology* **1994,** *75* (7), 1861-1876.
3. Fargione, J.; Hill, J.; Tilman, D.; Polasky, S.; Hawthorne, P., *Science* **2008,** *319* (5867), 1235-1238.
4. Lewis, N. S.; Nocera, D. G., *Proceedings of the National Academy of Sciences* **2006,** *103* (43), 15729-15735.
5. Turner, J. A., *Science* **1999,** *285* (5428), 687-689.
6. Dimroth, F.; Grave, M.; Beutel, P.; Fiedeler, U.; Karcher, C.; Tibbits, T. N. D.; Oliva, E.; Siefer, G.; Schachtner, M.; Wekkeli, A.; Bett, A. W.; Krause, R.; Piccin, M.; Blanc, N.; Drazek, C.; Guiot, E.; Ghyselen, B.; Salvetat, T.; Tauzin, A.; Signamarcheix, T.; Dobrich, A.; Hannappel, T.; Schwarzburg, K., *Progress in Photovoltaics: Research and Applications* **2014,** *22* (3), 277-282.
7. Powell, D. M.; Winkler, M. T.; Choi, H. J.; Simmons, C. B.; Needleman, D. B.; Buonassisi, T., *Energy & Environmental Science* **2012,** *5* (3), 5874-5883.
8. Joshi, P.; Xie, Y.; Ropp, M.; Galipeau, D.; Bailey, S.; Qiao, Q., *Energy & Environmental Science* **2009,** *2* (4), 426-429.
9. Fairley, P., *Spectrum, IEEE* **2005,** *42* (7), 28-33.
10. Brabec, C. J.; Sariciftci, N. S.; Hummelen, J. C., *Advanced Functional Materials* **2001,** *11* (1), 15-26.
11. Son, H. J.; Carsten, B.; Jung, I. H.; Yu, L., *Energy & Environmental Science* **2012,** *5* (8), 8158-8170.
12. He, Z.; Zhong, C.; Huang, X.; Wong, W.-Y.; Wu, H.; Chen, L.; Su, S.; Cao, Y., *Advanced Materials* **2011,** *23* (40), 4636-4643.
13. Chu, T.-Y.; Lu, J.; Beaupré, S.; Zhang, Y.; Pouliot, J.-R.; Zhou, J.; Najari, A.; Leclerc, M.; Tao, Y., *Advanced Functional Materials* **2012,** *22* (11), 2345-2351.
14. Lou, S. J.; Szarko, J. M.; Xu, T.; Yu, L.; Marks, T. J.; Chen, L. X., *Journal of the American Chemical Society* **2011,** *133* (51), 20661-20663.
15. He, Z.; Zhong, C.; Su, S.; Xu, M.; Wu, H.; Cao, Y., *Nat Photon* **2012,** *6* (9), 591-595.
16. http://www.heliatek.com/en/press/press-releases/details/heliatek-consolidates-its-technology-leadership-by-establishing-a-new-world-record-for-organic-solar-technology-with-a-cell-effi.
17. Dennler, G.; Scharber, M. C.; Brabec, C. J., *Advanced Materials* **2009,** *21* (13), 1323-1338.
18. Kalowekamo, J.; Baker, E., *Solar Energy* **2009,** *83* (8), 1224-1231.
19. Blom, P. W. M.; Mihailetchi, V. D.; Koster, L. J. A.; Markov, D. E., *Advanced Materials* **2007,** *19* (12), 1551-1566.
20. Mayer, A. C.; Scully, S. R.; Hardin, B. E.; Rowell, M. W.; McGehee, M. D., *Materials Today* **2007,** *10* (11), 28-33.
21. *Organic Solar Cells*. 1 ed.; SPringer-Verlag: Londdon, 2013; p VI,266.
22. Günes, S.; Neugebauer, H.; Sariciftci, N. S., *Chemical Reviews* **2007,** *107* (4), 1324-1338.
23. Brabec, C. J.; Zerza, G.; Cerullo, G.; De Silvestri, S.; Luzzati, S.; Hummelen, J. C.; Sariciftci, S., *Chemical Physics Letters* **2001,** *340* (3–4), 232-236.

24. Kietzke, T., *Advances in OptoElectronics* **2007,** *2007*, 15.
25. Nunzi, J.-M., *Comptes Rendus Physique* **2002,** *3* (4), 523-542.
26. Halls, J. J. M.; Pichler, K.; Friend, R. H.; Moratti, S. C.; Holmes, A. B., *Applied Physics Letters* **1996,** *68* (22), 3120-3122.
27. Theander, M.; Yartsev, A.; Zigmantas, D.; Sundström, V.; Mammo, W.; Andersson, M. R.; Inganäs, O., *Physical Review B* **2000,** *61* (19), 12957-12963.
28. Haugeneder, A.; Neges, M.; Kallinger, C.; Spirkl, W.; Lemmer, U.; Feldmann, J.; Scherf, U.; Harth, E.; Gügel, A.; Müllen, K., *Physical Review B* **1999,** *59* (23), 15346-15351.
29. Stübinger, T.; Brütting, W., *Journal of Applied Physics* **2001,** *90* (7), 3632-3641.
30. Zhang, F.; Johansson, M.; Andersson, M. R.; Hummelen, J. C.; Inganäs, O., *Advanced Materials* **2002,** *14* (9), 662-665.
31. Lim, Y.-F.; Lee, S.; Herman, D. J.; Lloyd, M. T.; Anthony, J. E.; Malliaras, G. G., *Applied Physics Letters* **2008,** *93* (19), 193301.
32. Lee, T.-W.; Chung, Y., *Advanced Functional Materials* **2008,** *18* (15), 2246-2252.
33. de Kok, M. M.; Buechel, M.; Vulto, S. I. E.; van de Weijer, P.; Meulenkamp, E. A.; de Winter, S. H. P. M.; Mank, A. J. G.; Vorstenbosch, H. J. M.; Weijtens, C. H. L.; van Elsbergen, V., *physica status solidi (a)* **2004,** *201* (6), 1342-1359.
34. Peumans, P.; Forrest, S. R., *Applied Physics Letters* **2002,** *80* (2), 338-338.
35. Li, G.; Chu, C.-W.; Shrotriya, V.; Huang, J.; Yang, Y., *Applied Physics Letters* **2006,** *88* (25), 253503.
36. Brown, T. M.; Kim, J. S.; Friend, R. H.; Cacialli, F.; Daik, R.; Feast, W. J., *Applied Physics Letters* **1999,** *75* (12), 1679-1681.
37. Yan, H.; Lee, P.; Armstrong, N. R.; Graham, A.; Evmenenko, G. A.; Dutta, P.; Marks, T. J., *Journal of the American Chemical Society* **2005,** *127* (9), 3172-3183.
38. De Jong, M. P.; Van Ijzendoorn, L. J.; De Voigt, M. J. A., *Applied Physics Letters* **2000,** *77* (14), 2255-2257.
39. Wong, K. W.; Yip, H. L.; Luo, Y.; Wong, K. Y.; Lau, W. M.; Low, K. H.; Chow, H. F.; Gao, Z. Q.; Yeung, W. L.; Chang, C. C., *Applied Physics Letters* **2002,** *80* (15), 2788-2790.
40. Ni, J.; Yan, H.; Wang, A.; Yang, Y.; Stern, C. L.; Metz, A. W.; Jin, S.; Wang, L.; Marks, T. J.; Ireland, J. R., *Journal of the American Chemical Society* **2005,** *127* (15), 5613-5624.
41. Greczynski, G.; Kugler, T.; Keil, M.; Osikowicz, W.; Fahlman, M.; Salaneck, W. R., *Journal of Electron Spectroscopy and Related Phenomena* **2001,** *121* (1), 1-17.
42. Ouyang, J.; Xu, Q.; Chu, C.-W.; Yang, Y.; Li, G.; Shinar, J., *Polymer* **2004,** *45* (25), 8443-8450.
43. Okuzaki, H.; Harashina, Y.; Yan, H., *European Polymer Journal* **2009,** *45* (1), 256-261.
44. Shrotriya, V.; Li, G.; Yao, Y.; Chu, C.-W.; Yang, Y., *Applied Physics Letters* **2006,** *88* (7), 073508.
45. Lee, Y. J.; Yi, J.; Gao, G. F.; Koerner, H.; Park, K.; Wang, J.; Luo, K.; Vaia, R. A.; Hsu, J. W. P., *Advanced Energy Materials* **2012,** *2* (10), 1193-1197.
46. Sgobba, V.; Guldi, D. M., *Journal of Materials Chemistry* **2008,** *18* (2), 153-157.
47. Chaudhary, S.; Lu, H.; Müller, A. M.; Bardeen, C. J.; Ozkan, M., *Nano Letters* **2007,** *7* (7), 1973-1979.
48. Hains, A. W.; Marks, T. J., *Applied Physics Letters* **2008,** *92* (2), 023504.
49. Limketkai, B. N.; Baldo, M. A., *Physical Review B* **2005,** *71* (8), 085207.
50. Gao, D.; Helander, M. G.; Wang, Z.-B.; Puzzo, D. P.; Greiner, M. T.; Lu, Z.-H., *Advanced Materials* **2010,** *22* (47), 5404-5408.

51. Jönsson, S. K. M.; Carlegrim, E.; Zhang, F.; Salaneck, W. R.; Fahlman, M., *Japanese Journal of Applied Physics* **2005,** *44* (6R), 3695.
52. Seo, J. H.; Gutacker, A.; Sun, Y.; Wu, H.; Huang, F.; Cao, Y.; Scherf, U.; Heeger, A. J.; Bazan, G. C., *Journal of the American Chemical Society* **2011,** *133* (22), 8416-8419.
53. He, C.; Zhong, C.; Wu, H.; Yang, R.; Yang, W.; Huang, F.; Bazan, G. C.; Cao, Y., *Journal of Materials Chemistry* **2010,** *20* (13), 2617-2622.
54. Scharber, M. C.; Muhlbacher, D.; Koppe, M.; Denk, P.; Waldauf, C.; Heeger, A. J.; Brabec, C. J., *ADVANCED MATERIALS-DEERFIELD BEACH THEN WEINHEIM-* **2006,** *18* (6), 789.
55. Lu, L.; Yu, L., *Advanced Materials* **2014,** *26* (26), 4413-4430.
56. Peters, C. H.; Sachs-Quintana, I. T.; Kastrop, J. P.; Beaupré, S.; Leclerc, M.; McGehee, M. D., *Advanced Energy Materials* **2011,** *1* (4), 491-494.
57. Sun, Y.; Welch, G. C.; Leong, W. L.; Takacs, C. J.; Bazan, G. C.; Heeger, A. J., *Nat Mater* **2012,** *11* (1), 44-48.
58. Sariciftci, N. S.; Smilowitz, L.; Heeger, A. J.; Wudl, F., *Science* **1992,** *258* (5087), 1474-1476.
59. Allemand, P. M.; Koch, A.; Wudl, F.; Rubin, Y.; Diederich, F.; Alvarez, M. M.; Anz, S. J.; Whetten, R. L., *Journal of the American Chemical Society* **1991,** *113* (3), 1050-1051.
60. Wöbkenberg, P. H.; Bradley, D. D. C.; Kronholm, D.; Hummelen, J. C.; de Leeuw, D. M.; Cölle, M.; Anthopoulos, T. D., *Synthetic Metals* **2008,** *158* (11), 468-472.
61. Hummelen, J. C.; Knight, B. W.; LePeq, F.; Wudl, F.; Yao, J.; Wilkins, C. L., *The Journal of Organic Chemistry* **1995,** *60* (3), 532-538.
62. Brabec, C. J.; Zerza, G.; Sariciftci, N. S.; Cerullo, G.; Lanzani, G.; De Silvestri, S.; Hummelen, J. C., Direct observation of the ultrafast electron transfer process in a polymer/fullerene blend. In *Ultrafast Phenomena XII*, Springer Berlin Heidelberg: 2001; Vol. 66, pp 589-591.
63. Neugebauer, H.; Brabec, C. J.; Hummelen, J. C.; Janssen, R. A. J.; Sariciftci, N. S., *Synthetic Metals* **1999,** *102* (1–3), 1002-1003.
64. Neugebauer, H.; Brabec, C.; Hummelen, J. C.; Sariciftci, N. S., *Solar Energy Materials and Solar Cells* **2000,** *61* (1), 35-42.
65. Wienk, M. M.; Kroon, J. M.; Verhees, W. J. H.; Knol, J.; Hummelen, J. C.; van Hal, P. A.; Janssen, R. A. J., *Angewandte Chemie International Edition* **2003,** *42* (29), 3371-3375.
66. Arbogast, J. W.; Foote, C. S., *Journal of the American Chemical Society* **1991,** *113* (23), 8886-8889.
67. Yao, Y.; Shi, C.; Li, G.; Shrotriya, V.; Pei, Q.; Yang, Y., *Applied Physics Letters* **2006,** *89* (15), 153507.
68. Tang, C. W., *Applied Physics Letters* **1986,** *48* (2), 183-185.
69. Hoppe, H.; Niggemann, M.; Winder, C.; Kraut, J.; Hiesgen, R.; Hinsch, A.; Meissner, D.; Sariciftci, N. S., *Advanced Functional Materials* **2004,** *14* (10), 1005-1011.
70. Yu, G.; Gao, J.; Hummelen, J. C.; Wudl, F.; Heeger, A. J., *Science* **1995,** *270* (5243), 1789-1791.
71. Koster, L. J. A.; Smits, E. C. P.; Mihailetchi, V. D.; Blom, P. W. M., *Physical Review B* **2005,** *72* (8), 085205.
72. Heeger, A. J., *Advanced Materials* **2014,** *26* (1), 10-28.
73. Padinger, F.; Rittberger, R. S.; Sariciftci, N. S., *Advanced Functional Materials* **2003,** *13* (1), 85-88.

74. Nam, Y. M.; Huh, J.; Jo, W. H., *Solar Energy Materials and Solar Cells* **2010,** *94* (6), 1118-1124.
75. Koster, L. J. A.; Mihailetchi, V. D.; Blom, P. W. M., *Applied Physics Letters* **2006,** *88* (9), 93511-93511.
76. Moulé, A. J.; Bonekamp, J. B.; Meerholz, K., *Journal of Applied Physics* **2006,** *100* (9), 094503.
77. Hoven, C. V.; Dang, X. D.; Coffin, R. C.; Peet, J.; Nguyen, T. Q.; Bazan, G. C., *Advanced Materials* **2010,** *22* (8), E63-E66.
78. Su, M. S.; Kuo, C. Y.; Yuan, M. C.; Jeng, U.; Su, C. J.; Wei, K. H., *Advanced Materials* **2011,** *23* (29), 3315-3319.
79. Rogers, J. T.; Schmidt, K.; Toney, M. F.; Kramer, E. J.; Bazan, G. C., *Advanced Materials* **2011,** *23* (20), 2284-2288.
80. Lee, J. K.; Ma, W. L.; Brabec, C. J.; Yuen, J.; Moon, J. S.; Kim, J. Y.; Lee, K.; Bazan, G. C.; Heeger, A. J., *Journal of the American Chemical Society* **2008,** *130* (11), 3619-3623.
81. Henson, Z. B.; Müllen, K.; Bazan, G. C., *Nature chemistry* **2012,** *4* (9), 699-704.
82. Coates, N. E.; Hwang, I.-W.; Peet, J.; Bazan, G. C.; Moses, D.; Heeger, A. J., *Applied Physics Letters* **2008,** *93* (7), 072105.
83. Hwang, I.-W.; Cho, S.; Kim, J. Y.; Lee, K.; Coates, N. E.; Moses, D.; Heeger, A. J., *Journal of Applied Physics* **2008,** *104* (3), 033706.
84. Guo, X.; Cui, C.; Zhang, M.; Huo, L.; Huang, Y.; Hou, J.; Li, Y., *Energy & Environmental Science* **2012,** *5* (7), 7943-7949.
85. Hu, X.; Wang, M.; Huang, F.; Gong, X.; Cao, Y., *Synthetic metals* **2013,** *164*, 1-5.
86. Photovoltaics, O., Concepts and Realization, ed. CJ Brabec, V. Dyakonov, J. Parisi and NS Sariciftci. Springer-Verlag, Heidelberg: 2003.
87. Peierls, R. E., *Quantum theory of solids*. Oxford University Press: 1955.
88. Yannoni, C. S.; Clarke, T. C., *Physical Review Letters* **1983,** *51* (13), 1191-1193.
89. Su, W. P.; Schrieffer, J. R.; Heeger, A. J., *Physical Review Letters* **1979,** *42* (25), 1698-1701.
90. Heeger, A. J.; Kivelson, S.; Schrieffer, J. R.; Su, W. P., *Reviews of Modern Physics* **1988,** *60* (3), 781-850.
91. Brédas, J. L.; Calbert, J. P.; da Silva Filho, D. A.; Cornil, J., *Proceedings of the National Academy of Sciences* **2002,** *99* (9), 5804-5809.
92. Zhou, H.; Yang, L.; You, W., *Macromolecules* **2012,** *45* (2), 607-632.
93. *Organic Photovoltaics*. Second ed.; Wiley-VCH: Weinheim, Germany, 2014; p 599.
94. Moliton, A.; Nunzi, J.-M., *Polymer International* **2006,** *55* (6), 583-600.
95. Scharber, M. C.; Mühlbacher, D.; Koppe, M.; Denk, P.; Waldauf, C.; Heeger, A. J.; Brabec, C. J., *Advanced Materials* **2006,** *18* (6), 789-794.
96. Soci, C.; Hwang, I. W.; Moses, D.; Zhu, Z.; Waller, D.; Gaudiana, R.; Brabec, C. J.; Heeger, A. J., *Advanced Functional Materials* **2007,** *17* (4), 632-636.
97. Thompson, B. C.; Fréchet, J. M. J., *Angewandte Chemie International Edition* **2008,** *47* (1), 58-77.
98. Schilinsky, P.; Waldauf, C.; Brabec, C. J., *Applied Physics Letters* **2002,** *81* (20), 3885-3887.
99. Vanlaeke, P.; Swinnen, A.; Haeldermans, I.; Vanhoyland, G.; Aernouts, T.; Cheyns, D.; Deibel, C.; D'Haen, J.; Heremans, P.; Poortmans, J.; Manca, J. V., *Solar Energy Materials and Solar Cells* **2006,** *90* (14), 2150-2158.

100. Roncali, J., *Macromolecular Rapid Communications* **2007,** *28* (17), 1761-1775.
101. Bredas, J. L.; Silbey, R.; Boudreaux, D. S.; Chance, R. R., *Journal of the American Chemical Society* **1983,** *105* (22), 6555-6559.
102. Shengqiang, X.; Samuel, C. P.; Huaxing, Z.; Wei, Y., Recent Progress on Highly Efficient Bulk Heterojunction Polymer Solar Cells. In *Functional Polymer Nanocomposites for Energy Storage and Conversion*, American Chemical Society: 2010; Vol. 1034, pp 71-80.
103. Brabec, C. J.; Dyakonov, V.; Parisi, J.; Sariciftci, N. S., *Organic photovoltaics: concepts and realization*. Springer Science & Business Media: 2013; Vol. 60.
104. Brédas, J. L., *The Journal of Chemical Physics* **1985,** *82* (8), 3808-3811.
105. Wudl, F.; Kobayashi, M.; Heeger, A. J., *The Journal of Organic Chemistry* **1984,** *49* (18), 3382-3384.
106. Price, S. C.; Stuart, A. C.; Yang, L.; Zhou, H.; You, W., *Journal of the American Chemical Society* **2011,** *133* (12), 4625-4631.
107. Cabanetos, C.; El Labban, A.; Bartelt, J. A.; Douglas, J. D.; Mateker, W. R.; Fréchet, J. M. J.; McGehee, M. D.; Beaujuge, P. M., *Journal of the American Chemical Society* **2013,** *135* (12), 4656-4659.
108. Fang, L.; Zhou, Y.; Yao, Y.-X.; Diao, Y.; Lee, W.-Y.; Appleton, A. L.; Allen, R.; Reinspach, J.; Mannsfeld, S. C. B.; Bao, Z., *Chemistry of Materials* **2013,** *25* (24), 4874-4880.
109. Intemann, J. J.; Yao, K.; Li, Y.-X.; Yip, H.-L.; Xu, Y.-X.; Liang, P.-W.; Chueh, C.-C.; Ding, F.-Z.; Yang, X.; Li, X.; Chen, Y.; Jen, A. K. Y., *Advanced Functional Materials* **2014,** *24* (10), 1465-1473.
110. Liang, Y.; Xu, Z.; Xia, J.; Tsai, S.-T.; Wu, Y.; Li, G.; Ray, C.; Yu, L., *Advanced Materials* **2010,** *22* (20), E135-E138.
111. Gao, J.; Dou, L.; Chen, W.; Chen, C.-C.; Guo, X.; You, J.; Bob, B.; Chang, W.-H.; Strzalka, J.; Wang, C.; Li, G.; Yang, Y., *Advanced Energy Materials* **2014,** *4* (5), n/a-n/a.
112. Lu, L.; Zheng, T.; Wu, Q.; Schneider, A. M.; Zhao, D.; Yu, L., *Chemical Reviews* **2015**.
113. Liu, J.; Wu, J.; Shao, S.; Deng, Y.; Meng, B.; Xie, Z.; Geng, Y.; Wang, L.; Zhang, F., *ACS Applied Materials & Interfaces* **2014,** *6* (11), 8237-8245.
114. Son, H. J.; Lu, L.; Chen, W.; Xu, T.; Zheng, T.; Carsten, B.; Strzalka, J.; Darling, S. B.; Chen, L. X.; Yu, L., *Advanced Materials* **2013,** *25* (6), 838-843.
115. He, F.; Wang, W.; Chen, W.; Xu, T.; Darling, S. B.; Strzalka, J.; Liu, Y.; Yu, L., *Journal of the American Chemical Society* **2011,** *133* (10), 3284-3287.
116. Zheng, T.; Lu, L.; Jackson, N. E.; Lou, S. J.; Chen, L. X.; Yu, L., *Macromolecules* **2014,** *47* (18), 6252-6259.
117. Scharber, M. C.; Koppe, M.; Gao, J.; Cordella, F.; Loi, M. A.; Denk, P.; Morana, M.; Egelhaaf, H.-J.; Forberich, K.; Dennler, G.; Gaudiana, R.; Waller, D.; Zhu, Z.; Shi, X.; Brabec, C. J., *Advanced Materials* **2010,** *22* (3), 367-370.
118. Morana, M.; Azimi, H.; Dennler, G.; Egelhaaf, H.-J.; Scharber, M.; Forberich, K.; Hauch, J.; Gaudiana, R.; Waller, D.; Zhu, Z.; Hingerl, K.; van Bavel, S. S.; Loos, J.; Brabec, C. J., *Advanced Functional Materials* **2010,** *20* (7), 1180-1188.
119. Zou, Y.; Najari, A.; Berrouard, P.; Beaupré, S.; Réda Aïch, B.; Tao, Y.; Leclerc, M., *Journal of the American Chemical Society* **2010,** *132* (15), 5330-5331.
120. Zhang, Y.; Hau, S. K.; Yip, H.-L.; Sun, Y.; Acton, O.; Jen, A. K. Y., *Chemistry of Materials* **2010,** *22* (9), 2696-2698.
121. Ye, L.; Jiao, X.; Zhang, H.; Li, S.; Yao, H.; Ade, H.; Hou, J., *Macromolecules* **2015,** *48* (19), 7156-7163.

122. Zhou, H.; Yang, L.; Stoneking, S.; You, W., *ACS Applied Materials & Interfaces* **2010,** *2* (5), 1377-1383.
123. Brédas, J. L.; Heeger, A. J., *Chemical Physics Letters* **1994,** *217* (5–6), 507-512.
124. Helbig, M.; Hörhold, H.-H., *Die Makromolekulare Chemie* **1993,** *194* (6), 1607-1618.
125. Greenham, N. C.; Moratti, S. C.; Bradley, D. D. C.; Friend, R. H.; Holmes, A. B., *Nature* **1993,** *365* (6447), 628-630.
126. Wong, S.; Ma, H.; Jen, A. K. Y.; Barto, R.; Frank, C. W., *Macromolecules* **2003,** *36* (21), 8001-8007.
127. Reichenbacher, K.; Suss, H. I.; Hulliger, J., *Chemical Society Reviews* **2005,** *34* (1), 22-30.
128. Wang, Y.; Parkin, S. R.; Gierschner, J.; Watson, M. D., *Organic Letters* **2008,** *10* (15), 3307-3310.
129. Zhou, H.; Yang, L.; Stuart, A. C.; Price, S. C.; Liu, S.; You, W., *Angewandte Chemie International Edition* **2011,** *50* (13), 2995-2998.
130. Chen, H.-Y.; Hou, J.; Zhang, S.; Liang, Y.; Yang, G.; Yang, Y.; Yu, L.; Wu, Y.; Li, G., *Nat Photon* **2009,** *3* (11), 649-653.
131. Liang, Y.; Feng, D.; Wu, Y.; Tsai, S.-T.; Li, G.; Ray, C.; Yu, L., *Journal of the American Chemical Society* **2009,** *131* (22), 7792-7799.
132. Liang, Y.; Yu, L., *Accounts of Chemical Research* **2010,** *43* (9), 1227-1236.
133. Zhou, H.; Yang, L.; Xiao, S.; Liu, S.; You, W., *Macromolecules* **2010,** *43* (2), 811-820.
134. Becke, A. D., *The Journal of Chemical Physics* **1993,** *98* (7), 5648-5652.
135. Lee, C.; Yang, W.; Parr, R. G., *Physical Review B* **1988,** *37* (2), 785-789.
136. Liang, Y.; Wu, Y.; Feng, D.; Tsai, S.-T.; Son, H.-J.; Li, G.; Yu, L., *Journal of the American Chemical Society* **2009,** *131* (1), 56-57.
137. Yang, L.; Zhou, H.; You, W., *The Journal of Physical Chemistry C* **2010,** *114* (39), 16793-16800.
138. Saadeh, H. A.; Lu, L.; He, F.; Bullock, J. E.; Wang, W.; Carsten, B.; Yu, L., *ACS Macro Letters* **2012,** *1* (3), 361-365.
139. Intemann, J. J.; Yao, K.; Yip, H.-L.; Xu, Y.-X.; Li, Y.-X.; Liang, P.-W.; Ding, F.-Z.; Li, X.; Jen, A. K. Y., *Chemistry of Materials* **2013,** *25* (15), 3188-3195.
140. Dou, L.; Chang, W.-H.; Gao, J.; Chen, C.-C.; You, J.; Yang, Y., *Advanced Materials* **2013,** *25* (6), 825-831.
141. Jeffries-El, M.; Kobilka, B. M.; Hale, B. J., *Macromolecules* **2014,** *47* (21), 7253-7271.
142. Chen, H.-Y.; Hou, J.; Hayden, A. E.; Yang, H.; Houk, K. N.; Yang, Y., *Advanced Materials* **2010,** *22* (3), 371-375.

CHAPTER 2

Part A

SYNTHESIS OF 3,7-DIIODO-2,6-DI(THIOPHEN-2-YL)BENZO[1,2-B:4,5-B']DIFURANS: FUNCTIONAL BUILDING BLOCKS FOR THE DESIGN OF NEW CONJUGATED POLYMERS

Chemical Communications 2012, 48, 8919.

DOI: 10.1039/C2CC34070D

Brandon M. Kobilka,[a] Anton V. Dubrovskiy,[a] **Monique D. Ewan**,[a] Aimée L. Tomlinson,[b] Richard C. Larock,[a] Sumit Chaudhary[c] and Malika Jeffries-EL[*a]

[a]Department of Chemistry, Iowa State University, Ames, IA 50011

[b]Department of Chemistry, North Georgia College & State University, Dalhonega, GA 30597

[c]Department of Electrical Engineering, Iowa State University, Ames, IA 50011

2.A.1 Abstract

3,7-Diiodo-2,6-di(thiophen-2-yl)benzo[1,2-*b*:4,5-*b*']difurans are efficiently prepared by an iodine-promoted double cyclization. This new heterocyclic core is readily modified by the attachment of alkyl chains for improved solubility. The use of these compounds for the synthesis of new conjugated polymers is also reported.

2.A.2 Introduction

Organic semiconductors are finding widespread use as replacements for their inorganic counterparts in a range of applications, including field effect transistors (OFET)s, light-emitting diodes (OLED)s, and photovoltaic cells (OPVC)s.[1-3] These materials offer advantages in the form of facile device fabrication via solution-based techniques and energy levels that can be tuned by chemical synthesis. Tuning can be accomplished through the synthesis of materials with alternating electron-donating and electron-accepting moieties.[4, 5] Among electron-donating building blocks, benzo[1,2-*b*:4,5-*b*′]dithiophene (BDT) is particularly promising, due to its planar conjugated structure that facilitates π–π stacking, leading to higher hole mobility.[6-9] Bulk heterojunction photovoltaic cells (BHJ-PVC)s using BDT copolymers as donors have achieved power-conversion efficiencies (PCE)s up to 7.4%.[8]

Recently, furan-containing molecules have been explored for the design of organic semiconductors.[10-13] Furan is an attractive alternative to thiophene, since it is isoelectronic, while possessing a Dewar resonance energy of 18.0 kJ mol^{-1}, which is less aromatic than that of thiophene (27.2 kJ mol^{-1}).[14] Thus, replacing thiophene with furan is expected to favor the formation of quinoid structures, leading to a reduction in the band gap of the resulting materials. Although benzo[1,2-*b*:4,5-*b*']difurans (BDF)s are known in the literature, the lack of methods for the synthesis of substituted derivatives has prevented their widespread use.[15-19] Encouraged by some of our earlier work on iodocyclization, we explored this approach for synthesizing BDFs.[20] Herein, we report the synthesis of

functional BDFs and their polymerization with isoindigo, an electron-deficient moiety that has been used in several polymers with high PCE, when used as donor materials in BHJ-PVCs.[21, 22]

2.A.3 Results and Discussion

The synthetic steps to the desired polymers are shown in Scheme 2-A.1. The hydrogenation of the alkynyl BDFs **3a** and **3b** afforded the alkylated derivatives **4a** and **4b** in yields of ~95% each. Subsequent stannylation afforded **5a** and **5b** in yields of ~94% each. The Stille cross-coupling polymerization of **5a** or **5b** with 6,6'-dibromo-*N*,*N*'-(2-octyldodecanyl)-isoindigo **6**[23]

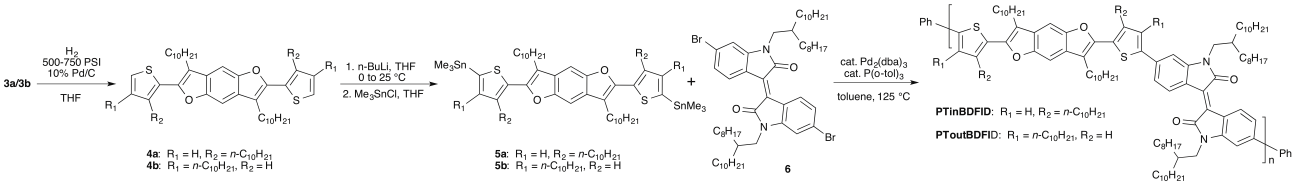

Scheme 2-A.1 Modification and polymerization of the 2,6-di(thiophen-2-yl)benzo[1,2-*b*:4,5-*b*']difurans.

afforded the polymers **PT$_{in}$BDFID** and **PT$_{out}$BDFID** in excellent yields after purification by Soxhlet extraction with methanol, followed by acetone, to remove residual catalyst and low molecular weight materials. Of the catalysts evaluated, $Pd_2(dba)_3$ gave the best results (Table 2-A.1). The polymers are soluble in standard organic solvents, such as THF and chloroform, at room temperature. Monomer **5a** consistently produced polymers with higher molecular weights. Presumably, this is due to the reduced steric hindrance at the 2- and 2'-positions of the BDF moiety.

Table 2-A.1. Reaction conditions and molecular weight data for PTBDFIDs

Polymer[a]	Catalyst	Yield (%)[c]	M_w[b]	M_w/M_n	DPn
PT_{out}BDFID	$Pd(PPh_3)_4$	82	20,500	1.3	12
PT_{out}BDFID	$Pd_2(dba)_3$	86	33,100	1.9	19
PT_{in}BDFID	$Pd(PPh_3)_4$	79	35,000	1.9	21
PT_{in}BDFID	$Pd_2(dba)_3$	84	76,200	2.3	45

[a] [monomer] = 0.2 M in toluene, and Pd catalyst loading = 2 mol%. [b] Molecular weight data was obtained by GPC (see ESI). [c] Isolated yield.

We anticipated that the differences in the regiochemistry of the BDFs would result in differences in the optical spectra. Compounds **2b**, **3b**, and **4b**, with the alkyl substituents on the 4 and 4' positions of the thiophene rings, have less interaction with the pseudo-peri iodine, alkyne, or alkane substituents, and exhibit greater vibrational structure than analogs **2a**-**4a**. Arguably, this is due to the greater rigidity of the overall aromatic chromophore, *i.e.* reduction of out-of-plane rotation of the thiophene moieties. The dramatically different band shapes between the members of each pair mean that comparisons of λ_{max} between "a" and "b" analogs is not particularly meaningful. However, the leading edge of the onset of strong S1 absorption for each "a-b" pair of compounds extrapolates to a very similar wavelength, with each pair distinct from the other two. This reflects the intrinsic electronic similarities between each pair of isomers.

As expected, the additional conjugation of the alkynyl groups of **3a** and **3b** produces a red shift in the onset of absorption and λ_{max} of the S1 absorption band. Compared to the alkyl substituents in compounds **4a** and **4b**, the iodo substituents in **2a** and **2b** induce a red-shift – albeit smaller than that of the alkyne – consistent with a reduction in conjugation length and orbital overlap. The UV–vis

Table 2-A.2. Electronic and optical properties of PTBDFIDs

Polymer	Media	λ_{max} (nm)	HOMO[a] (eV)	LUMO[b] (eV)	E_g^{opt} (eV)[c]	E_g^{EC} (eV)[d]
PT_{out}BDFID	THF	399, 582				
PT_{out}BDFID	Film	403, 612	-5.7	-3.8	1.7	1.9
PT_{in}BDFID	THF	378, 600				
PT_{in}BDFID	Film	415, 653	-5.7	-3.8	1.6	1.9

[a] HOMO= -(E_{onset}^{ox} + 5.1) (eV). [b] LUMO = -(E_{onset}^{red} + 5.1) (eV). [c] Estimated from the optical absorption edge. [d] Onset of potentials (vs Fc).

absorption spectra of **PT_{in}BDFID** and **PT_{out}BDFID** in solution and in thin films are shown in Figure 2-A.1 and the optical and electronic properties are summarized in Table 2-A.2. Both polymers exhibit two main absorption bands. The high-energy bands can be attributed to the π-π* transition, whereas the low energy bands are due to intramolecular charge transfer between the donor and acceptor units. In solution, the λ_{max} of **PT_{in}BDFID**'s low energy band is red-shifted 18 nm relative to **PT_{out}BDFID**, whereas the λ_{max} of **PT_{in}BDFID's** high-energy band is blue-shifted 21 nm relative to **PT_{out}BDFID**. In the solid state, the λ_{max} for the low energy band of **PT_{out}BDFID** is blue-shifted 41 nm relative to **PT_{in}BDFID** and the difference in the high-energy band is only 12 nm. These results suggest that **PT_{out}BDFID** has a more twisted backbone than **PT_{in}BDFID**. The optimized geometries obtained for isoindigo/BDF oligomers calculated using density functional theory also support the notion that **PT_{out}BDFID** has a more twisted structure. The similarity **PT_{out}BDFID's** solution and film spectra indicates the steric interaction between the out facing side chain and the isoindigo group inhibits planarization.

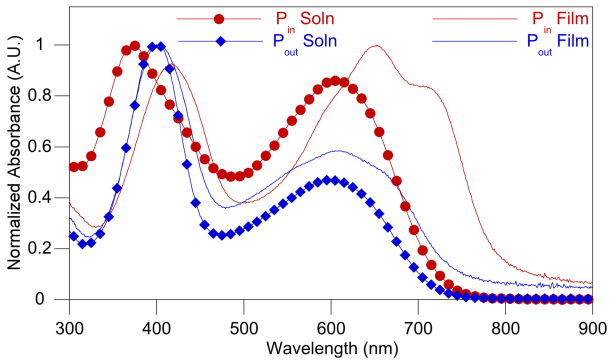

Fig. 2-A.1 UV-vis absorption of the polymers in solution and thin films.

The electrochemical properties of the polymers have been investigated by cyclic voltammetry (CV). Both polymers exhibit measureable and reproducible oxidation and reduction processes. The electrochemical band gaps are both approximately 0.3 eV higher than the optical band gaps (E_g^{opt}) determined via the tangent lines on the absorption spectra. This difference can be attributed to the electron injection barrier in the electrochemistry.[24, 25] The HOMO and LUMO values of both polymers are similar to those reported previously for **PBDT-OIO**, a related terpolymer of **6**, thiophene and BDT (LUMO -3.91 eV and HOMO -5.74 eV).[26] Unfortunately, we cannot arrive at a conclusion regarding the relative donor strength of BDF, as the BDT group had two electron-donating alkoxy groups on the central benzene ring. Although, the LUMO values are less than 0.3 eV lower than those of the $PC_{61}BM$ acceptor, impeding charge transfer the HOMO level of both polymers are deep enough to ensure air stability, while providing for good open-circuit voltage (V_{oc}).[27, 28]

The performance of both polymers in BHJ-PVCs was evaluated using $PC_{61}BM$ as the electron acceptor with a device configuration of indium tin oxide (ITO)/poly(3,4-ethylene dioxythiophene):polystyrene sulfonate (PEDOT:PSS)/polymer: $PC_{61}BM$ (1:4, w/w)/LiF/Al. The active layer processing conditions were chosen to yield a layer thickness less than 100 nm. In general (for P3HT systems), thicker layers (~200 nm) are better, because they absorb more light. However, since new generation donor/acceptor polymer films do not have a long-range order like P3HT, thicker layers

tend to have increased recombination due to hole traps, and thus lower efficiencies.[29] The fabrication conditions and PVC parameters (fill factor (FF), short-circuit current density (J_{sc}) and V_{oc}) are summarized in Table 2-A.3. The current-voltage (*I-V*) characteristics of our devices are shown in Figure 2-A.2.

Overall, **PT_{in}BDFID** PVCs performed better than **PT_{out}BDFID**-based devices in all categories. This is most likely an effect of the polymer's planarity on morphology, and is currently being evaluated further. Although the performance of these devices is lower than other conjugated polymers, this is our first attempt toward fabricating PVCs from these materials. We note that the performance of most new systems can be dramatically improved by the optimization of processing parameters.

Table 2-A.3. Photovoltaic performance of **P12** and **P13** with PCBM

Polymer	**V_{OC} (V)**	**I_{SC} (mA)**	**J_{SC} (mA/cm^2)**	**FF (%)**	**PCE (%)**
P_{in}BDFID	0.7366	0.208	1.66	48.6	0.590
P_{out}BDFID	0.6410	0.164	1.306	36	0.301

*Polymers films were prepared from solutions in *o*-DCB 10 mg/mL.

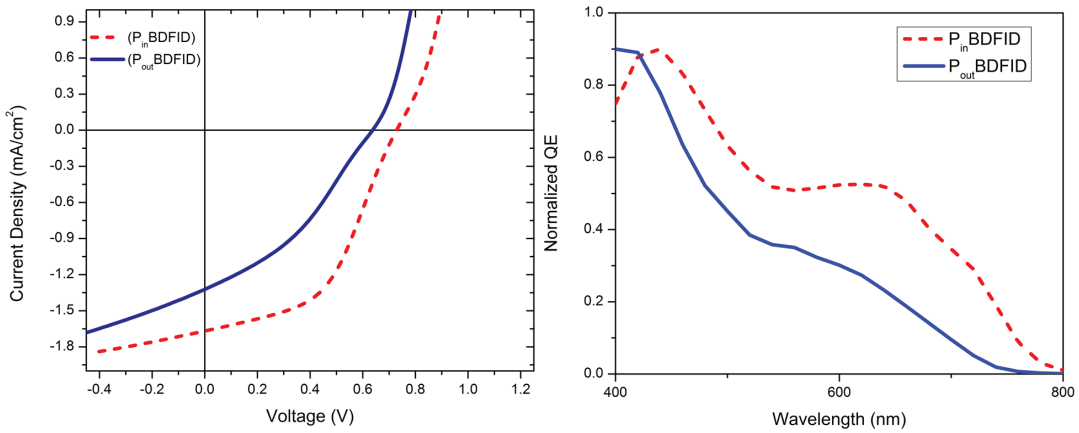

Fig. 2-A.2. Current-voltage characteristics of polymer PVCs (left). Normalized external quantum efficiency vs. wavelength curve of the PVCs (right).

2.A.4 Conclusions

In conclusion, we report the efficient synthesis of novel electron-rich building blocks based on 2,6-di(thiophen-2-yl)benzo[1,2-*b*:4,5-*b*']difurans and their use for the development of donor-acceptor copolymers. The highlights of this work are the overall high yields of the reactions and the versatility of the synthetic approach. The energy levels of the new polymers are suitable for use as donor materials in BHJ-PVCs. Preliminary device studies have shown good V_{oc} and FF, but low overall performance. We are currently working to optimize the device performance in addition to developing new materials based on BDFs.

2.A.5 Supporting Information

2.A.5.1 Device Fabrication and Characterization

All these devices were produced via a solution-based spin-casting fabrication process. All polymers were mixed with PC60BM (Sigma-Aldrich) (mixed 1:4 at 14 mg/mL for polymer and 56 mg/mL for PC60BM) then dissolved in o-dichlorobenzene and magnetically stirred at 60 °C for 48 hours. ITO coated glass slides (Delta Technologies) were cleaned by consecutive 5 minute sonications in (i) isopropanol and acetone, (ii) precision cleaner detergent (dissolved in deionized water), (iii) ethanol and methanol, and then (iv) deionized water. The slides were then dried with nitrogen and cleaned with air plasma (Harrick Scientific plasma cleaner) for 10 minutes. Filtered (0.45μm) PEDOT:PSS (Clevios PTM) was spin-coated onto the prepared substrates (9000 rpm/65 sec) after first being heated and stirred for one hour (80 °C, 1200 rpm). The casted PEDOT:PSS films were then annealed at 48 140 °C for 20 minutes. After cooling, the substrates were transferred to an argon-filled glovebox. After 48 hours of mixing, the Polymer:PCBM solutions were filtered (0.2 μm pore, VWR Scientific) and then stirred for an additional 5 hours at 60 °C . The solutions were heated up to 90 °C approximately 5 minutes prior to spin coating, after which the solutions were dropped onto the PEDOT:PSS-coated substrates by micropipette and spin-cast at 2000 rpm for 45 seconds. The active layer of the films was covered with a petri dish and annealed at 70 °C for 10 minutes. LiF (2 nm) and Al (120 nm) were successively thermally evaporated through a shadow mask under vacuum to complete the devices. J-V data was generated by illuminating the devices using an ETH quartzline lamp at 1 sun (calibrated using a crystalline silicon photodiode with a KG-5 filter).

PART B

INFLUENCE OF HETEROATOMS ON PHOTOVOLTAIC PERFORMANCE OF DONOR-ACCEPTOR COPOLYMERS BASED ON 2,6-DI(THIOPHEN-2-YL)BENZO[1,2-B:4,5-B']DIFURANS AND DIKETOPYRROLOPYRROLE

Polymer Chemistry, 2013, 4, 5329.
DOI: 10.1039/C3PY00138E

Brandon M. Kobilka,[a] **Monique D. Ewan**,[a§]Benjamin J. Hale,[a§] Anton V. Dubrovskiy,[a] Toby L. Nelson,[b] Volodimyr Duzhko[c] and Malika Jeffries-EL[*a]

[a]Department of Chemistry, Iowa State University, Ames, IA 50011
[b]Department of Chemistry, Oklahoma State University, 107 Physical Science I, Stillwater, OK
[c]Department of Polymer Science and Engineering, University of Massachusetts – Amherst, 120 Governors Drive, Conte A529, Amherst, MA 01003-9263, USA
§Both authors contributed equally to this work.

2.B.1 Abstract

Donor–acceptor conjugated polymers based on the novel donor 3,7-didodecyl-2,6-di(thiophen-2-yl)benzo[1,2-*b*:4,5-*b'*]difuran, and either 3,6-di-2-furanyl-1,4-diketopyrrolo[3,4-*c*]pyrrole or 3,6-di-2-thienyl-1,4-diketopyrrolo[3,4-*c*]pyrrole as the acceptor were synthesized via the Stille cross-coupling reaction. The alkyl chains on the diketopyrrolopyrrole monomers were varied to engineer the solubility and morphology of the materials. All of the polymers have similar optoelectronic properties with optical band-gaps of 1.3-1.4 eV, LUMO levels of -3.7 to -3.8 eV and HOMO levels of -5.5 to -5.6 eV. However, the furan containing polymers have much better solubility; as a result they have significantly higher molecular weights. When the polymers were used as donor materials along with $PC_{71}BM$ as the electron-acceptor in bulk-heterojunction photovoltaic cells, power conversion efficiencies of up to 2.9% were obtained, with the furan-containing polymers giving the best results.

2.B.2 Introduction

Since their discovery over 35 years ago, conjugated polymers have evolved from being mere academic curiosities into a booming global enterprise in both academic and industrial labs.[30, 31] These organic semiconductors are being evaluated for use in a range of optoelectronic applications as they offer several advantages over their inorganic counterparts, including the potential to fabricate large-area films using low cost solution processing techniques, to manufacture lightweight and flexible devices and to alter the materials' properties through chemical synthesis.[1, 2, 32, 33] Currently, the synthesis of material comprising alternating electron-donating and electron-accepting moieties is an effective way to alter its optical and electronic properties.[5, 34] Using this approach, a number of materials possessing beneficial properties, such as broad absorption bands, LUMO levels that are appropriately offset from the acceptor, low-lying HOMO levels, and high charge carrier mobilities for use as donor-materials in bulk-heterojunction organic photovoltaic cells (OPVs) have been synthesized. As a result, power conversion efficiencies (PCE)s for polymer OPVs have exceeded

9%.[35-38]

The steady increase in the performance of OPVs over the past few years is a combination of many improvements including the development of new device architectures, the band-gap engineering of the donor materials, and the optimization of film morphology. Early success in the development of devices based on organic semiconductors was first seen with regioregular poly(3-hexylthiophene) (P3HT), which possesses excellent solubility, oxidative stability, and good charge carrier mobility.[39, 40] However, since P3HT has a high-lying HOMO level and a fairly wide band-gap, a number of new thiophene-based materials have been developed in order to address these issues while maintaining high charge carrier mobility. In contrast, furan has not been widely used for the synthesis of conjugated polymers, largely due to the difficulty involved with synthesizing substituted furans. However, furan has several advantages over thiophene making it a promising building block for developing conjugated polymers. For example, furan is isoelectronic to thiophene, but less aromatic, which can facilitate the formation of quiniodal structures, stabilizing the HOMO level.[41] Additionally, furan based polymers have better solubility than their thiophene containing analogs.[10, 42]

Previously, the synthesis of a furan-containing monomer 3,6-di-2-furanyl-1,4-diketopyrrolo[3,4-*c*]pyrrole (FDPP) and its use in polymers has been reported.[10, 13, 43-45] Diketopyrrolopyrrole (DPP) is a strong electron-accepting moiety that can increase the intramolecular charge transfer along the polymer chain and stabilize both the LUMO and HOMO energy levels of the resulting materials. The DPP ring system also has a symmetric coplanar structure that enhances interchain interactions, increasing charge carrier mobility. Since the DPP moiety is a bis-lactam, it is always synthesized between two arenes. Initially, 3,6-di-2-thienyl-

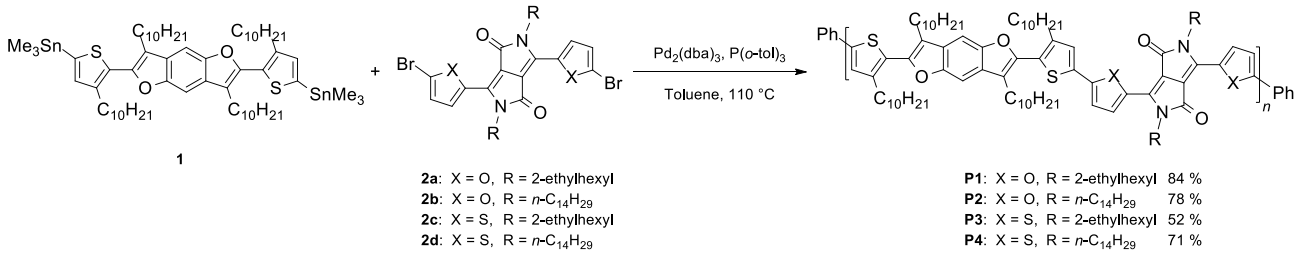

Scheme 2-B.1. Synthesis of copolymers **P1-P4**

1,4-diketopyrrolo[3,4-*c*]pyrrole (TDPP) was widely investigated for the synthesis of narrow band-gap polymers for use in OPVs with PCEs of up to 5.6%.[46] Recently, FDPP-based polymers have been reported that exhibit better solubility than TDPP polymers. The resulting improvement in the film-forming properties has lead to PCEs as high as 6.5%.[43, 47]

At the same time, the electron-donating benzo[1,2-*b*:4,5-*b*′]dithiophene (BDT) moiety has been widely investigated for the synthesis of conjugated polymers. BDT has a planar conjugated structure that facilitates π–π stacking, leading to good charge carrier mobility.[6, 8, 9, 48] As a result, PCEs approaching 8% have been obtained for BDT copolymers.[8, 49] Recently, our group[50] and others[41, 51-55] have investigated the use of the benzo[1,2-*b*:4,5-*b*']difuran (BDF) as a building block for the synthesis of new conjugated polymers. In addition to the positive attributes of BDT, the smaller atomic radius of the oxygen relative to thiophene is expected to reduce steric hindrance between adjacent units, increasing planarity and conjugation.[56] Consequently, BDF-containing conjugated polymers are expected to possess smaller band-gaps than their BDT-containing counterparts.

Based on the aforementioned considerations, we have synthesized four new donor-acceptor copolymers composed of BDF and either FDPP or TDPP. The FDPP monomer

was chosen to compare with the TDPP due to its potential to enhance solubility. The alkyl side chains were varied to further evaluate the trade-off between improved solubility afforded by the branched 2-ethylhexyl chains and enhanced film forming properties of the linear tetradecyl chains. The performance of these materials was evaluated in OPVs to ascertain whether side-chain modification or heteroatom substitution had a greater impact on performance.

2.B.3 Results And Discussion

2.B.3.1 Synthesis and characterization

The synthetic route to the copolymers is illustrated in Scheme 2-B.1. The Stille cross-coupling reaction of benzodifuran **1** and the corresponding DPPs **2a-d** afforded polymers **P1-P4** in good yields (52-84%) after purification by stirring with functionalized silica, followed by Soxhlet extraction. All of the polymers were soluble in common organic solvents, such as THF, chloroform and chlorobenzene at room temperature. The polymers were characterized by ^{1}H NMR and the spectra are in agreement with the expected polymer structures. The molecular weights were estimated using gel permeation chromatography (GPC) at 50 °C using THF as the eluent and the resulting data is summarized in Table 2-B.1. All polymers displayed strong intermolecular interactions in solution leading to aggregation at temperatures below 40 °C during analysis; thus, increasing the run temperatures allowed for the proper measurement of the molecular weight of individual polymer chains. The furan-containing polymers, **P1** and **P2**, showed considerably higher molecular weights but also had better solubilities than their thiophene-containing analogues **P3** and **P4**. This is consistent with the results reported by Fréchet *et al*, where FDPP copolymers exhibited better solubility and higher molecular

weight over those comprising TDPP.[10] In our case, due to synthetic constraints, our two furan-containing copolymers have an equal number of thiophene and furan units. Of these, the polymer bearing branched 2-ethylhexyl side chains, **P1**, had a higher molecular weight than the one bearing linear tetradecyl side chains, **P2**. This trend was also observed in the set of polymers containing only thiophene in the polymer backbone, indicating that the improved solubility within each set is a result of the branched side chains. Interestingly, Fréchet and co-workers also observed that DPP-copolymers with both furan and thiophene in the polymer backbone had higher molecular weights than those containing only furan. This is increase in solubility was also seen in a series of oligomers containing both thiophene and furan.[57, 58] Given the difficulty associated with synthesizing functionalized furans, increasing its content within the polymer backbone would be challenging. However, the previous reports indicate that such efforts may not improve the solubility of the resulting polymer.

Table 2-B.1 Molecular weight and thermal data for **P1-P4**

Polymer	Yield (%)[a]	M_w[b] (kDa)	M_n[b] (kDa)	PDI	DP_n	T_d[c] (°C)
P1	84	55.6	28.9	1.9	40	333
P2	78	44.2	19.9	2.2	29	353
P3	53	24.0	9.5	2.5	17	349
P4	71	8.1	6.1	1.3	5	359

[a] Isolated yield. [b] Molecular weight data was obtained by GPC. [c] 5% weight loss determined by TGA in air.

2.B.3.2 Thermal properties

The thermal properties of the polymers were evaluated using thermal gravimetric analysis (TGA) and differential scanning calorimetry (DSC). TGA results are summarized in Table 1 and indicate that 5 % weight loss onsets occurred between 333-359 °C. DSC did not reveal any observable phase transitions for temperatures up to 200 °C; however, observable melting points were seen for all four polymers above 335 °C. These thermal characteristics are indicative of good stability above the operational temperature threshold of organic photovoltaic devices.

Table 2-B.2 Optical and electronic properties for **P1-P4**

Polymer	λ_{max}^{soln} (nm)	λ_{max}^{film} (nm)	E_g^{opt} [a] (eV)	HOMO [b] (eV)	LUMO [b] (eV)	E_g^{EC} [d] (eV)
P1	658	774, 668	1.4	-5.5	-3.7	1.8
P2	663	739, 668	1.4	-5.5	-3.8	1.7
P3	657	752, 673	1.3	-5.6	-3.8	1.8
P4	671	678	1.4	-5.6	-3.7	1.9

[a] Estimated from the absorption onset of the film. [b] HOMO= -(E_{onset}^{ox} + 5.1) eV. [c] LUMO = -(E_{onset}^{red} + 5.1) eV. [d] E_g^{EC} = LUMO - HOMO.

2.B.3.3 Optical and electrochemical properties

The normalized absorption spectra of **P1-P4** in dilute $CHCl_3$ solution and thin films are shown in Figures 2-B.1 and 2-B.2, respectively, and the optical data is summarized in Table 2-B.2. All four polymers exhibit two distinct absorption bands in both solution and film. The high-energy band is attributable to localized π-π* transitions,

while the broad, low-energy band corresponds to intermolecular charge transfers between the electron-donating and electron-accepting units. In solution, the λ_{max} of both polymers **P1** and **P3** is nearly identical, at 658 nm and 657 nm, respectively. For **P2** and **P4**, the λ_{max} has a slight bathochromic shift, but both polymers exhibit a significant low-energy shoulder that their structural counterparts do not. This shoulder results from the interaction between aggregated polymer backbones, and is thus more abundant in both **P2** and **P4**, which bear linear side chains, than it is in **P3** and **P4** that bear branched side chains.

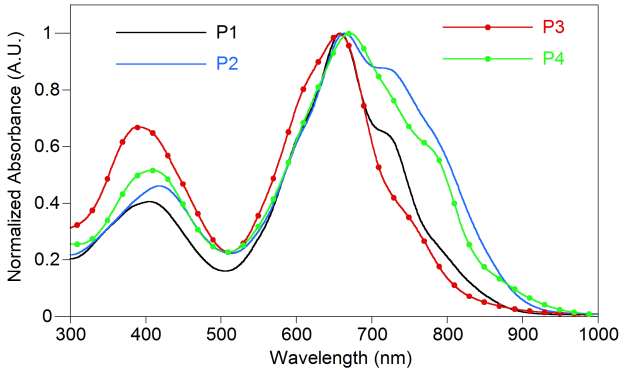

Fig. 2-B.1 UV-Vis absorption of **P1-P4** in solution

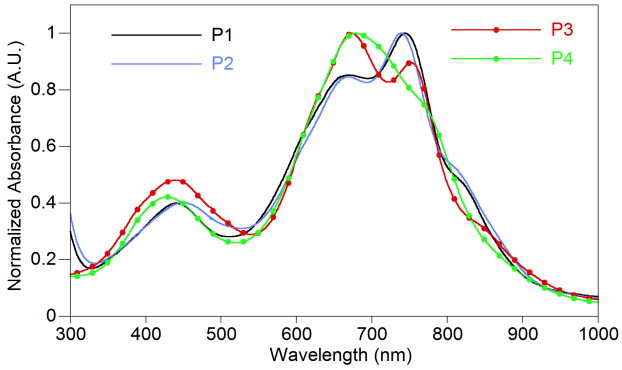

Fig. 2-B.2 UV-Vis absorption of **P1-P4** in film

As thin films, all four polymers display a large bathochromic shift (~100 nm), which suggests stronger molecular interactions or aggregation than in solution. Additionally, all four polymers have optical band-gaps within 0.1 eV of each other, as estimated from the onset wavelength of the film absorption, indicating that effective conjugation was reached in each case. Despite this similarity, the polymers displayed moderate variations in the low energy absorption bands. The furan-containing polymers, **P1** and **P2**, have the most red-shifted absolute λ_{max} at 744 nm and 739 nm, respectively, whereas the thiophene-containing polymer **P3** has only a local λ_{max} in the same region at 752 nm and **P4** only displays a weakly defined shoulder around 750 nm. This data suggests that the presence of this absorption band in **P1** and **P2** correlates well with the higher molecular weights, while its presence diminishes as the molecular weight declines in **P3** and **P4**.

To further elucidate the electrochemical properties of the polymers, the redox behaviour was measured by cyclic voltammetry. All four polymers exhibit measureable and reproducible oxidation and reduction processes. The HOMO and LUMO levels were estimated from the onset of oxidation and reduction using the absolute energy level of ferrocene/ferrocenium (Fc/Fc^{+}) as 5.1 eV under vacuum and are summarized in Table 2. For all four polymers, the HOMO levels ranged between -5.5 to -5.6 eV, deep enough to guarantee good air stability. The LUMO levels ranged from -3.7 to -3.8 eV giving an average electrochemical band-gap of 1.8 ± 0.1eV. These values are statistically similar enough to suggest that replacing the furans in **P1** and **P2** to the thiophenes in **P3** and **P4** has only a minor influence on the electrochemical properties. It is also of note that the optical band-gaps are all estimated to be slightly larger than the electrochemical band-

gap, which correlates well to the expected energy barrier associated with the interface of the polymer film and the electrode surface.[24, 25]

2.B.3.4 Photovoltaic devices

The performance of all four polymers in OPVs was evaluated using [6,6]-phenyl-C_{71}-butyric acid methyl ester ($PC_{71}BM$) as the electron acceptor with a device configuration of indium tin oxide (ITO)/poly(3,4-ethylene dioxythiophene): polystyrene sulfonate (PEDOT:PSS)/polymer:$PC_{71}BM$ (1 : 2, w/w)/LiF/Al. The active layer was deposited from 30 mg/mL *o*-DCB solutions, using processing conditions selected to yield a thickness of about 100 nm. In some cases, analogous devices were prepared using 3% of 1-chloronapthalene (CN) as a high-boiling solvent additive to improve polymer/PCBM blend morphology. The current density-voltage (*J*-*V*) curves of the OPVs are shown in Figure 2-B.2. The resultant photovoltaic performance, including short circuit current density (J_{SC}), open circuit voltage (V_{OC}), fill factor (FF) and power conversion efficiency (PCE) are shown in Table 2-B.3.

Among the devices fabricated without solvent additive, **P2** gave the highest PCE, at 2.77%. Conversely, the **P1**- and **P3**-based devices had somewhat lower efficiencies with respective values of 2.28% and 2.10%. While all three of these polymers gave open circuit voltages of ~0.70 V, **P2** combines superior photocurrent with a good fill factor. This is a result of the polymer's good molecular weights and the presence of linear alkyl chains, which typically results in ideal blends without the addition of additives. Expectantly, the devices fabricated from **P4** performed significantly worse, only returning PCEs of ~1.0 %, a result of decreases in all categories. This outcome is a consequence of the poor solubility and significantly lower molecular weights of **P4**. Due

to these deficiencies, no attempts were made to optimize **P4**'s devices through solvent additives.

We initially evaluated the use of diiodooctane as a solvent additive,[59] but saw no improvement in the PCE. However, when CN was used as a solvent additive,[60] the device performance improved in all cases. The most notable increase was observed in the **P1**-based devices, where the PCE improved to 2.89%, largely due to an increase in the photocurrent. While both the **P2**- and **P3**-based devices also saw an increase in photocurrent, this improvement was less than in the case of **P1**. Accordingly, the **P2**- and **P3**-based devices had much smaller gains in overall PCE.

Table 2-B.3 Photovoltaic device performance of **P1-P4** with PCBM

Polymer	**Additive**	J_{SC} **(mA/cm^2)**	V_{OC} **(V)**	**FF**	**PCE (%)**
P1	none	-5.1	0.70	0.63	2.28
	3% CN	-7.0	0.69	0.60	2.89
P2	none	-7.0	0.66	0.60	2.77
	3% CN	-7.7	0.65	0.57	2.81
P3	none	-6.7	0.67	0.47	2.10
	3% CN	-7.4	0.66	0.47	2.28
P4	none	-4.2	0.59	0.39	0.97

When comparing devices based on the furan-containing polymers **P1** and **P2**, both with identical polymer backbones, the impact that solvent additives can have on blend morphology is made clear. With the 3% CN additive, the devices from **P2** experienced a

negligible improvement in PCE (+0.04%); however, **P1**-based devices consistently gave better efficiencies with the CN additive. Thus, solvent additives have the potential to neutralize morphological defects resulting from the use of branched side chains. Arguably, this effect is not as pronounced in the devices based on **P3** where reduced molecular weights lead to poorer film morphologies that cannot be overcome.

Since all four polymers show similar optical and electronic properties, factors related to morphology and charge carrier mobility play a larger role in overall device performance. Again, these crucial device characteristics appear to coincide with higher molecular weights.

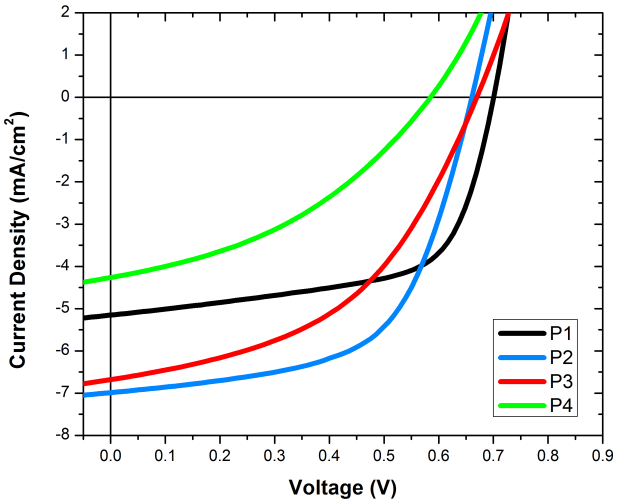

Fig. 2-B.3. Current-voltage characteristics **P1**-**P4**-based OPVs without solvent additives.

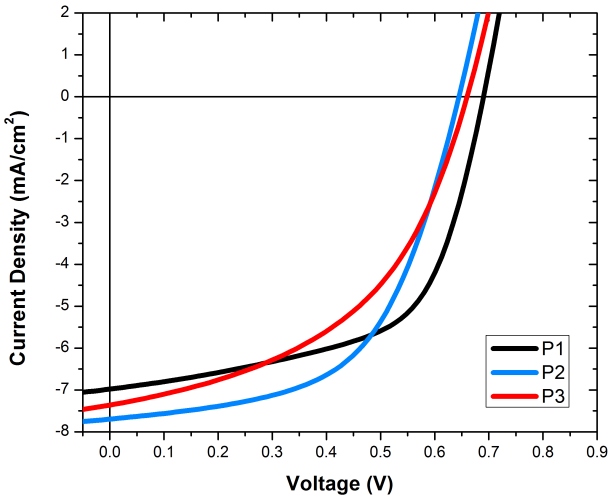

Fig. 2-B.4. Current-voltage characteristics for **P1**-**P3**-based OPVs using 3% CN as a solvent additive.

2.B.4 Conclusions

A related series of new donor-acceptor copolymers based on diketopyrrolopyrrole and 2,6-di(thiophen-2-yl)benzo[1,2-b:4,5-b']difuran have been synthesized. The substitution of the DPP monomer has been modified to bear all possible combinations of either thiophene or furan, and branched 2-ethylhexyl or linear tetradecyl alkyl chains. All four polymers displayed similar optoelectronic properties with an estimated average HOMOs of -5.6 eV, LUMOs of -3.8 eV and optical band-gaps of around 1.4 eV. Despite these similarities, the polymers displayed varied molecular weights due to the aforementioned modifications to the DPP unit. The furan-containing polymers **P1** and **P2** achieved higher molecular weights than either of the thiophene-containing analogues. Likewise, the branched side chains afforded greater solubility than did the linear side chains. Interestingly, when OPVs were fabricated from the polymers, those based on **P2**

exhibited the best PCE (~3%) owing to the presence of linear side chains. Devices from **P1** were able to achieve comparable efficiencies to the **P2** devices through the use of solvent additives. However, devices based on **P3** and **P4** achieved maximum efficiencies of only ~2.3% and 1.0%, respectively, due to poor solubility. These results further demonstrate that incorporating furan into polymer backbones typically dominated by thiophene can vastly improve solubility and molecular weights eliminating the need for large, branched alkyl side chains. These fundamental improvements are integral to the creation of new, high-efficiency OPVs by enhancing both film morphology and charge-carrier mobility.

2.B.5 Supporting Information

2.B.5.1 Fabrication of photovoltaic devices

All devices were produced via a solution-based, spin-casting fabrication process. All polymers were mixed with $PC_{71}BM$ (SES Research) (mixed 1:2 with a total solution concentration of 30 mg/mL for $PC_{71}BM$) then dissolved in *o*-dichlorobenzene and stirred at 95°C for 48 hours. ITO coated glass slides (Delta Technologies) were cleaned by consecutive 10 minute sonications in (i) Mucasol™ detergent (dissolved in deionized water), 2x, (ii) deionized water, (iii) acetone, and then (iv) isopropanol. The slides were then dried in an oven for at least 3 hours and cleaned with air plasma (Harrick Scientific plasma cleaner) for 10 minutes. Filtered (0.45 μm) PEDOT:PSS (Clevios P™) was spin-coated onto the prepared substrates (2000 rpm/60 sec) after first being stirred for 10 minutes at room temperature. The PEDOT:PSS films were annealed at 150 °C for 30 minutes. After cooling, the substrates were transferred to an argon-filled glovebox. After 48 hours of mixing, the polymer:PCBM solutions were filtered (0.45 μm pore, GS-Tek) and simultaneously dropped onto the PEDOT:PSS-coated substrates and spin-cast at 1000 rpm for 120 seconds. The films were dried under vacuum overnight. LiF (1 nm) and Al (100 nm) were successively thermally evaporated through a shadow mask under vacuum to complete the devices. *J-V* data was generated by illuminating the devices using an ETH quartzline lamp at 1 sun (calibrated using a crystalline silicon photodiode with a KG-5 filter).

2.C REFERENCES

1. Facchetti, A., *Chem. Mater.* **2010,** *23* (3), 733-758.
2. Grimsdale, A. C.; Leok Chan, K.; Martin, R. E.; Jokisz, P. G.; Holmes, A. B., *Chem. Rev.* **2009,** *109* (3), 897-1091.
3. Cheng, Y.-J.; Yang, S.-H.; Hsu, C.-S., *Chem. Rev.* **2009,** *109* (11), 5868-5923.
4. Havinga, E. E.; Hoeve, W.; Wynberg, H., *Polym. Bull.* **1992,** *29* (1), 119-126.
5. Havinga, E. E.; ten Hoeve, W.; Wynberg, H., *Synth. Met.* **1993,** *55* (1), 299-306.
6. Hou, J.; Park, M.-H.; Zhang, S.; Yao, Y.; Chen, L.-M.; Li, J.-H.; Yang, Y., *Macromolecules* **2008,** *41* (16), 6012-6018.
7. Sista, P.; Biewer, M. C.; Stefan, M. C., *Macromol. Rapid Comm.* **2012,** *33* (1), 9-20.
8. Liang, Y.; Xu, Z.; Xia, J.; Tsai, S.-T.; Wu, Y.; Li, G.; Ray, C.; Yu, L., *Adv. Mater.* **2010,** *22* (20), E135-E138.
9. Najari, A.; Beaupré, S.; Berrouard, P.; Zou, Y.; Pouliot, J.-R.; Lepage-Pérusse, C.; Leclerc, M., *Adv. Funct. Mater.* **2011,** *21* (4), 718-728.
10. Woo, C. H.; Beaujuge, P. M.; Holcombe, T. W.; Lee, O. P.; Fréchet, J. M. J., *J. Am. Chem. Soc.* **2010,** *132* (44), 15547-15549.
11. Peart, P. A.; Tovar, J. D., *Macromolecules* **2009,** *42* (13), 4449-4455.
12. Li, H.; Tang, P.; Zhao, Y.; Liu, S.-X.; Aeschi, Y.; Deng, L.; Braun, J.; Zhao, B.; Liu, Y.; Tan, S.; Meier, W.; Decurtins, S., *J. Poly. Sci. A.* **2012,** *50* (14), 2935–2943.
13. Bijleveld, J. C.; Karsten, B. P.; Mathijssen, S. G. J.; Wienk, M. M.; de Leeuw, D. M.; Janssen, R. A. J., *J. Mater. Chem.* **2011,** *21* (5), 1600-1606.
14. Hosmane, R. S.; Liebman, J. F., *Tetrahedron Lett.* **1992,** *33* (17), 2303-2306.
15. Liang, Z.; Ma, S.; Yu, J.; Xu, R., *J. Org. Chem.* **2007,** *72* (24), 9219-9224.
16. Huo, L.; Huang, Y.; Fan, B.; Guo, X.; Jing, Y.; Zhang, M.; Li, Y.; Hou, J., *Chem. Commun.* **2012,** *48* (27), 3318-3320.
17. Yi, C.; Blum, C.; Lehmann, M.; Keller, S.; Liu, S.-X.; Frei, G.; Neels, A.; Hauser, J.; Schürch, S.; Decurtins, S., *J. Org. Chem.* **2010,** *75* (10), 3350-3357.
18. Tsuji, H.; Mitsui, C.; Ilies, L.; Sato, Y.; Nakamura, E., *J. Am. Chem. Soc.* **2007,** *129* (39), 11902-11903.
19. Keller, S.; Yi, C.; Li, C.; Liu, S.-X.; Blum, C.; Frei, G.; Sereda, O.; Neels, A.; Wandlowski, T.; Decurtins, S., *Org. Biomol. Chem.* **2011,** *9* (18), 6410-6416.
20. Yue, D.; Yao, T.; Larock, R. C., *J. Org. Chem.* **2005,** *70* (25), 10292-10296.
21. Stalder, R.; Mei, J.; Reynolds, J. R., *Macromolecules* **2010,** *43* (20), 8348-8352.
22. Wang, E.; Ma, Z.; Zhang, Z.; Vandewal, K.; Henriksson, P.; Inganàs, O.; Zhang, F.; Andersson, M. R., *J. Am. Chem. Soc.* **2011,** *133* (36), 14244-14247.
23. Lei, T.; Cao, Y.; Fan, Y.; Liu, C.-J.; Yuan, S.-C.; Pei, J., *J. Am. Chem. Soc.* **2011,** *133* (16), 6099-6101.
24. Cardona, C. M.; Li, W.; Kaifer, A. E.; Stockdale, D.; Bazan, G. C., *Adv. Mater.* **2011,** *23* (20), 2367-2371.
25. Zhu, Y.; Champion, R. D.; Jenekhe, S. A., *Macromolecules* **2006,** *39* (25), 8712-8719.
26. Ma, Z.; Wang, E.; Jarvid, M. E.; Henriksson, P.; Inganas, O.; Zhang, F.; Andersson, M. R., *J. Mater. Chem.* **2012,** *22* (5), 2306-2314.

27. Thompson, B. C.; Kim, Y.-G.; Reynolds, J. R., *Macromolecules* **2005,** *38* (13), 5359-5362.
28. Scharber, M.; Mühlbacher, D.; Koppe, M.; Denk, P.; Waldauf, C.; Heeger, A.; Brabec, C., *Adv. Mater.* **2006,** *18* (6), 789-794.
29. Beiley, Z. M.; Hoke, E. T.; Noriega, R.; Dacuña, J.; Burkhard, G. F.; Bartelt, J. A.; Salleo, A.; Toney, M. F.; McGehee, M. D., *Adv. Energy Mater.* **2011,** *1* (5), 954-962.
30. Service, R. F., *Science* **2011,** *332* (6027), 293.
31. Nelson, J., *Materials Today* **2011,** *14* (10), 462-470.
32. Thomas, S. W., III; Joly, G. D.; Swager, T. M., *Chem. Rev.* **2007,** *107* (4), 1339-1386.
33. Thompson, B. C.; Frechet, J. M. J., *Angew. Chem. Int. Ed. Engl.* **2008,** *47* (1), 58-77.
34. Havinga, E. E.; ten Hoeve, W.; Wynberg, H., *Polym. Bull.* **1992,** *29* (1), 119-126.
35. He, Z.; Zhong, C.; Su, S.; Xu, M.; Wu, H.; Cao, Y., *Nat Photon* **2012,** *6* (9), 591-595.
36. He, Z.; Zhong, C.; Huang, X.; Wong, W.-Y.; Wu, H.; Chen, L.; Su, S.; Cao, Y., *Advanced Materials* **2011,** *23* (40), 4636-4643.
37. Small, C. E.; Chen, S.; Subbiah, J.; Amb, C. M.; Tsang, S.-W.; Lai, T.-H.; Reynolds, J. R.; So, F., *Nat. Photonics* **2012,** *6* (2), 115-120.
38. Li, X.; Choy, W. C. H.; Huo, L.; Xie, F.; Sha, W. E. I.; Ding, B.; Guo, X.; Li, Y.; Hou, J.; You, J.; Yang, Y., *Adv. Mater.* **2012,** *24* (22), 3046-3052.
39. McCullough, R. D.; Lowe, R. D.; Jayaraman, M.; Anderson, D. L., *J. Org. Chem.* **1993,** *58* (4), 904-912.
40. Jeffries-El, M.; McCullough, R. D., Regioregular polythiophene. In *Handbook of Conducting Polymers*, 3rd ed / edited by Terje A. Skotheim and John Reynolds. ed.; Skotheim, T. A., Reynolds, John R., Ed. London: Boca Raton, Fla, 2007; pp 331-380.
41. Huo, L.; Huang, Y.; Fan, B.; Guo, X.; Jing, Y.; Zhang, M.; Li, Y.; Hou, J., *Chem. Commun.* **2012,** *48* (27), 3318-3320.
42. Gidron, O.; Diskin-Posner, Y.; Bendikov, M., *J. Am. Chem. Soc.* **2010,** *132* (7), 2148-2150.
43. Yiu, A. T.; Beaujuge, P. M.; Lee, O. P.; Woo, C. H.; Toney, M. F.; Fréchet, J. M. J., *J. Am. Chem. Soc.* **2011,** *134* (4), 2180-2185.
44. Sonar, P.; Foong, T. R. B.; Singh, S. P.; Li, Y.; Dodabalapur, A., *Chem. Commun.* **2012,** *48* (67), 8383-8385.
45. Sonar, P.; Singh, S. P.; Williams, E. L.; Li, Y.; Soh, M. S.; Dodabalapur, A., *J. Mater. Chem.* **2012,** *22* (10), 4425-4435.
46. Bijleveld, J. C.; Gevaerts, V. S.; Di Nuzzo, D.; Turbiez, M.; Mathijssen, S. G. J.; de Leeuw, D. M.; Wienk, M. M.; Janssen, R. A. J., *Adv. Mater.* **2010,** *22* (35), E242-E246.
47. Yuan, J.; Huang, X.; Zhang, F.; Lu, J.; Zhai, Z.; Di, C.; Jiang, Z.; Ma, W., *J. Mater. Chem.* **2012,** *22* (42), 22734-22742.
48. Toba, M.; Nakashima, T.; Kawai, T., *J. Poly. Sci. A.* **2011,** *49* (8), 1895-1906.
49. Chen, H.-Y.; Hou, J.; Zhang, S.; Liang, Y.; Yang, G.; Yang, Y.; Yu, L.; Wu, Y.; Li, G., *Nat. Photonics* **2009,** *3* (11), 649-653.
50. Kobilka, B. M.; Dubrovskiy, A. V.; Ewan, M. D.; Tomlinson, A. L.; Larock, R. C.; Chaudhary, S.; Jeffries-El, M., *Chem. Commun.* **2012,** *48* (71), 8919-8921.

51. Sista, P.; Huang, P.; Gunathilake, S. S.; Bhatt, M. P.; Kularatne, R. S.; Stefan, M. C.; Biewer, M. C., *J. Poly. Sci. A.* **2012,** *50* (20), 4316-4324.
52. Hu, C.; Fu, Y.; Li, S.; Xie, Z.; Zhang, Q., *Polym. Chem.* **2012,** *3* (10), 2949-2955.
53. Chen, X.; Liu, B.; Zou, Y.; Xiao, L.; Guo, X.; He, Y.; Li, Y., *J. Mater. Chem.* **2012,** *22* (34), 17724-17731.
54. Liu, B.; Chen, X.; Zou, Y.; He, Y.; Xiao, L.; Xu, X.; Li, L.; Li, Y., *Polym. Chem.* **2013,** *4* (3), 470-476.
55. Liu, B.; Chen, X.; Zou, Y.; Xiao, L.; Xu, X.; He, Y.; Li, L.; Li, Y., *Macromolecules* **2012,** *45* (17), 6898-6905.
56. Bunz, U. H. F., *Angew, Chem. Int. Ed.* **2010,** *49* (30), 5037-5040.
57. Hucke, A.; Cava, M. P., *J. Org. Chem.* **1998,** *63* (21), 7413-7417.
58. Miyata, Y.; Nishinaga, T.; Komatsu, K., *J. Org. Chem.* **2005,** *70* (4), 1147-1153.
59. Lee, J. K.; Ma, W. L.; Brabec, C. J.; Yuen, J.; Moon, J. S.; Kim, J. Y.; Lee, K.; Bazan, G. C.; Heeger, A. J., *Journal of the American Chemical Society* **2008,** *130* (11), 3619-3623.
60. Peet, J.; Kim, J. Y.; Coates, N. E.; Ma, W. L.; Moses, D.; Heeger, A. J.; Bazan, G. C., *Nat. Mater.* **2007,** *6* (7), 497-500.

CHAPTER 3

THE EFFECT OF HETEROATOM SUBSTITUTION ON THE SOLAR CELL PERFORMANCE OF COPOLYMERS BASED ON TWO DIMENSIONAL BENZO[1,2-B:4,5-B']DIFURAN-BASED DONOR-ACCEPTOR

Monique D. Ewan, Brandon M. Kobilka and Malika Jeffries-EL*

Department of Chemistry, Iowa State University, Ames, IA 50011

3.1 Abstract

A series of donor-acceptor copolymers based on two-dimensional benzo[1,2-*b*'4,5-*b*']difuran (BDF) and either benzothiadiazole (BT) or benzoselenadiazole (BSe) were synthesized by Stille cross-coupling reactions in order to evaluate the effect of the heteroatom substitution on the properties of the resulting polymers. The performance of the polymers as an active layer donor material in solar cells was evaluated. The BT based polymer obtained the better solar cell performance with a power conversion efficiency of 1.03%.

3.2 Introduction

The recent years have seen an incredible increase in the performance of bulk heterojunction solar cells. Through these improvements organic solar cells have become closer to being a viable replacement for their inorganic counterparts due to their cheaper production costs and abilities to be used in flexible substrates[1-5]. Another major advantage of organic solar cells is the ability to fine-tune the energy levels of the their

active materials. This is readily accomplished trough the use of donor – acceptor (D-A) polymers, which also enable tuning of the materials, bandgaps, charge carrier mobility and film morphology [6-10]. To date, D-A conjugated polymers have been used as a active components in OSC and have resulted in some of the highest reported power conversion efficiencies (PCEs) for this field[11-14].

There have been a lot of studies done to examine the effect of replacing sulfur (S) with selenium (Se) within the aromatic rings of conjugated polymers[15-18]. The replacement of sulfur with selenium tends to induce a redshift in the absorption spectrum[19, 20]. This is because, even though it is isoelectronic with sulfur, the selenium atom is much larger in size and is less electronegative than sulfur[21, 22]. Therefore, selenium-containing polymers are expected to be more effective than sulfur at extending the absorption spectrum towards the infrared region. Selenium is also more polarizable than sulfur, and therefore polymers experience Se-Se lone pair interactions and can achieve high charge carrier mobilities[23].

Benzothiadiazole (BT) has been widely used as an electron acceptor unit in high efficiency D-A copolymers[24-26]. Recently, there have been efforts to replace the sulfur with selenium[17, 27, 28] to yield benzoselenadiazole (BSe). However, there has not been a lot of work in this area and therefore there still remains a need to compare the properties anaogous copolymers to get a more in depth understanding of the effects of selenium substitution[17].

The synthesis of two-dimensional (2-D) conjugated polymers is another way to improve the performance of organic semiconductors in bulk heterojunction solar cells. Here, functionalized aromatic groups are used as side chains instead of the usual alkyl or

alkoxy substitutions[29]. This provides the advantage of broader UV-Vis absorption due to the increased conjugation from the aromatic side chains[30, 31]. Additionally, 2-D systems show a greater planarization, which leads to improved π- π interactions and higher hole mobilities[32]. The area of 2-D polymers also needs to be further explored. Some of the current polymers are based on the donor-type molecule benzo[1,2-*b*'4,5-*b*']dithiophene (BDT) and benzo[1,2-*b*'4,5-*b*']difuran (BDF), where the aromatic side chains are on the 4 and 8 positions of the molecule[33-36]. However, only a few groups have evaluated the impact of 2-D conjugation on BDT in the 3 and 7 positions[37] , and no one has looked at this effect in BDF. In this work we report the synthesis of copolymers based on 2-D BDF and BT or BSe comonomers.

3.3 Results and Discussion

3.3.1 Synthesis and characterization

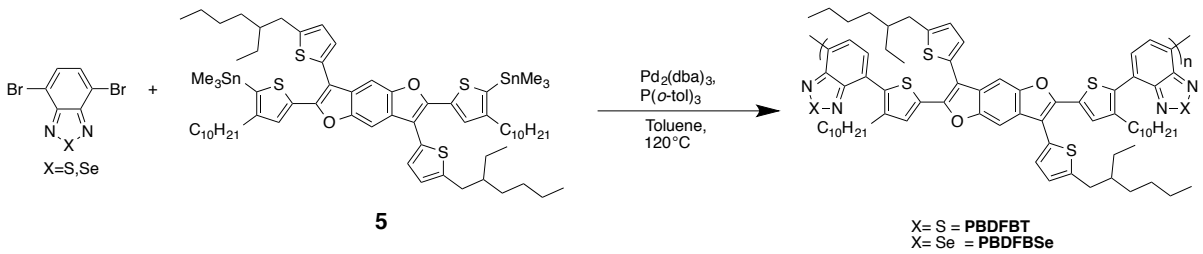

Scheme 3-1

The synthetic route for the benzo[1,2-*b:4,5*-b']difuran-based polymers is depicted in Scheme 3-1. Compound **5** was synthesized according to our group procedure, while Compounds **2** and **4** were synthesized according to literature procedures. The polymerizations were carried out by Stille cross-coupling of either monomer **2** or **4** with the 2-D BDF monomer to produce polymers **PBDFBT** and **PBDFBSe**. This polymerization was followed by Sohxlet extraction with acetone, methanol, hexanes and

chloroform followed by stirring with functionalized silica, and precipitation into methanol. Both polymers were soluble in common organic solvents such as THF and chloroform at room temperature. The molecular weights of the polymers were estimated using gel permeation chromatography (GPC) at 40 °C using $CHCl_3$ as the eluent and the resulting data is summarized in Table 3-1.**PBDFBSe** had a higher molecular weight (M_w) relative to **PBDFBT** and also a lower polydispersity index (PDI). Overall molecular weights were low and the degrees of polymerization were 6 and 7 for **PBDFBT** and **PBDFBSe** respectively.

Table 3-1. Molecular weight data for polymers

Polymer	M_w (kDa)	M_n (kDa)	PDI	DP_n
PBDFBT	12.7	8.0	1.6	6
PBDFBSe	15.3	10.0	1.5	7

3.3.2 Optical Properties

Normalized UV-Vis absorption spectra of the copolymers in dilute chloroform solutions and as solid thin films on glass substrates are shown in Figures 3-1 and 3-2. The absorption spectra of the polymers were similar and contained two major absorption bands. The higher energy peak is attributed to the π- π* transition of the main chains[38, 39]. The lowest energy peak at the longer wavelength is attributed to the strong intramolecular charge transfer typical of D-A copolymers[40]. In solution the λ_{max} of **PBDFBSe** low

energy band is red-shifted 29 nm relative to **PBDFBT** and also red-shifted 5 nm for the higher energy band. In the solid state, the λ_{max} for the lower energy band of **PBDFBSe** is 3 nm red-shifted relative to **PBDFBT**. However, the higher energy band was blue-shifted by 8 nm relative to **PBDFBT**. Going from solution to solid state, a larger redshift (~ 41 nm) was observed for PBDFBT film than for the **PBDFBSe**. This suggests that the **PBDFBT** polymer may have stronger interactions between polymer chains than **PBDFBSe** in the solid state[41]. The estimated optical band gaps were identical for both polymers.

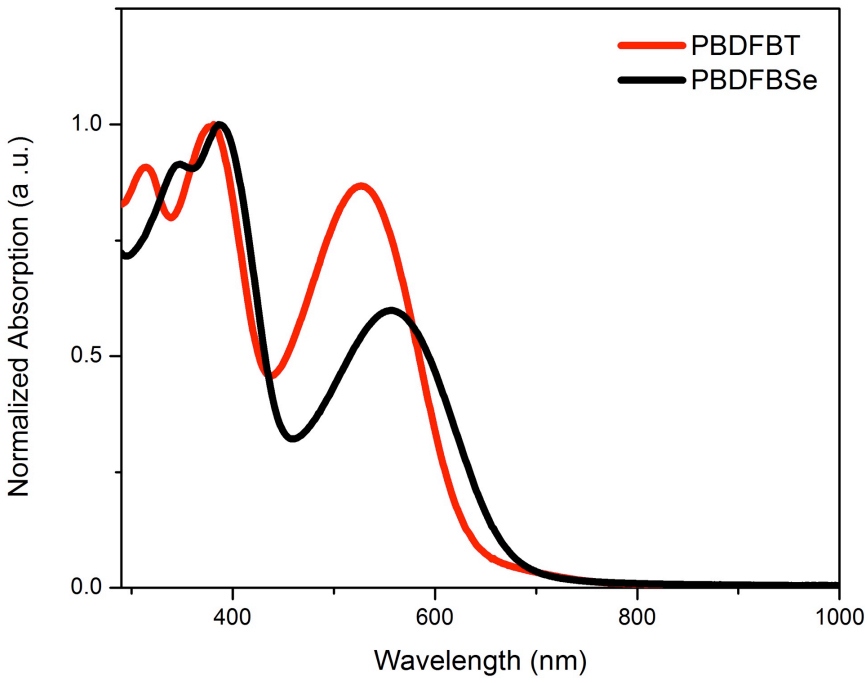

Figure 3-1. Normalized UV-Vis absorption spectra of the polymers in chloroform solution

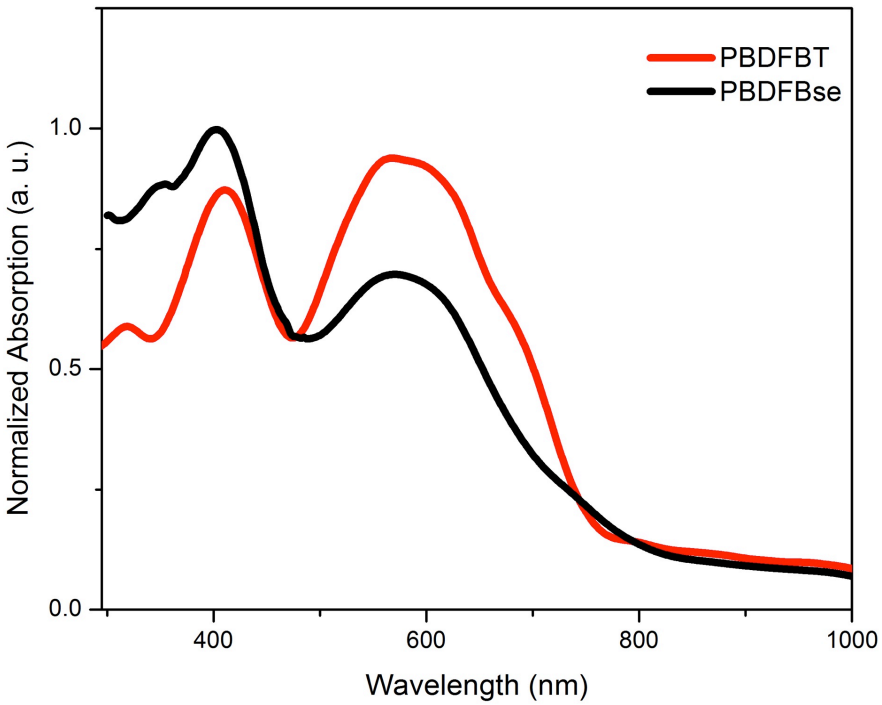

Figure 3-2. Normalized UV-Vis absorption spectra of polymer thin films

Table 3-2. Optoelectronic properties of polymers

Polymer	λ_{max}, soln (nm)	λ_{max}, film (nm)	E_g^{opt} (eV)	HOMO (eV)	LUMO (eV)	E_g^{EC} (eV)
PBDFBT	314,381,527	319,411,568	1.6	-5.5	-3.6	1.9
PBDFBSe	347,386,556	355,403,571	1.6	-5.5	-3.5	2.0

3.3.3 Electrochemical properties

Cyclic voltammetry (CV) was employed to investigate the redox behavior of the polymers and to estimate their HOMO and LUMO levels. These HOMO/LUMO levels were estimated from the onset of oxidation and reduction using ferrocene/ferrocenium (Fc/Fc+) as 4.8 eV under vacuum and are summarized in Table 3-2. Both polymers exhibit measurable oxidation and reduction processes. The electrochemical bandgaps are approximate 0.3 – 0.4 eV larger than the optical bandgaps. This difference is attributed to the electron injection barrier in electrochemistry[42]. The HOMO levels were identical at -5.5 eV, and are deep enough to ensure air stability[43]. PBDFBT had a slightly lower LUMO of -3.6 eV compared to -3.5 for **PBDFBS**e. As a result, it had the smaller electrochemical bandgap. It is important to note that with the errors associated with CV, this difference might be negligible. The LUMO levels of the polymers are all 0.3 eV greater than that for PCBM (-3.9 eV), which provides enough driving force for charge separation and transfer [43].

5.3.4 Evaluation of Photovoltaic Properties

The performance of all two polymers in OPVs was evaluated using $PC_{71}BM$ as the electron acceptor with a device configuration of ITO/PEDOT:PSS/polymer:PBCM (1:2), w/w)/Ca/Al. The active layer processing conditions were chosen so that the thickness of the active layer blend was ~100 nm. The solar cell performances are summarized in Table 3-3. The current density- voltage (J-V) characteristics of the devices

are shown in Figures 3-3 and 3-4. **PBDFBT** had better solar cell performances relative to **PBDFBSe**. This could be due to the fact that it showed a stronger absorbance in the longer wavelength range. Also, because PBDFBT showed more of a redshift going from solution to film, it is possible that the film morphology of PBDFBT in active layer was better, promoting better charge transport. In the solar cell devices, it produced a much higher V_{OC}, as well as a higher current and a slightly higher FF.

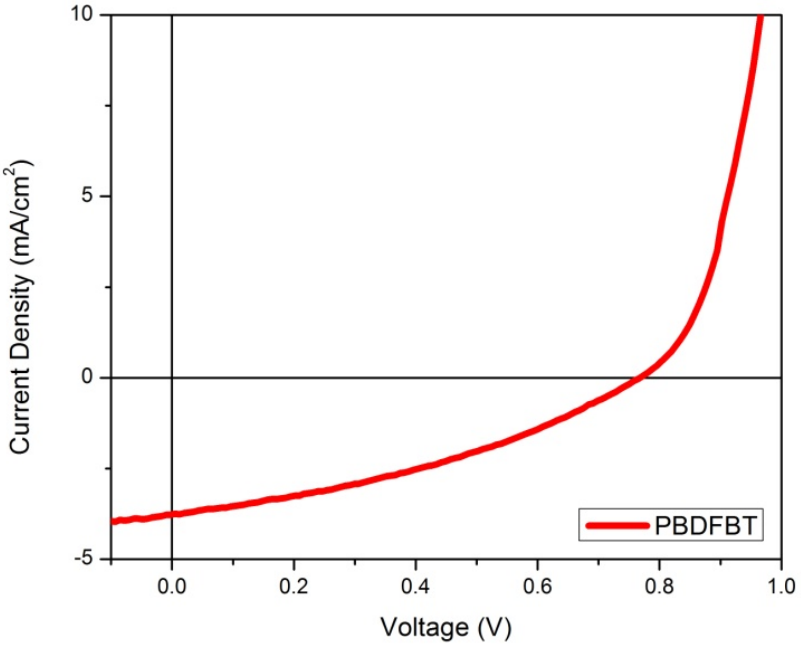

Figure 3-3. J-V curve for PBDFBT polymer

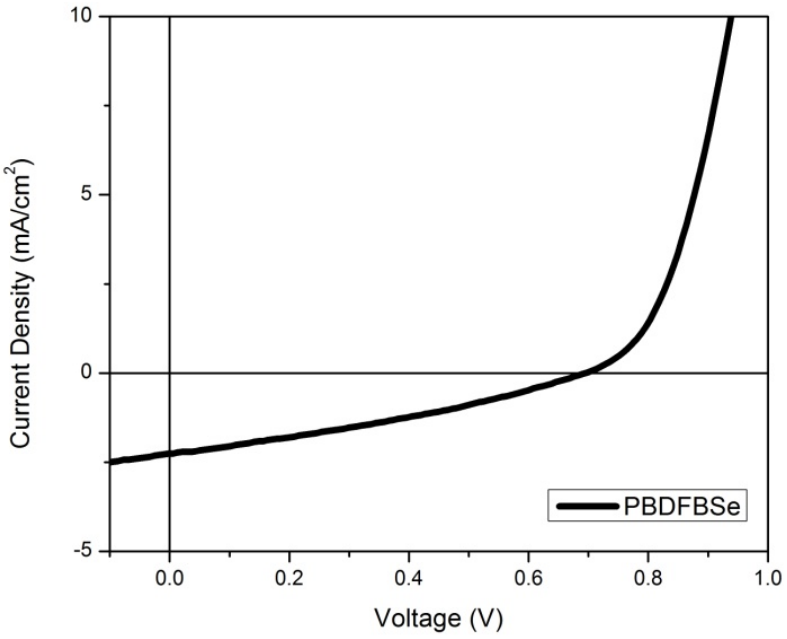

Figure 3-4. J-V curve for PBDFBSe polymer

Table 3-3.Photovoltaic properties of the OSCs based on the two copolymers

Polymer	Polymer: PCBM ratio	V_{OC} (V)	J_{SC} (mA/cm^2)	FF (%)	PCE (%)
PBDFBT	1:3	0.76	3.78	35.8	1.03
PBDFBSe	1:2	0.69	2.27	31.6	0.49

3. 4 Conclusions

A new series of conjugated copolymers based on BT or BSe with two dimensional benzo[1,2-b:4,5-b']difuran were synthesized. The position of the thienyl side

chains were on the, relatively unexplored, 3 and 7 positions of the BDF core. The resulting polymers had similar electronic but slightly different optical properties. The photovoltaic performances, overall, were low. However, we were able to ascertain that, for this polymer series, the BT analogue had a distinctly better performance. More work needs to be done to evaluate the morphology of the films, using atomic force microscopy (AFM) as well as to reproduce the polymers with higher molecular weights.

3. 5 Experimental

3.5.1 Materials and General Experimental Details.

Toluene was dried using an Innovative Technologies solvent purification system. Air and moisture sensitive reactions were performed using standard Schlenk techniques. Solvents used for palladium-catalyzed reactions were deoxygenated prior to use by bubbling a stream of argon through the solvent with vigorous stirring for approximately 60 minutes. All chemical reagents were purchased from commercial sources and used without further purification unless otherwise noted. SiliaMetS® Cysteine was purchased from SiliCycle, Inc. 4,7 dibromobenzo[*c*][1,2,5]thiadiazole (**2**), 3,6-dibromobenzene-1,2-diamine (**3**) and 4,7 dibromobenzo[*c*][1,2,5]thiadiazole (**4**) were synthesized according to literature procedures. Nuclear magnetic resonance (NMR) spectra were carried out in $CDCl_3$ and recorded on Varian MR (400 MHz) or a Bruker Advance-III (600 MHz). ^1H NMR spectra were internally referenced to the residual protonated solvent peak. In all spectra, chemical shifts are given in ppm (δ) relative to the solvent. Gel permeation chromatography (GPC) measurements were performed on a separation module equipped with two 10 μm AMGPC-gel columns (cross-linked styrene-divinyl benzene copolymer) connected in series (guard, 10,000 Å, 1,000 Å) with a UV-Vis detector. Analyses were

performed at 40 °C temperature using chloroform as the eluent with a flow rate of 1.0 mL min^{-1}. Calibration was based on polystyrene standards. Cyclic voltammetry was performed using a e-DAQ e-corder 410 potentiostat with a scanning rate of 100 mV s^{-1}. The polymer solutions (1-2 mg mL^{-1}) were drop-cast onto a platinum electrode. Ag/Ag^+ was used as the reference electrode and a platinum wire as the auxiliary electrode. The reported values are referenced to Fc/Fc^+ (-4.8 eV versus vacuum). All electrochemistry experiments were performed in deoxygenated CH_3CN under an argon atmosphere using 0.1 M tetrabutylammonium hexafluorophosphate as the electrolyte. Absorption spectra were obtained on a photodiode-array Agilent 8453 UV-visible spectrophotometer using polymer solutions in $CHCl_3$ and thin films. The films were made by spin-coating 25 x 25 x 1 mm glass slides using solutions of polymer (2 mg/mL) in $CHCl_3$ at a spin rate of 1200 rpm on a Headway Research, Inc. PWM32 spin-coater.

3.5.2 General Polymerization Procedure.

To a stirred, deoxygenated solution of bisstannane (**5**) and either **2** or **4** in 10 mL of toluene was added $Pd_2(dba)_3$ (2 mol %) and tri(o-tolyl)phosphine (8 mol %). The reaction mixture was heated to reflux, under argon, and stirred for 12-36 hours. The polymer was end-capped by the addition of an excess amount of trimethyl(phenyl)tin and iodobenzene, each followed by a 4 hour period of reflux. The reaction mixture was cooled to 50 °C and diluted with chloroform. A small portion of SiliaMetS® Cysteine was added and the reaction mixture was stirred for 8 hours followed by precipitation into cold methanol and filtration. The polymer was purified via Soxhlet extraction by subsequently rinsing with methanol, acetone and hexanes and finally extracted with

chloroform. Most of the chloroform was removed in vacuo and the polymer was precipitated into methanol, collected by filtration and dried in vacuo.

Poly(4,4'-((3,7-bis(5-(2-ethylhexyl)thiophen-2-yl)benzo[1,2-*b*:4,5-*b'*]difuran-2,6-diyl)bis(3-decylthiophene-5,2-diyl))bis(benzo[*c*][1,2,5]thiadiazole))(PBDFBT).

Polymer was obtained as purple solid from **5** and **2**; GPC: M_n =8.0 kDa, M_w = 12.7 kDa, PDI = 1.6.

Poly(4,4'-((3,7-bis(5-(2-ethylhexyl)thiophen-2-yl)benzo[1,2-*b*:4,5-*b'*]difuran-2,6-diyl)bis(3-decylthiophene-5,2-diyl))bis(benzo[*c*][1,2,5]selenadiazole))(PBDFBSe).

Polymer obtained as a dark purple solid (275 mg, 83% yield) from **5** and **4**; GPC: M_n = 10.0 kDa, M_w = 15.3 kDa, PDI = 1.5.

3.5.3 Device Fabrication and Characterization.

All polymers were mixed with $PC_{71}BM$ (mixed at a 1:2 weight ratio with a total solution concentration of 30 mg/mL) then dissolved in *o*-dichlorobenzene and stirred at 90 °C for 48 hours. ITO-coated glass substrates were cleaned sequentially by ultrasonication in Mucasol™ detergent (dissolved in deionized water), deionized water, acetone and acetone. The slides were dried in an oven for at least three hours followed by O_2 plasma exposure for 10 minutes. Filtered (0.45 μm) PEDOT: PSS was then spin-coated onto the prepared substrates (2000 rpm/60 s). The PEDOT: PSS films were then annealed at 150 °C for 30 minutes. At this point, the substrates were transferred to an argon – filled glovebox. The thickness of PEDOT: PSS layer was approximately 40 nm. After 48 hours of mixing, the polymer: PCBM solutions were filtered (0.45 μm) and immediately dropped onto the PEDOT:PSS coated substrates and spincast at 1000 rpm for 120 seconds. Photovoltaic devices with a configuration of ITO/PEDOT:PSS/

Polymer:$PC_{71}BM$/Ca/Al were fabricated. A cathode was prepared by sequentially depositing a Ca film (20 nm) and an Al film (100 nm) through a shadow mask. The photovoltaic devices had an area of 0. 06 cm^2 and were tested under simulated AM 1.5 G irradiation (100 $mWcm^{-2}$, calibrated with Daystar Meter) using a SoLux Solar Simulator, and the current-voltage (*I-V*) curves were measured using a Keithley 2400 multisource meter.

3.6 Acknowledgements

We would like to thank the Iowa State University (ISU) Institute for Physical Research and Tecnology for proving the author with a Katron fellowship. We also thank the National Science Foundation Materials Research Facilities Network (DMR-1250372) and Polymer-Based Materials for Harvesting Solar Energy, an Energy Frontier Research Center funded by the U.S. Department of Energy, Office of Science, Office of Basic Energy Sciences under Award Number DE-SC0001087 for support of the device fabrication

3.7 Supporting Information

3.7.1 Synthetic Procedures

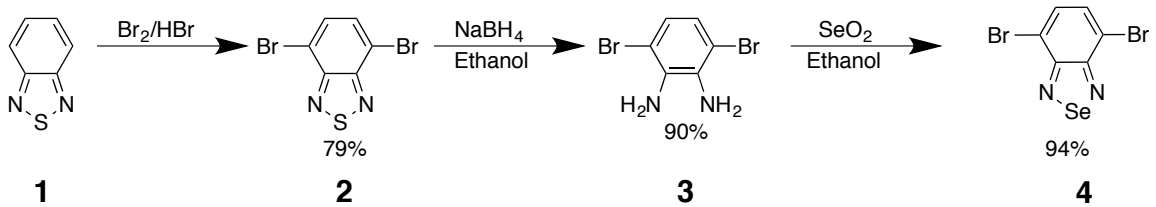

Scheme S3-1

4,7 dibromobenzo[*c*][1,2,5]thiadiazole (2). To a stirred solution of benzo[*c*][1,2,5]thiadiazole (10.15 g, 74.5 mmol) and 48% HBr (150 mL) was added Br_2 (36.69 g 229.5 mmol) in HBr (100 mL). The addition for the Br_2 solution was drop-wise over 4-6 hours. The reaction was heated to reflux for 16 hours after which time it was cooled to room temperature. A solution of $NaHSO_3$ was added. The reaction mixture filtered and washed with excess H_2O as well as cold ether. The solid product was recrystallized using acetone to yield yellow needles. (17.19 g 78.5%). ^{1}H NMR (400 MHz; $CDCl_3$) δ (7.73 s, 2H).

3,6-dibromobenzene-1,2-diamine (3). $NaBH_4$ (2.94 g, 77.9 mmol) was added portion-wise to a suspension of 4,7 dibromobenzo[*c*][1,2,5]thiadiazole (**2**) (1.23 g, 4.18 mmol) in ethanol (42 mL) at 0° C. The reaction mixture was stirred for 20 hours at rt. The solvent was then evaporated and water (200 mL was added). The mixture was extracted with ether, washed with brine and dried over $MgSO_4$. The solvent was removed in vacuo to afford the product as a tan solid (0.9 g. 81%). ^{1}H NMR (400 MHz; $CDCl_3$) δ (6.85, s, 2H).

4,7 dibromobenzo[*c*][1,2,5]thiadiazole (4). 3,6-dibromobenzene-1,2-diamine **(3)** (1.15 g, 3.92mmol) and SeO_2 (0.52 g, 4.7 mmol) were refluxed in ethanol overnight. The reaction mixture was extracted with DCM and washed with water three times. It was then dried over $MgSO_4$ and the solvent was evaporated. The product was recrystallized from acetone to give yellow crystals (1.21 g, 94%). ^{1}H NMR (400 MHz; $CDCl_3$) δ (7.65, s, 2H)

3.7.2 ^{1}H NMR spectra of monomers

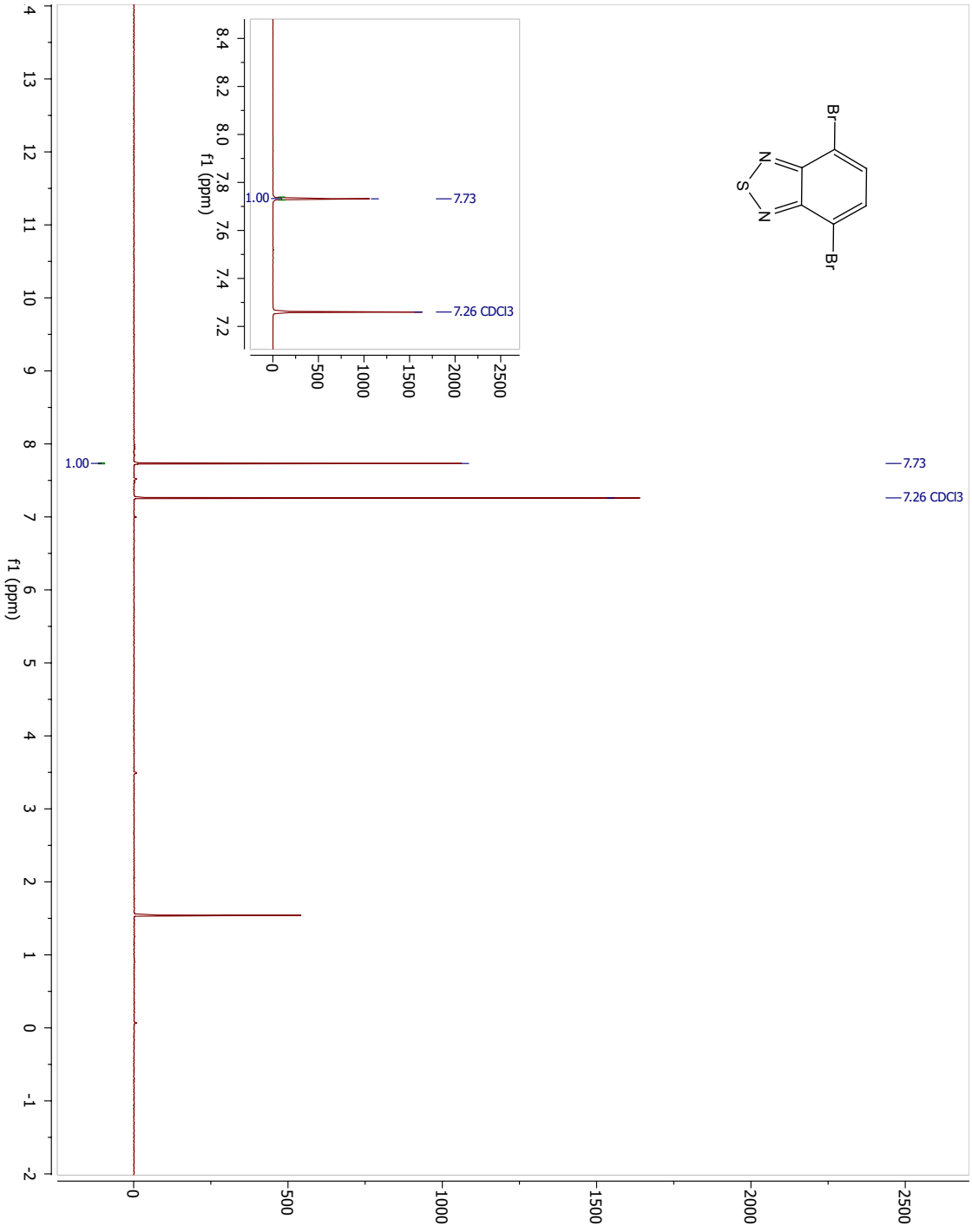

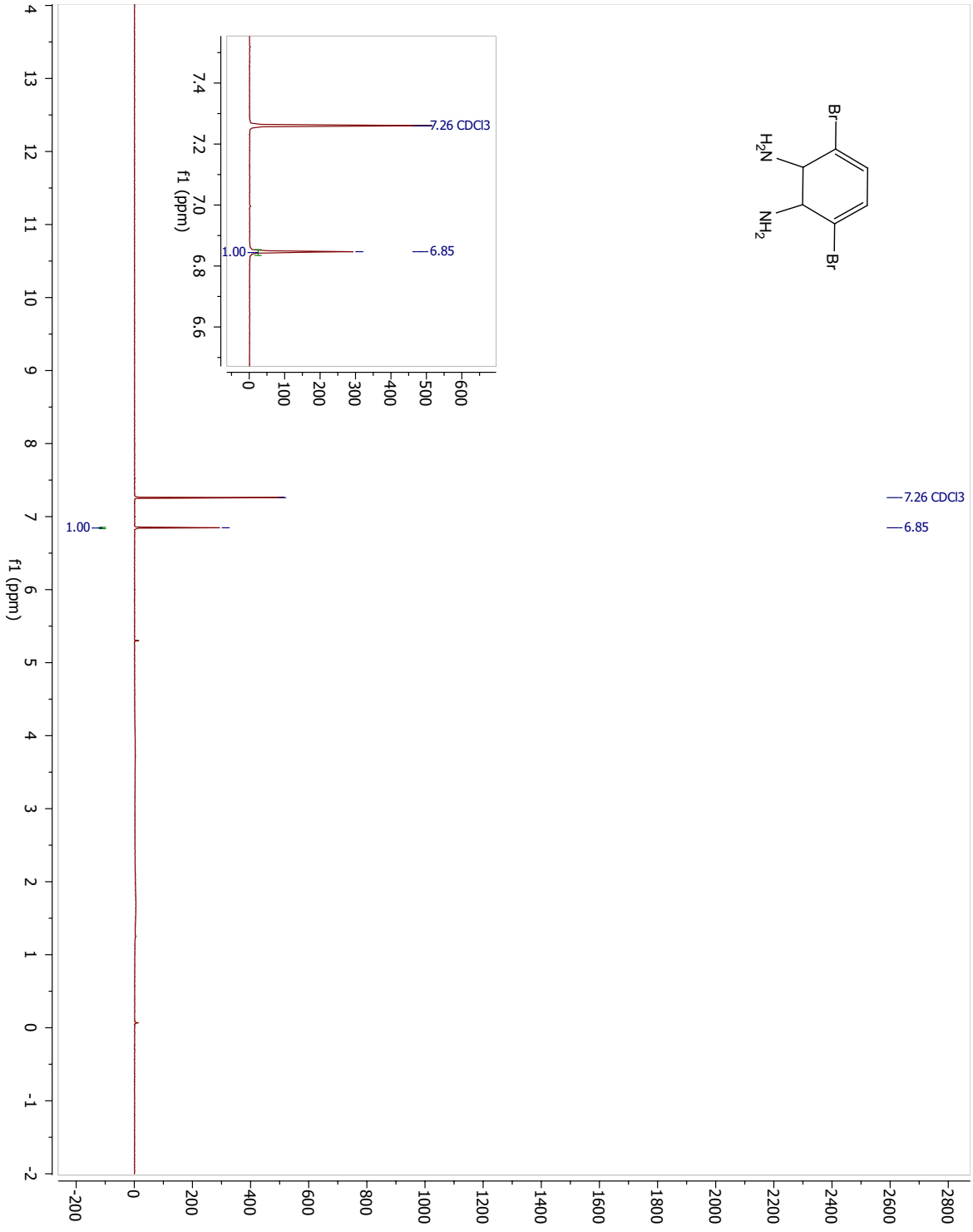

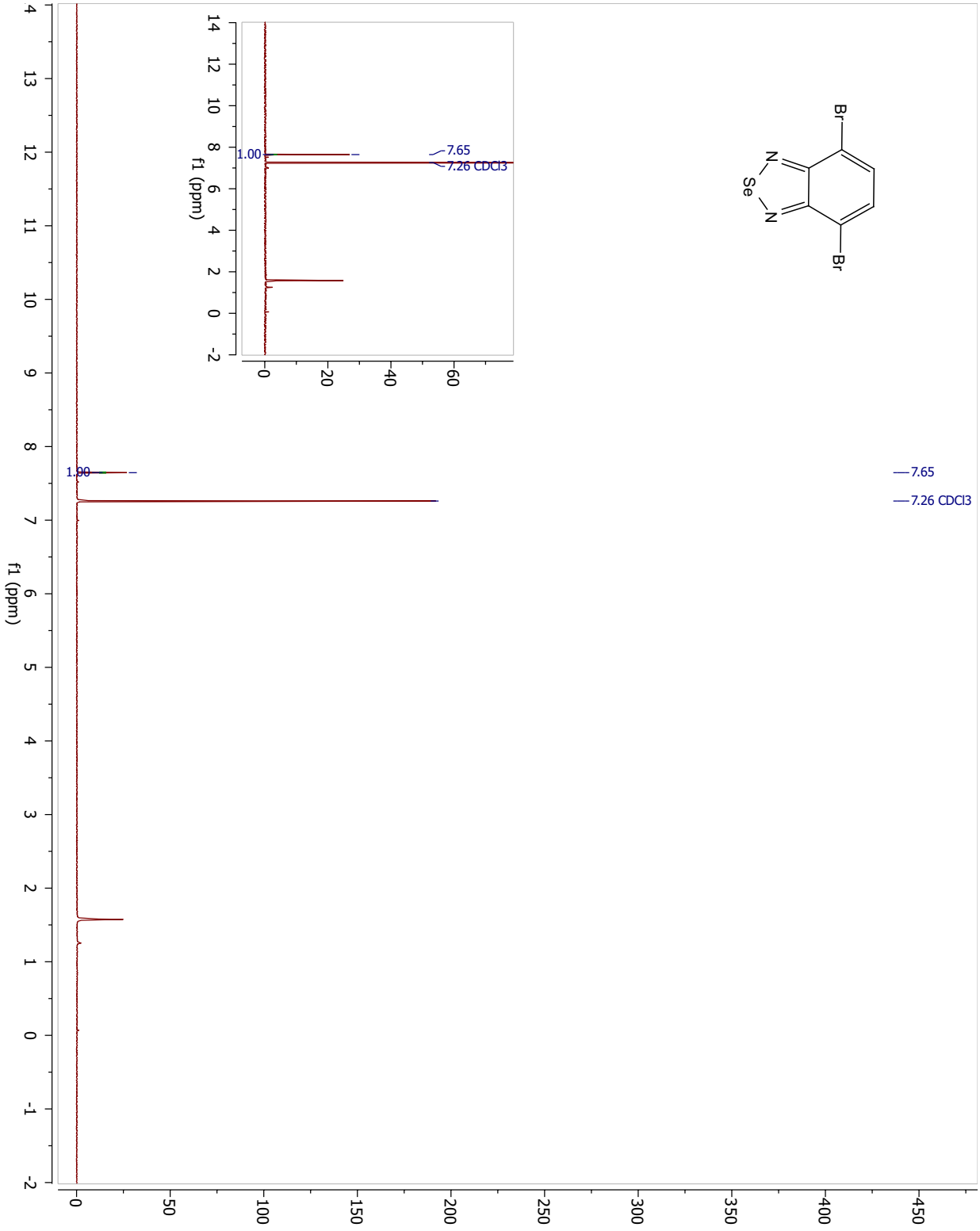

3.8 REFERENCES

1. Bijleveld, J. C.; Zoombelt, A. P.; Mathijssen, S. G. J.; Wienk, M. M.; Turbiez, M.; de Leeuw, D. M.; Janssen, R. A. J., *Journal of the American Chemical Society* **2009,** *131* (46), 16616-16617.
2. Lewis, N. S., *science* **2007,** *315* (5813), 798-801.
3. Zhou, H.; Yang, L.; You, W., *Macromolecules* **2012,** *45* (2), 607-632.
4. Zhan, X.; Zhu, D., *Polymer Chemistry* **2010,** *1* (4), 409-419.
5. Li, G.; Zhu, R.; Yang, Y., *Nature Photonics* **2012,** *6* (3), 153-161.
6. Facchetti, A., *Chemistry of Materials* **2010,** *23* (3), 733-758.
7. Grimsdale, A. C.; Leok Chan, K.; Martin, R. E.; Jokisz, P. G.; Holmes, A. B., *Chemical reviews* **2009,** *109* (3), 897-1091.
8. Thomas, S. W.; Joly, G. D.; Swager, T. M., *Chemical Reviews* **2007,** *107* (4), 1339-1386.
9. Thompson, B. C.; Frechet, J. M. J., *Angewandte chemie international edition* **2008,** *47* (1), 58-77.
10. Roncali, J., *Chemical reviews* **1997,** *97* (1), 173-206.
11. Chu, T.-Y.; Lu, J.; Beaupré, S.; Zhang, Y.; Pouliot, J.-R.; Wakim, S.; Zhou, J.; Leclerc, M.; Li, Z.; Ding, J., *Journal of the American Chemical Society* **2011,** *133* (12), 4250-4253.
12. He, Z.; Zhong, C.; Su, S.; Xu, M.; Wu, H.; Cao, Y., *Nature Photonics* **2012,** *6* (9), 591-595.
13. Liang, Y.; Xu, Z.; Xia, J.; Tsai, S. T.; Wu, Y.; Li, G.; Ray, C.; Yu, L., *Advanced Materials* **2010,** *22* (20), E135-E138.
14. Liang, Y.; Yu, L., *Accounts of chemical research* **2010,** *43* (9), 1227-1236.
15. Jeffries-El, M.; Kobilka, B. M.; Hale, B. J., *Macromolecules* **2014,** *47* (21), 7253-7271.
16. Saadeh, H. A.; Lu, L.; He, F.; Bullock, J. E.; Wang, W.; Carsten, B.; Yu, L., *ACS Macro Letters* **2012,** *1* (3), 361-365.
17. Shen, P.; Bin, H.; Zhang, Y.; Li, Y., *Polymer Chemistry* **2014,** *5* (2), 567-577.
18. Chung, D. S.; Kong, H.; Yun, W. M.; Cha, H.; Shim, H.-K.; Kim, Y.-H.; Park, C. E., *Organic Electronics* **2010,** *11* (5), 899-904.
19. Shiroudi, A.; Zahedi, E., *Chinese Journal of Chemistry* **2011,** *29* (11), 2249-2256.
20. Kang, I.; An, T. K.; Hong, J.; Yun, H. J.; Kim, R.; Chung, D. S.; Park, C. E.; Kim, Y. H.; Kwon, S. K., *Advanced Materials* **2013,** *25* (4), 524-528.
21. Kronemeijer, A. J.; Gili, E.; Shahid, M.; Rivnay, J.; Salleo, A.; Heeney, M.; Sirringhaus, H., *Advanced Materials* **2012,** *24* (12), 1558-1565.
22. Ha, J. S.; Kim, K. H.; Choi, D. H., *Journal of the American Chemical Society* **2011,** *133* (27), 10364-10367.
23. Shahid, M.; McCarthy-Ward, T.; Labram, J.; Rossbauer, S.; Domingo, E. B.; Watkins, S. E.; Stingelin, N.; Anthopoulos, T. D.; Heeney, M., *Chemical Science* **2012,** *3* (1), 181-185.
24. Chen, M. H.; Hou, J.; Hong, Z.; Yang, G.; Sista, S.; Chen, L. M.; Yang, Y., *Advanced Materials* **2009,** *21* (42), 4238-4242.

25. Blouin, N.; Michaud, A.; Gendron, D.; Wakim, S.; Blair, E.; Neagu-Plesu, R.; Belletete, M.; Durocher, G.; Tao, Y.; Leclerc, M., *Journal of the American Chemical Society* **2008,** *130* (2), 732-742.
26. Huo, L.; Chen, H.-Y.; Hou, J.; Chen, T. L.; Yang, Y., *Chem. Commun.* **2009,** (37), 5570-5572.
27. Zhao, W.; Cai, W.; Xu, R.; Yang, W.; Gong, X.; Wu, H.; Cao, Y., *Polymer* **2010,** *51* (14), 3196-3202.
28. Yang, R.; Tian, R.; Yan, J.; Zhang, Y.; Yang, J.; Hou, Q.; Yang, W.; Zhang, C.; Cao, Y., *Macromolecules* **2005,** *38* (2), 244-253.
29. Hou, J.; Tan, Z. a.; Yan, Y.; He, Y.; Yang, C.; Li, Y., *Journal of the American Chemical Society* **2006,** *128* (14), 4911-4916.
30. Hou, J.; Huo, L.; He, C.; Yang, C.; Li, Y., *Macromolecules* **2006,** *39* (2), 594-603.
31. Hou, J.; Tan, Z. a.; He, Y.; Yang, C.; Li, Y., *Macromolecules* **2006,** *39* (14), 4657-4662.
32. Li, Y.; Zou, Y., *Advanced materials* **2008,** *20* (15), 2952-2958.
33. Huo, L.; Hou, J.; Zhang, S.; Chen, H. Y.; Yang, Y., *Angewandte Chemie International Edition* **2010,** *49* (8), 1500-1503.
34. Huo, L.; Zhang, S.; Guo, X.; Xu, F.; Li, Y.; Hou, J., *Angewandte Chemie* **2011,** *123* (41), 9871-9876.
35. Duan, R.; Ye, L.; Guo, X.; Huang, Y.; Wang, P.; Zhang, S.; Zhang, J.; Huo, L.; Hou, J., *Macromolecules* **2012,** *45* (7), 3032-3038.
36. Zhang, Y.; Gao, L.; He, C.; Sun, Q.; Li, Y., *Polymer Chemistry* **2013,** *4* (5), 1474-1481.
37. Kumagai, J.; Hirano, K.; Satoh, T.; Seki, S.; Miura, M., *The Journal of Physical Chemistry B* **2011,** *115* (26), 8446-8452.
38. Kim, J.-H.; Kim, H. U.; Mi, D.; Jin, S.-H.; Shin, W. S.; Yoon, S. C.; Kang, I.-N.; Hwang, D.-H., *Macromolecules* **2012,** *45* (5), 2367-2376.
39. Kim, J.-H.; Song, C. E.; Kang, I.-N.; Shin, W. S.; Hwang, D.-H., *Chemical Communications* **2013,** *49* (31), 3248-3250.
40. Jenekhe, S. A.; Lu, L.; Alam, M. M., *Macromolecules* **2001,** *34* (21), 7315-7324.
41. Iyer, A.; Bjorgaard, J.; Anderson, T.; Köse, M. E., *Macromolecules* **2012,** *45* (16), 6380-6389.
42. Janietz, S.; Bradley, D. D. C.; Grell, M.; Giebeler, C.; Inbasekaran, M.; Woo, E. P., *Applied physics letters* **1998,** *73* (17), 2453-2455.
43. Heeger, A. J.; Kivelson, S.; Schrieffer, J. R.; Su, W. P., *Reviews of Modern Physics* **1988,** *60* (3), 781-850.

CHAPTER 4

SYNTHESIS, CHARACTERIZATION AND PHOTOVOLTAIC PROPERTIES OF DITHIENYLBENZOBISAZOLE-DITHIENYLSILOLE COPOLYMERS

J. Polym. Sci., Part A: Polym. Chem. **2015**, *53*, 1533–1540

DOI: 10.1002/pola.27603

Achala Bhuwalka,[1] **Monique D. Ewan**,[1] Jared F. Mike, [1] Moneim Elshobaki,[3,4] Brandon Kobilka,[1] Sumit Chaudhary,[2] Malika Jeffries-EL[1]

[1]Department of Chemistry Iowa State University, Ames IA, 50011, USA

[2]Department of Electrical and Computer Engineering, Iowa State University, Ames IA, 50011 USA

[3]Department of Materials Science & Engineering, Iowa State University, Ames, IA, 50011, USA.

[4]Physics Department, Mansoura University, Mansoura, 35516, Egypt.

4.1 Abstract

Three conjugated polymers comprised of dioctyl-dithieno-[2,3-*b*:2',3'-*d*]silole and a donor-acceptor-donor triad of either *cis*-benzbisoxazole, *trans*-benzobisoxazole or *trans*-benzobisthiazole were synthesized via the Stille cross-coupling reaction. The impact of varying the heteroatoms and/or the location within the benzobisazole moiety on the optical and electronic properties of the resulting polymers was evaluated via cyclic voltammetry and UV-Visible spectroscopy. All of the polymers have similar optical band-gaps of ~1.9 eV and highest occupied molecular orbital levels of -5.2 eV. However, the lowest unoccupied molecular orbitals (LUMO) ranged from -3.0 – -3.2 eV. Interestingly, when the polymers were used as donor materials in bulk-heterojunction photovoltaic cells with $PC_{71}BM$ as the electron-acceptor, the benzobisoxazole-åbased polymers gave slightly better results than the benzobisthiazole-containing polymers with power conversion efficiencies up to 3.5 %. These results indicate that benzobisoxazoles are promising materials for use in OPVs.

4.2 Introduction

Nowadays conjugated polymers (CP)s have become ubiquitous in applications such as field-effect transistors,[1, 2] light emitting diodes,[3-5] photovoltaic cells,[6-8] and sensors.[9, 10] CPs offer several advantages over their inorganic counterparts including solution processability potentially reducing fabrication costs, and the ability to tune their properties via organic synthesis, which enables optimization for use in specific applications. Currently, one of the most effective strategies for tuning the optical and electronic properties of CPs is through the incorporation of alternating electron donating and electron accepting comonomers within the polymer backbone.[11-13] This approach has afforded many materials with narrow band-gaps suitable for

effective harvesting of solar energy. However, in most organic photovoltaic cells (OPV)s a bulk heterojunction is formed by using the CP as a donor material and blending it with a fullerene acceptor, such as $PC_{61}BM$ or $PC_{71}BM$. Thus, the energy levels of both materials must be well aligned for efficient electron transfer between the two materials.[14, 15] Additionally, the morphology should be fine enough to enable efficient dissociation of electron-hair pairs at the donor:acceptor interfaces; at the same time coarser domains are also required to efficiently transport the charges to the electrodes. Although CP based OPVs are rapidly approaching the 10 % power conversion efficiency (PCE) recommended for them to be competitive commercially, the development of new materials remains an important area of research.[16-18] In particular the development of efficient donor materials that address practical aspects of commercialization such as facile synthesis and purification of monomers, and enhanced thermal and environmental stability of the resulting material are still needed.[19]

Polybenzobisazoles are a class of polymers that are known for their exceptional thermal stability and high tensile strength of fibers spun from them.[20-23] For example, poly(*p*-phenylene-2,6-benzobisoxazole) is a liquid crystalline polymer based on benzo[1,2-*d*; 4,5-*d*']benzobisoxazole that is spun into fibers commercially sold under the name Zylon®.[21] Due to the previous use of polybenzobisazoles in high performance applications, all of the necessary monomers can be synthesized on industrial scale, and purified without the use of column chromatography. This is advantageous for large-scale synthesis. Furthermore, the benzobisazole ring system is electron-deficient and planar, which leads strong intermolecular interactions and good charge transport properties within polymer films.[24-26] Despite these advantages, the use of benzobisazoles in optoelectronic materials has been nominal due to the harsh reaction conditions used for their synthesis and their poor solubility. Traditionally, benzobisazoles are synthesized

by an acid catalyzed condensation reaction at high temperatures.[22, 23] Such reaction conditions not only limit the types of substituents that can be on the monomer but residual acid also results in undesirable doping of the polymer and can also catalyze the degradation of the material in sunlight.[27] To address these limitations, our group has developed a mild high yielding synthesis of functional benzobisazoles via an orthoester condensation reaction.[28-30]

To date, there are only a few reports on the synthesis and photovoltaic properties of donor-acceptor polymers comprising benzobisazoles.[31-37] Jenekhe and coworkers reported a PCE of 2.1 % for a quarterthiophene benzobisthiazole polymer.[31] Our group reported a PCE of only 0.6 % for a related benzobisthiazole polymer, but obtained a PCE of 1.1 % for the isoelectronic benzobisoxazole polymer.[33] Although all of these polymers exhibited good charge carrier mobilities, they had relatively wide band gaps (1.9 – 2.1 eV), limiting the harvesting of solar energy. To improve on the properties of this system, we decided to evaluate the electron rich dithienosilole (DTS) moiety. This silicon bridged fused bithiophene system features two alkyl chains that impart excellent solubility to the resulting polymer, while the long C-Si bonds move the alkyl chains away from the ring system, thereby allowing for improved π-stacking. Additionally, the σ*-orbital in DTS is able to interact with the π*-orbital of the bithiophene, giving a conjugated, planar system further increasing π-stacking interactions and the long-range order.[38] Furthermore, DTS has a lower-lying (LUMO) and highest occupied molecular orbital (HOMO) than other bithiophene derivatives, which can reduce the polymer band gap and increase the open circuit voltage (V_{oc}) of the devices fabricated from them affording PCEs as high as 7.3 %.[39] Jenekhe and coworkers reported a PCE of 2.1 % for a BHJ device using a dithienosilole-dithienylbenzobisthiazole polymer as the donor and $PC_{71}BM$ as the acceptor.[32] Since, our previous results indicate that polymers incorporating the benzobisoxazole moiety

exhibited higher V_{oc} and PCE in comparison to the analogous benzobisthiazole polymers, we set out to evaluate the optical and electronic properties of a series of polymers containing DTS and the isomeric benzo[1,2-*d*; 5,4-*d*']bisoxazole (*cis*-BBO) and benzo[1,2-*d*; 4,5-*d*']bisoxazole (*trans*-BBO) and the isoelectronic benzo[1,2-*d*; 4,5-*d*']bisthiazole (*trans*-BBZT). We note that could not include the *cis*-BBZT polymer in our studies as the synthesis of the required starting material, 4,6-diamino-1,3- benzenedithiol has not been reported in the modern era. Our attempts to prepare this compound according to literature procedure yield different products from the reports. Furthermore, all efforts to synthesize this compound in our labs using new approaches have been unsuccessful. Scheme 4-1 summarizes all polymer syntheses.

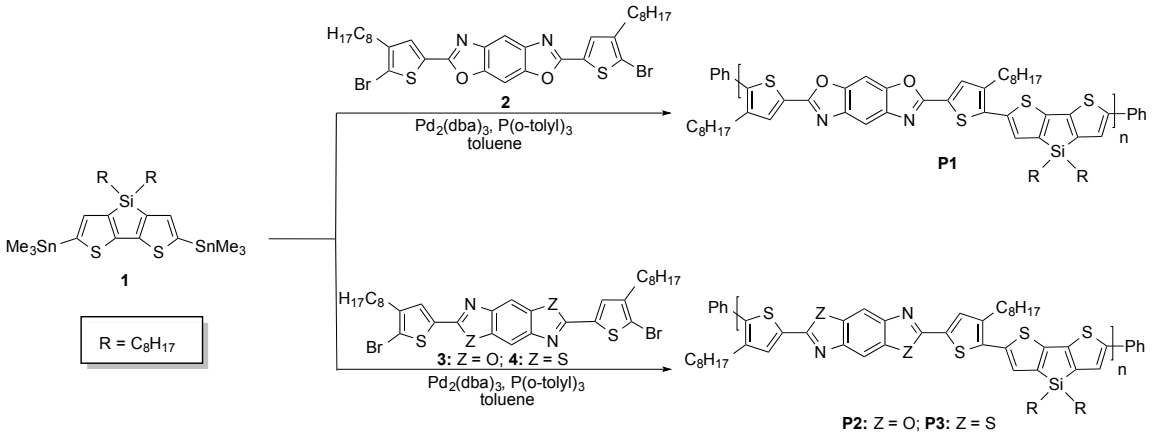

Scheme 4-1

4.3 Results and Discussion

The weight-averaged (M_w), number-averaged (M_n) molecular weights and polydispersity index (PDI) as estimated using GPC are summarized in Table 1. The number averaged degree of polymerization (DP_n) for the polymers was determined to range from 9-12. Unfortunately, the limited solubility of the polymers the disproportionate ratio of alkyl to aryl protons and the

generally lower signal to noise obtained for quarternary protons prevented analysis by ^{1}H NMR spectroscopy. Thermogravimetric analysis (TGA) revealed that all polymers were thermally stable with 5 % weight loss onsets occurring above 300 °C under air. None of the polymers exhibited any glass transitions as shown by differential scanning calorimetry (DSC) . The results are summarized in Table 1.

Table 4-1. Physical characterization of **P1 – P3**.

Polymer	yield[a] (%)	M_n[b] (kDa)	PDI[b]	DP_n	T_d (°C)[c]
P1	89	11.6	2.3	12	308
P2	83	12.4	2.6	12	306
P3	55	9.5	2.2	9	315

[a] Isolated yield [b]Determined by GPC in $CHCl_3$ using polystyrene standards.. [c] 5% weight loss temperature by TGA in air.

4.3.1 Optical and Electrochemical Properties.

The optical properties of the polymers were investigated using UV-Visible absorption spectroscopy in solution and solid state. The normalized absorbance spectra of the polymer solutions in dilute chloroform solution and in the solid state are shown in Figures 4-1 and 4-2, respectively. The data is summarized in Table 2. In solution, the λ_{max} of all the polymers are similar. However, **P1** and **P2** have small shoulders arising from aggregation in polymer backbone,[31] whereas **P3** exhibits a single, featureless absorbance band. As thin films, the λ_{max} values for **P1**, **P2** and **P3** are 524 nm, 536 nm and 549 nm respectively. These absorbance

spectra are slightly broader than the corresponding solution spectra, resulting in bathochromic shifts of 2 nm – 30 nm in the absorption maximum. This suggests a slight increase in the backbone planarization and π- stacking in the solid state.[41] The film λ_{max} of **P3** is the same as that reported by Jenekhe for a similar polymer which had branched alkyl chains on the dithienosilole unit and the alkyl chain on the thiophenes flanking the benzobisthiazole moiety was facing inwards.[32] The solution and thin film λ_{max} values of **P1 – P3** are bathochromically shifted by 70 – 95 nm relative to our previous reported polymers which employed bithiophene as the donor.[33] This can be attributed to the fused dithienosilole ring system which can lead to a more rigid, coplanar backbone thereby increasing the effective π-conjugation length, decreasing the band gap and red-shifting the absorbance spectra.

The optical band gaps for **P1 – P3** were estimated from the onset wavelength of the polymers films and range from 1.9 – 2.0 eV.

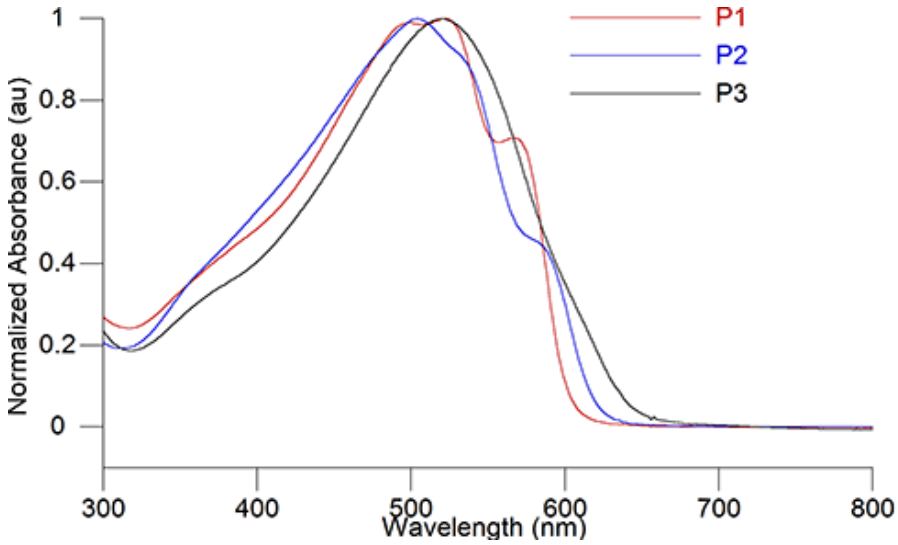

Figure 4-1. UV-Vis absorption spectra of **P1 – P3** in dilute chloroform solutions.

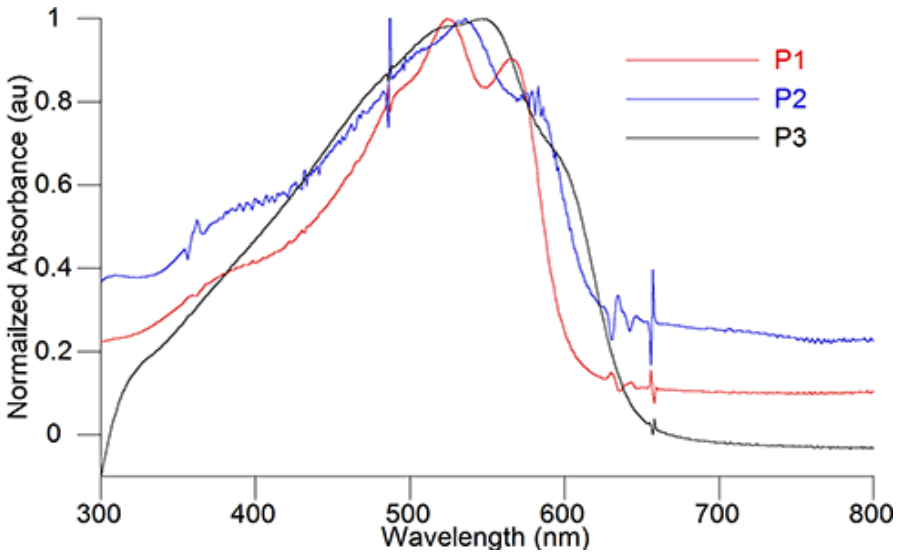

Figure 4-2. UV-Vis absorption spectra of **P1 – P3** as thin films. Thin films were spun from polymer solutions in 1:1 (v/v) $CHCl_3$:*o*DCB (2 mg/mL).

Table 4-2. Electronic and optical properties of benzobisazole-thiophene-dithienosilole terpolymers.

Polymer	Solution	Film							
	λ_{max}^{soln} (nm)	λ_{max}^{film} (nm)	λ_{onset} (nm)	E_g^{opt}(eV)[a]	E_g^{EC}(eV)[b]	E_{onset}^{ox}	E_{onset}^{red}	LUMO (eV)[c]	HOMO (eV)[d]
P1	522	524	610	2.0	2.2	0.4	-1.8	-3.0	-5.2
P2	505	536	640	1.9	2.0	0.4	-1.6	-3.2	-5.2
P3	520	549	650	1.9	--	0.5	---	---	-5.2

[a] Estimated from the optical absorption edge. [b] Estimated from HOMO-LUMO. [c] LUMO = -4.8- (E^{red}_{onset}) (eV). [d] HOMO = -4.8- (E^{ox}_{onset}) (eV). Electrochemical properties were measured using a three-electrode cell (electrolyte: 0.1 mol/L $TBAPF_6$ in acetonitrile) with an Ag/Ag^+ reference electrode, a platinum auxiliary electrode, and a platinum button electrode as the working electrode. Reported values are referenced to Fc/Fc^+. Polymer films were drop cast on to the working electrode from an *o*-DCB solution of **P1 – P3**. No reduction peak was seen for **P3.**

As expected, these band-gaps are slightly narrower than those reported previously for the benzobisazole-quarterthiophene system which ranged from 2.1 eV – 2.2 eV.[33] This further demonstrates that using a stronger fused electron-donating comonomer was beneficial in narrowing the band gap.

Using cyclic voltammetry, the electrochemical properties of the polymers were evaluated and the results are summarized in Table 2. **P1** and **P2** showed reproducible oxidation and reduction processes, whereas **P3** only showed a clear wave during the oxidation cycle. The HOMO levels were all ranged from -5.2 to -5.3 eV and were estimated using the absolute energy level of ferrocene/ferrocenium (Fc/Fc^+) as 4.8 eV under vacuum and the onsets of oxidation.[42] These are deep enough to provide good air stability.[15] Similarly, the LUMO levels of -3.0 eV and -3.2 eV were estimated using the onsets of reduction for the BBO polymers **P1** and **P2**, respectively. The *trans*-BBZT polymer **P3** did not exhibit a measurable reduction wave. These results indicate that the HOMO level of these polymers are unaffected by changing the configuration of the oxygen atoms or replacing them with sulphur. In contrast, switching the oxygen from the *cis*- to the *trans*- configuration reduced the LUMO level by ~0.2 eV. The LUMO levels for all of the polymers are also lower than those of their quarterthiophene counterparts.[33] Thus replacing the bithiophene with DTS was beneficial. The difference between the electrochemical band gaps of **P1** and **P2** and their optical band gaps is typical for these measurements due to the energy barrier associated with the interface of the polymer film and the electrode surface.[42, 43]

4.3.2 Photovoltaic Properties

The OPV performances of the polymers was evaluated using photovoltaic devices with a configuration of ITO/PEDOT:PSS/**Polymer**:$PC_{71}BM$/Ca/Al and a 1:2 weight ratio of polymer to

$PC_{71}BM$ with a total solution concentration of 21 mg/mL. These devices were evaluated with and without the solvent additive, DIO. The photovoltaic parameters including short circuit current density (J_{SC}), open circuit voltage (V_{OC}), fill factor (*FF*) and power conversion efficiency (PCE) are listed in Table 4-3. The current density-voltage (*J-V*) curves of **P1**:$PC_{71}BM$, **P2**:$PC_{71}BM$, and **P3**:$PC_{71}BM$ photovoltaic devices under AM 1.5 G illumination (100 mW/cm^2) are shown in Figure 4-3. We were able to obtain maximum PCE values of 2.47, 3.51 and 2.15 for **P1**, **P2**, and **P3**, respectively. However, we were unable to obtain these values reproducibly in subsequent runs. This is indicative of the difficulty in obtaining ideal nanoscale morphology within the polymer:fullerene blends. On average the devices based on the benzobisoxazole polymers **P1** and **P2** had similar performance with PCEs of ~1.5 % without the use of solvent additives. Whereas, the performance of the devices made from the benzobisthiazole polymer **P3** were slightly lower with a PCEs of 1.22 %. We also evaluated the use of DIO as a solvent additive,[44]

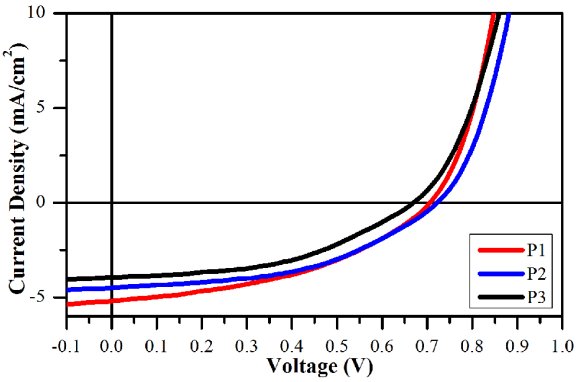

Figure 4-3. Current density-voltage *(J-V)* curves of polymer:$PC_{71}BM$, photovoltaic devices under AM 1.5 G illumination (100 mW cm^{-2}).

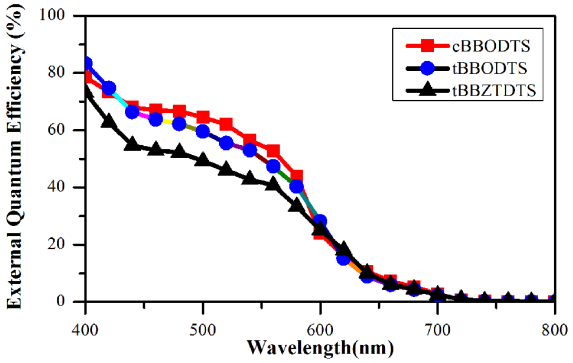

Figure 4-4. The external quantum efficiency of polymer:$PC_{71}BM$, photovoltaic devices under AM 1.5 G illumination (100 mW cm^{-2}).

but only observed a nominal improvement in the PCE for **P3**, and a minor decrease in the performance of **P1** and **P2**. In general, the performances of these devices were modest as a result of both J_{SC} and V_{OC} and moderate *FF*. The external quantum efficiency (EQE) curves for the best devices are shown in Figure 4. All of the devices had broad photoresponses between 400 to 690 nm, with a maximum EQE of 79% at 400nm, 83% at 400nm, and 73% at 400nm, for **P1**, **P2**, and **P3**, respectively. These overall performance of these polymers represent a modest improvement over our previously results on poly(quarterthiophene benzobisazoles), in which the best performance was a PCE of 1.14 % for the *trans*-BBO polymer.[33] The OPV performance of **P3** is comparable to that reported by Jenekhe *et al* for a related benzobisthiazole polymer, poly[(4,4' -bis(2- ethylhexyl)dithieno[3,2-*b*:2' ,3' -*d*]silole)-2,6-diyl-alt- (2,5-bis(3-dodecylthiophen-2-yl)benzo[1,2-*d*;4,5-*d'*]bisthiazole)] (PBTEHS), which had a PCE of 1.24 % that increased to 2.02 % with the use of additives.[32] Although PBTEHS and **P3** have different substituents on both the flanking thiophenes and benzodithiophene, the

Table 4-3. Photovoltaic device performance of **P1 - P3** with $PC_{71}BM$.

Polymer	Additive (% DIO)	J_{SC} (mA/cm^2)	V_{OC} (V)	*FF*	PCE (%)	Max PCE (%)	R_{SH} (Ω cm^2)
P1	None	8.07±5.89	0.69±0.03	0.40±0.05	2.01±1.00	3.51	457±259
P1	0.5	3.14±0.07	0.69±0.02	0.49±0.02	1.08±0.02	1.11	1,656±127
P1	2.5	4.00±0.21	0.65±0.05	0.46±0.01	1.20±0.20	1.34	982±134
P2	None	5.13±1.49	0.71±0.01	0.46±0.04	1.67±0.44	2.57	818±209
P2	0.5	4.47±0.07	0.71±0.01	0.46±0.01	1.43±0.03	1.45	792±34
P2	2.5	4.80±0.04	0.69±0.01	0.42±0.01	1.39±0.02	1.42	708±37
P3	None	5.27±3.11	0.66±0.01	0.44±0.08	1.44±0.48	2.15	944±455
P3	0.5	3.78±0.13	0.68±0.02	0.46±0.01	1.17±0.03	1.21	970±40
P3	2.5	4.23±0.15	0.67±0.01	0.43±0.01	1.22±0.03	1.25	835±146

Photovoltaic devices with a configuration of ITO/PEDOT:PSS/Polymer:$PC_{71}BM$/Ca/Al were fabricated at a 1:2 weight ratio of polymer to $PC_{71}BM$ and a total solution concentration of 21mg /mL. DIO was used as the additive (% v/v).

similarities in their initial performance but different behavior upon the addition of the co-solvents suggest that the polymers' structure has a negative impact on the morphology of the blends thin film.

The hole mobilities of the polymers were examined using the space-charge-limited current (SCLC) method with a hole only device structure of ITO/PEDOT:PSS/Polymer/Al and are summarized in Table 4-4.[45] The mobilites were calculated according to equation 4-1:

$$J_{SCLC} = \frac{9\varepsilon_0\varepsilon_r\mu_h V^2}{8L^3} \qquad (4\text{-}1)$$

in which $\varepsilon_0\varepsilon_r$ is the permittivity of the polymer, μ_h is the carrier mobility, and L is the device thickness.[46] The mobilities of the polymers were on the same order of magnitude as each other, with **P3** having the lowest mobility. This is consistent with the OPV data, with **P3** giving the worst performance, by only by a small margin.

4.3.3 Film Morphology

The surface roughness and phase distribution of the three polymer systems were studied by atomic force microscopy (AFM) (Figure 4-5). The AFM height images reveal smooth topography for all three polymers with root-mean square (RMS) surface roughness values less than 1.30 nm (Table 4-4). In the phase images, **P1**:$PC_{71}BM$ and **P2**:$PC_{71}BM$ thin-films show a bi-phasic distribution. However, the phase image of **P3**:$PC_{71}BM$ thin film is notably different and shows a strong vertical phase separation, which hampers both exciton dissociation and charge transport, and explains the poorest performance of the **P3** based devices. It is known that the BBZT containing polymers have poorer solubility than the BBO based ones.[29, 33] The reduced solubility of **P3** relative to **P1** and **P2** strongly affects the polymer/fullerene intermixing, and potentially increases tendency for aggregation.

Table 4-4. Mobility of **P1 - P3** hole-only devices and AFM data of polymer: $PC_{71}BM$ blends.

Polymer	μ_h ($cm^2 V^{-1} s^{-1}$)	RMS Roughness (nm)
P1	8.04E-06	1.08
P2	5.06E-06	0.97
P3	2.34E-06	1.30

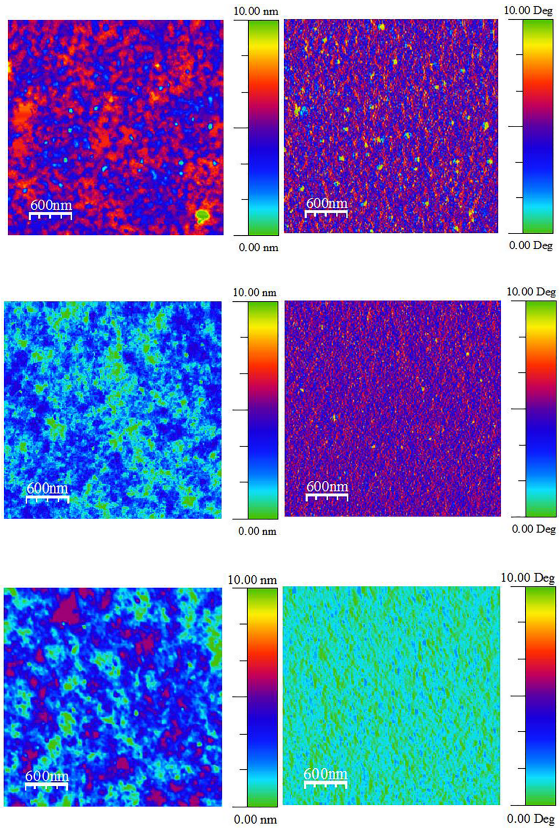

FIGURE 4-5. AFM height (left) and phase (right) images at 3 μm x 3 μm of devices with polymer:$PC_{71}BM$ blends at a 1:2 weight ratio. From top to bottom: **P1**:$PC_{71}BM$, **P2**:$PC_{71}BM$ and **P3:**$PC_{71}BM$

The surface morphology of the **P1**:$PC_{71}BM$ and **P2**:$PC_{71}BM$ thin films with varying amounts of DIO (0, 0.5 and 2.5 vol %) was also investigated by AFM (Figure 6). The RMS surface roughness values of the films with 0.5 vol % (1.86 nm for **P1** and 2.05 nm for **P2**) and 2.5 vol % (2.12 nm for **P1** and 1.56 nm for **P2**) DIO additives were larger than the films processed without any additives (0.47 nm for **P1** and 0.48 nm for **P2**). On the other hand, AFM phase images of the DIO-treated thin films display larger domain sizes, which indicate the existence of large polymer aggregates. This suppresses the exciton dissociation, short-circuit-current, and consequently the power conversion efficiency of the DIO-treated devices (Table 4-3). While the role of the solvent additive generally is to facilitate the crystallization of the polymer around the fullerene,[47] in the case of these polymers the large aggregates obtained are not favorable. In the future, different solvent additives will be investigated to further optimize the OPV performance of polybenzobisazoles-based solar cells.

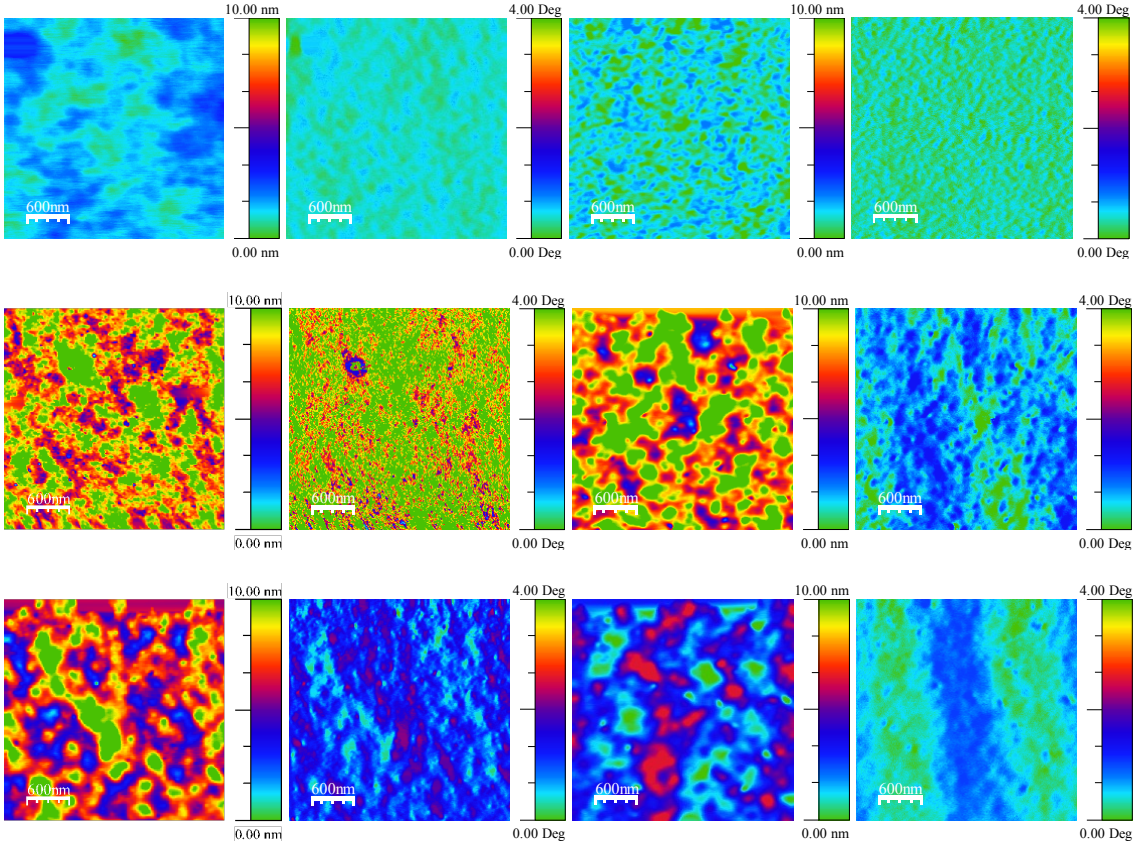

FIGURE 4-6. AFM height (first and third column) and phase (second and fourth column) of **P1**:$PC_{71}BM$ blends and **P2**:$PC_{71}BM$ blends, respectively. Images at 3 μm x 3 μm of devices with a 1:2 weight ratio. From top to bottom: control. 0.5% DIO and 2.5% DIO

4.4 Conclusions

In summary, a series of donor-acceptor copolymers based on dithienylbenzobisazole and dithieno[3,2-*b*:2’ ,3’ -*d*]silole were synthesized in an effort to improve the OPV performance of benzobisazole polymers. Although the polymers differed in the location and/or nature of the heteroatoms within the benzobisazole moiety they had identical

HOMO levels (- 5.2 eV) and fairly similar LUMO levels (-3.0 to 3.2 eV). The use of the DTS monomer had only a moderate effect on the band gap of these polymers. However, these materials did outperform our previously reported benzobisazoles. Furthermore our data indicates that among this series, benzobisoxazole based polymers are the most promising due to improved solubility and thin film formation. Research is ongoing in our lab to further improve upon the properties of this class of polymers.

4.5 Supporting Information

4.S.1 Device Fabrication and Characterization.

All polymers were mixed with $PC_{71}BM$ (mixed at a 1:2 weight ratio with a total solution concentration of 21mg/mL) then dissolved in *o*-dichlorobenzene and stirred at 90 °C for 48 hours. ITO-coated glass substrates were cleaned sequentially by ultrasonication in Mucasol™ detergent (dissolved in deionized water), deionized water, acetone and acetone. The slides were dried in an oven for at least three hours followed by O_2 plasma exposure for 10 minutes. Filtered (0.45 μm) PEDOT:PSS was then spin-coated onto the prepared substrates (2000 rpm/60 s). The PEDOT:PSS films were then annealed at 150 °C for 30 minutes. The thickness of PEDOT:PSS layer was approximately 40 nm. The PEDOT:PSS films were then transferred to an argon-filled glovebox. After 48 hours of mixing, the polymer:PCBM solutions were filtered (0.45 μm) and immediately dropped onto the PEDOT:PSS coated-coated substrates and spincast at 1000 rpm for 120 seconds. Photovoltaic devices with a configuration of ITO/PEDOT:PSS/ Polymer:$PC_{71}BM$/Ca/Al were fabricated. These devices were evaluated with and without the solvent additive, 1,8-diiodooctane (DIO). A cathode was prepared by sequentially depositing a Ca film (20 nm) and an Al film (100 nm) through a shadow mask. The photovoltaic devices had an

area of 0. 06 cm^2 and were tested under simulated AM 1.5 G irradiation (100 $mWcm^{-2}$, calibrated with Daystar Meter) using a SoLux Solar Simulator, and the current-voltage (*I-V*) curves were measured using a Keithley 2400 multisource meter. A Veeco Digital Instruments atomic force microscope (AFM) was used to map the surface profile of the investigated thin films. Both the surface roughness and phase images were captured simultaneously at scan rate and size of 0.5 Hz and 3μm × 3μm, respectively. The images were analyzed using Nanotec Electronica WSxM software.[40]

4.8 REFERENCES

1. Facchetti, A., *Mater. Today* **2007,** *10* (3), 28-37.
2. Bao, Z.; Lovinger, A. J., *Chemistry of Materials* **1999,** *11* (9), 2607-2612.
3. Friend, R. H.; Gymer, R. W.; Holmes, A. B.; Burroughes, J. H.; Marks, R. N.; Taliani, C.; Bradley, D. D. C.; Dos Santos, D. A.; Bredas, J. L.; Logdlund, M.; Salaneck, W. R., *Nature* **1999,** *397* (6715), 121-128.
4. Tang, C. W.; VanSlyke, S. A., *Applied Physics Letters* **1987,** *51* (12), 913-915.
5. Grimsdale, A. C.; Leok Chan, K.; Martin, R. E.; Jokisz, P. G.; Holmes, A. B., *Chemical reviews* **2009,** *109* (3), 897-1091.
6. Tang, C. W., *Applied Physics Letters* **1986,** *48* (2), 183-185.
7. Facchetti, A., *Chem. Mater.* **2011,** *23* (3), 733-758.
8. Günes, S.; Neugebauer, H.; Sariciftci, N. S., *Chemical Reviews* **2007,** *107* (4), 1324-1338.
9. McQuade, D. T.; Pullen, A. E.; Swager, T. M., *Chem. Rev.* **2000,** *100* (7), 2537-2574.
10. Thomas, S. W.; Joly, G. D.; Swager, T. M., *Chemical reviews* **2007,** *107* (4), 1339-1386.
11. van Mullekom, H. A. M.; Vekemans, J. A. J. M.; Havinga, E. E.; Meijer, E. W., *Materials Science and Engineering: R: Reports* **2001,** *32* (1), 1-40.
12. Havinga, E. E.; ten Hoeve, W.; Wynberg, H., *Polymer Bulletin* **1992,** *29* (1), 119-126.
13. Havinga, E. E.; ten Hoeve, W.; Wynberg, H., *Synthetic Metals* **1993,** *55* (1), 299-306.
14. Koster, L. J. A.; Mihailetchi, V. D.; Blom, P. W. M., *Applied Physics Letters* **2006,** *88* (9), 93511-93511.
15. Thompson, B. C.; Kim, Y.-G.; Reynolds, J. R., *Macromolecules* **2005,** *38* (13), 5359-5362.
16. Son, H. J.; Carsten, B.; Jung, I. H.; Yu, L., *Energy & Environmental Science* **2012,** *5* (8), 8158-8170.
17. Dennler, G.; Scharber, M. C.; Brabec, C. J., *Advanced Materials* **2009,** *21* (13), 1323-1338.
18. Kalowekamo, J.; Baker, E., *Solar Energy* **2009,** *83* (8), 1224-1231.
19. Po, R.; Bernardi, A.; Calabrese, A.; Carbonera, C.; Corso, G.; Pellegrino, A., *Energy & Environmental Science* **2014,** *7* (3), 925-943.
20. Wolak, M. A.; Jang, B. B.; Palilis, L. C.; Kafafi, Z. H., *J. Phys. Chem. B* **2004,** *108*, 5492.
21. Wolfe, J. F., Polybenzothiazoles and Polybenzoxazoles. In *Encyclopedia of Polymer Science and Engineering*, John Wiley and Sons: New York, NY, 1988; Vol. 11, pp 601-635.
22. Wolfe, J. F.; Arnold, F. E., *Macromolecules* **1981,** *14*, 909-915.
23. Wolfe, J. F.; Loo, B. H.; Arnold, F. E., *Macromolecules* **1981,** *14*, 915-920.
24. Alam, M. M.; Jenekhe, S. A., *Chemistry of Materials* **2002,** *14* (11), 4775-4780.
25. Pang, H.; Vilela, F.; Skabara, P. J.; McDouall, J. J. W.; Crouch, D. J.; Anthopoulos, T. D.; Bradley, D. D. C.; de Leeuw, D. M.; Horton, P. N.; Hursthouse, M. B., *Advanced Materials* **2007,** *19* (24), 4438-4442.

26. Osaka, I.; Takimiya, K.; McCullough, R. D., *Advanced Materials* **2010,** *22* (44), 4993-4997.
27. Song, B.; Fu, Q.; Ying, L.; Liu, X.; Zhuang, Q.; Han, Z., *Journal of Applied Polymer Science* **2012,** *124* (2), 1050-1058.
28. Mike, J. F.; Inteman, J. J.; Ellern, A.; Jeffries-El, M., *The Journal of Organic Chemistry* **2009,** *75* (2), 495-497.
29. Mike, J. F.; Intemann, J. J.; Cai, M.; Xiao, T.; Shinar, R.; Shinar, J.; Jeffries-EL, M., *Polym. Chem.* **2011,** *2* (10), 2299-2305.
30. Mike, J. F.; Makowski, A. J.; Jeffries-El, M., *Org. Lett.* **2008,** *10* (21), 4915-4918.
31. Ahmed, E.; Kim, F. S.; Xin, H.; Jenekhe, S. A., *Macromolecules* **2009,** *42* (22), 8615-8618.
32. Ahmed, E.; Subramaniyan, S.; Kim, F. S.; Xin, H.; Jenekhe, S. A., *Macromolecules* **2011,** *44* (18), 7207-7219.
33. Bhuwalka, A.; Mike, J. F.; He, M.; Intemann, J. J.; Nelson, T.; Ewan, M. D.; Roggers, R. A.; Lin, Z.; Jeffries-El, M., *Macromolecules* **2011,** *44* (24), 9611-9617.
34. Patil, A. V.; Park, H.; Lee, E. W.; Lee, S.-H., *Synthetic Metals* **2010,** *160* (19-20), 2128-2134.
35. Tsuji, M.; Saeki, A.; Koizumi, Y.; Matsuyama, N.; Vijayakumar, C.; Seki, S., *Advanced Functional Materials* **2014,** *24* (1), 28-36.
36. Saeki, A.; Tsuji, M.; Yoshikawa, S.; Gopal, A.; Seki, S., *Journal of Materials Chemistry A* **2014,** *2* (17), 6075-6080.
37. Subramaniyan, S.; Kim, F. S.; Ren, G.; Li, H.; Jenekhe, S. A., *Macromolecules* **2012,** *45* (22), 9029-9037.
38. Chen, H.-Y.; Hou, J.; Hayden, A. E.; Yang, H.; Houk, K. N.; Yang, Y., *Advanced Materials* **2010,** *22* (3), 371-375.
39. Chu, T.-Y.; Lu, J.; Beaupré, S.; Zhang, Y.; Pouliot, J.-R.; Wakim, S.; Zhou, J.; Leclerc, M.; Li, Z.; Ding, J.; Tao, Y., *Journal of the American Chemical Society* **2011,** *133* (12), 4250-4253.
40. Horcas, I.; Fernández, R.; Gómez-Rodríguez, J. M.; Colchero, J.; Gómez-Herrero, J.; Baro, A. M., *Review of Scientific Instruments* **2007,** *78* (1), 013705.
41. Kokubo, H.; Sato, T.; Yamamoto, T., *Macromolecules* **2006,** *39* (11), 3959-3963.
42. Cardona, C. M.; Li, W.; Kaifer, A. E.; Stockdale, D.; Bazan, G. C., *Advanced Materials* **2011,** *23* (20), 2367-2371.
43. Admassie, S.; Inganäs, O.; Mammo, W.; Perzon, E.; Andersson, M. R., *Synthetic Metals* **2006,** *156* (7–8), 614-623.
44. Lee, J. K.; Ma, W. L.; Brabec, C. J.; Yuen, J.; Moon, J. S.; Kim, J. Y.; Lee, K.; Bazan, G. C.; Heeger, A. J., *Journal of the American Chemical Society* **2008,** *130* (11), 3619-3623.
45. Mihailetchi, V. D.; Wildeman, J.; Blom, P. W. M., *Physical Review Letters* **2005,** *94* (12), 126602.
46. Shrotriya, V.; Yao, Y.; Li, G.; Yang, Y., *Applied Physics Letters* **2006,** *89* (6), 063505-3.
47. Chen, H.-Y.; Yang, H.; Yang, G.; Sista, S.; Zadoyan, R.; Li, G.; Yang, Y., *J. Phys. Chem. C* **2009,** *113* (18), 7946-7953.

CHAPTER 5

SYNTHESIS AND PHOTOVOLTAIC PROPERTIES OF 2,6-BIS(2-THIENYL) BENZOBISAZOLE AND 4,8-BIS(THIENYL)-BENZO[1,2-*B*:4,5-*B'*]DITHIOPHENE COPOLYMERS

J. Polym. Sci., Part A: Polym. Chem. **2015**

DOI: 10.1002/pola.27793

Achala Bhuwalka,[1] **Monique D. Ewan**,[1] Moneim Elshobaki,[2,3] Jared F. Mike,[1] Brian Tlach,[1] Sumit Chaudhary,[4] Malika Jeffries-EL[1]

[1]Department of Chemistry, Iowa State University, Ames IA, 50011, USA

[2]Department of Materials Science & Engineering, Iowa State University, Ames, IA, 50011, USA.

[3]Physics Department, Mansoura University, Mansoura, 35516, Egypt.

[4]Department of Electrical and Computer Engineering, Iowa State University, Ames IA, 50011 USA

5.1 Abstract

In an effort to design efficient low cost polymers for use in organic photovoltaic cells the easily prepared donor-acceptor-donor triad of a either *cis*-benzobisoxazole, *trans*-benzobisoxazole or *trans*-benzobisthiazole flanked by two thiophene rings was combined with the electron-rich 4,8-bis(5-(2-ethylhexyl)--thien-2-yl)-benzo[1,2-*b*:4,5-*b'*]dithiophene. The electrochemical, optical, morphological, charge transport and photovoltaic properties of the resulting terpolymers were investigated. Although the polymers differed in the arrangement and/or nature of the chalcogens, they all had similar HOMO energy levels (-5.2 to -5.3 eV) and optical band gaps (2.1 to 2.2 eV). However, the LUMO energy levels ranged from - 3.1 to -3.5 eV. When the polymers were used as electron donors in bulk heterojunction photovoltaic devices with $PC_{71}BM$ ([6,6]-phenyl C_{71}-butyric acid methyl ester) as the acceptor, the *trans*-benzobisoxazole polymer had the best performance with a power conversion efficiency of 2.8 %.

5.2 Introduction

Organic photovoltaic cells (OPVs) continue to garner a large amount of interest due to their potential for use in the development of lightweight and large area panels for efficient solar energy conversion. Currently, the most efficient OPVs are based on the bulk-heterojunction concept in which an electron accepting material, such as a functionalized fullerene, is blended with an electron donating conjugated polymer.[1] Achieving high power conversion efficiency (PCE) in these systems requires concurrent optimization of several parameters including the nanoscale morphology of the polymer film formed upon blending with the donor conjugated polymers the fullerene acceptor and the alignment of energy levels of these two components.[2] In an effort to optimize the properties of the donor polymers, there has been extensive research on

the design and synthesis of new materials. A popular approach is the synthesis of polymers composed of alternating electron rich and electron poor moieties as the intramolecular charge transfer (ICT) between these groups can be modified by adjusting the strength of the two monomers, thereby enabling tuning of the polymer's highest occupied molecular orbital (HOMO) and lowest unoccupied molecular orbital (LUMO) levels.[3-5] Although there are many known donor-acceptor conjugated polymers, only a few combinations have resulted in high PCEs. Moreover, many of these polymers utilize complex heterocycles that are challenging to synthesize and purify on large scale.[2, 6, 7]

Accordingly, benzo[1,2-*d*;5,4-*d*']bisoxazole (*cis*-BBO), benzo[1,2-*d*;4,5-*d*']bisoxazole (*trans*-BBO), and benzo[1,2-*d*;4,5-*d*']bisthiazole (*trans*-BBZT), are particularly promising for the development low-cost solution processible OPVs. Collectively referred to as the benzobisazoles, these electron deficient heterocycles are present in a variety of materials including high performance rigid-rod polymers,[8-10] non-linear optical materials,[11] emissive polymers for use in organic light emitting diodes,[12-17] electron transporting layers,[18] field-effect transistors (OFET)s,[19-22] and OPVs.[21, 23-28] Benzobisazoles have planar conjugated structure that facilitates π–π stacking, improving charge carrier mobility.[18, 22] Additionally, polybenzobisazoles are among some of the most thermally and environmentally stable materials known, which is benefical for long term device stability.[8-10] As a result of their origins as high performance materials, the monomers required for the synthesis of benzobisazoles can be prepared in large quantities, and purified without the use of column chromatography, making scale-up feasible.[8, 9, 29] Historically, the use of polybenzobisazoles was hampered by their poor solubility and the harsh conditions used for their synthesis. However, new synthetic methods have enabled the development of solution processable polybenzobisazoles.[17, 21, 23]

Previously, we reported the synthesis and photovoltaic properties of copolymers comprising a donor-acceptor-donor tri triad of a benzobisazole flanked by two thiophene rings and 3,3'-dioctylbithiophene.[25] These copolymers exhibited hole mobilities as high as 4.9 x 10^{-3} $cm^2V^{-1}s^{-1}$ when used in OFETs and modest PCEs up to 1.14%, with the *trans*-BBO polymer giving the best performance in both devices. In an effort to improve upon the performance of these polymers we replaced the bithiophenes with benzo[1,2-*b*:4,5-*b*′]dithiophene (BDT). This electron rich building block has a planar structure that facilitates π–π stacking thus improving hole mobility.[30-34] As a result, there are several copolymers comprised of BDT and various electron-deficient moieties with reported PCEs approaching the 10% PCE sought after for commercial viability.[35-40] In this work, we have utilized the two dimensional donor moiety 4,8-bis(5-(2-ethylhexyl)thien-2-yl)-benzo[1,2-*b*:4,5-*b'*]dithiophene. Replacing the electron rich alkoxy-side chains with thiophene rings lowers the HOMO level of the resulting polymers, while the extended conjugation created by the flanking thiophene rings increases absorption. As a result, polymers made from thiophene substituted BDTs often have better OPV performance than their alkoxy substituted analogs.[41, 42] This selection proved to be advantegous as when the polymers were used as electron donors in bulk heterojunction photovoltaic devices with $PC_{71}BM$ as the acceptor, the *trans*-benzobisoxazole polymer had the best performance with a PCE of 2.8%. This nearly a three-fold increase over the previously reported devices based on the bithiophene comonomers,[25] and rivals the performance of our copolymers with dithienylsilole.[43]

5.3 Results and Discussion

5.3.1 Synthesis and physical characterization

The synthesis of the polymers is shown in Scheme 1. The required monomers 4,8-bis(5-(2-ethylhexyl) thien-2-yl)-benzo[1,2-*b*:4,5-*b'*]dithiophene **1**,[44] 2,6-bis(4-octylthiophen-2-yl)-benzo[1,2-*d*; 5,4-*d'*]bisoxazole **2**,[17] 2,6-bis(4-octylthiophen-2-yl)-benzo[1,2-*d*; 4,5-*d*']bisoxazole **3**,[17] and 2,6-bis(4-octylthiophen-2-yl)-benzo[1,2-*d*; 4,5-*d*']bisthiazole **4**[17] were synthesized according to the literature procedure. The use of the thiophene-benzobisazole-thiophene triad prevents ring opening side reactions at the 2- and 6-positions of the benzobisazole ring during the cross-coupling reaction.[45] The Stille cross-coupling polymerization of monomer **1** with **2**, **3,** or **4** with afforded polymers **P1**, **P2** and **P3** respectively in yields ranging from 60 – 76% (Scheme 5-1). All polymers had limited solubility in common organic solvents, such as THF, and chloroform at room temperature, preventing characterization via NMR spectroscopy. However, characterization via gel permeation chromatography (GPC) was possible. The reported molecular weight of **P3** appears to be half that of **P1** and **P2** due to the reduced solubility of the sulfur containing polymer. We also believe that the limited solubility of **P3** has impeded its analysis as only the fraction soluble

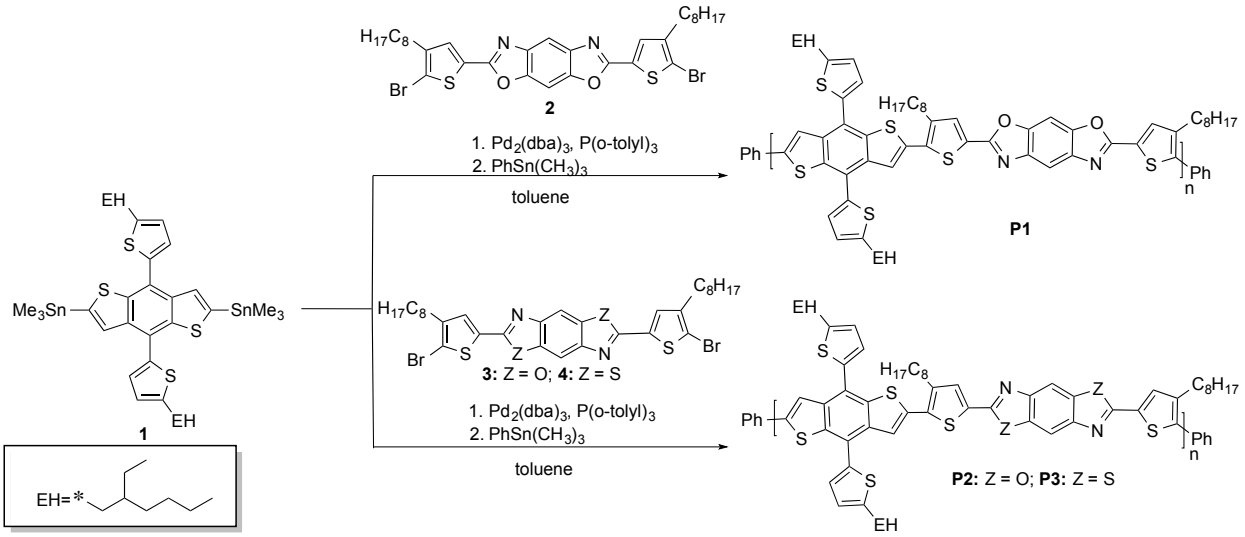

Scheme 5-1. Synthesis of benzodithiophene-thiophene-benzobisazole copolymers.

in chloroform at room temperature was evaluated. Nonetheless, all of the polymers showed excellent film-forming abilities. Thermogravimetric analysis (TGA) revealed that all polymers were thermally stable with 5% weight loss onsets occurring above 240 °C under air. The results are summarized in Table 1.

Table 5-1. Physical characterization of **P1 – P3**.

Polymer	Yield [a] (%)	M_n [b] (kDa)	Đ [b]	DP_n	T_d (ºC) [c]
P1	76	15.9	1.9	17	387
P2	71	10.9	2.1	12	246
P3	60	5.3	1.5	4	250

[a] Isolated yield [b]Determined by GPC in $CHCl_3$ using polystyrene standards. [c] 5% weight loss temperature by TGA in air.

5.3.2 Optical and electrochemical Properties.

The normalized absorbance spectra of the polymer solutions in chloroform and in the solid state are shown in Figure 1 and 2, respectively, and the data is summarized in Table 2. In solution the UV-Visible spectrum for **P2** has a single, featureless absorbance band, whereas vibronic coupling is seen in the spectra of **P1** and **P3**. The absorption maximum for **P2** is hypsochromically shifted 26 nm relative to the absorbance maximum for its isomer, **P1**, whereas the absorption maximum of **P3** is red-shifted 87 nm relative to the isoelectronic **P2**. All of the spectra are fairly broad and lack a second low-energy absorption seen when intermolecular charge transfer between the electron donating and electron accepting units is occuring.[5] As thin films, the absorbance maximum for all of the polymers are bathochromically shifted indicating increased backbone planarization and π-stacking in the solid state.[46] Interestingly, the absorbance maxima of **P1** and **P2** in thin film are significantly red-shifted relative to their solution spectra, while the absorbance maxima of **P3** is only slightly red-shifted relative to its solution spectra. The difference is likely a result of the lower molecular weight of **P3**. Despite the lower molecular weight of the polymer, **P3** exhibited the most red-shifted absorbance maximum of the series. Overall, the absorption maxima for these polymers is also red-shifted relative to the analogous quarter thiophene benzobisazoles, which had absorption maxima of 460, 475, and 462 nm for the *cis*-BBO, *trans*-BBO, and *trans*-BBZT polymers, respectively and similar molecular weights.[25] Although the optical band gaps for both series of polymers were similar, the red-shifted absorption in this series of polymers is beneficial in improving the photovoltaic properties of the polymers.

The electrochemical properties of the polymers were evaluated by cyclic voltammetry. All three polymers exhibit measureable and reproducible oxidation and reduction processes . The HOMO and LUMO levels were estimated from the onset of oxidation and reduction using the absolute energy level of ferrocene/ferrocenium (Fc/Fc^{+}) as -4.8 eV under vacuum and are summarized in Table 2.[47] The HOMO levels ranged from -5.2 to -5.3 eV, all of which are deep enough to guarantee good air stability.[48] The LUMO levels ranged from -3.1 to -3.5 eV, with the *trans*-BBZT being the lowest. As a result, **P3** had the smallest electrochemical band gap of the series. The electrochemical band gaps for **P1** and **P2** are both similar to their optical band gaps, whereas the electrochemical band gap of **P3** is significantly smaller than its optical band gap. We note that the current of the cyclic voltammogram of **P3** is also smaller than that of the other polymers which could be a result of difference in the morphology of the polymer film on the electrodes surface among other issues.[47] This data demonstrates that changing the position of the oxygen atoms from the *cis*- configuration to the *trans*- configuration has a negligible impact on the HOMO level and a negligible impact on the LUMO level. However, replacing the oxygen atoms of *trans*-BBO with sulfur had a negligible impact on the HOMO level, while reducing the LUMO level by ~0.3 eV. As a result the benzobisthiazole polymer has the smallest electrochemical bandgap.

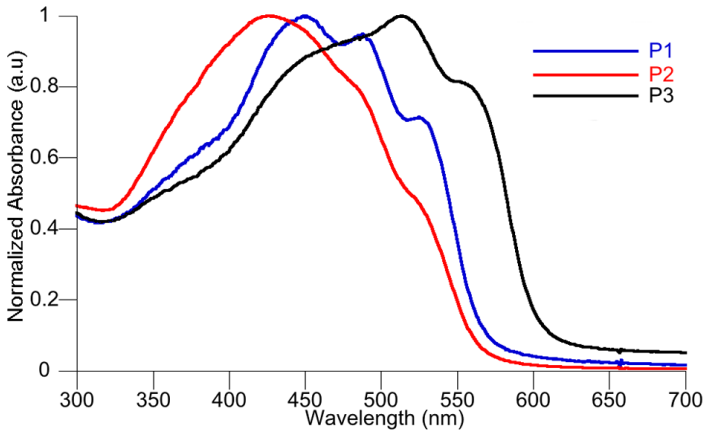

Figure 5-1. UV-Vis absorption spectra of **P1 – P3** in dilute chloroform solutions.

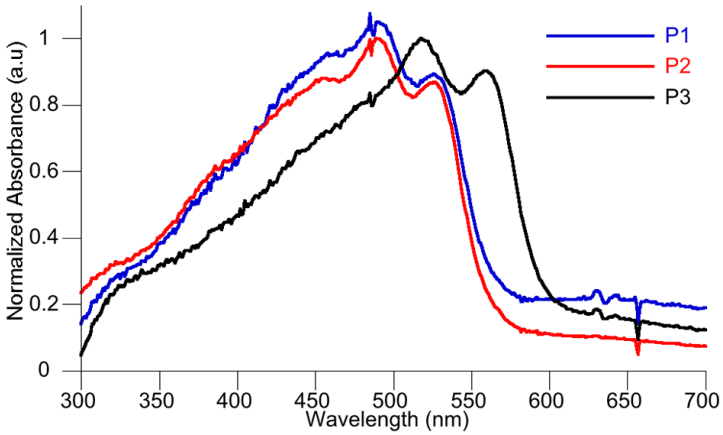

Figure 5-2. UV-Vis absorption spectra of **P1 – P3** as thin films spun from polymer solutions in *o*DCB (2 mg/mL).

Table 5-2. Electronic and optical properties of benzobisazole-thiophene-dithienosilole terpolymers.

Polymer	Solution	Film							
	λ_{max}^{soln} (nm)	λ_{max}^{film} (nm)	λ_{onset} (nm)	E_g^{opt} (eV)[a]	E_g^{EC} (eV)[b]	E_{onset}^{ox}	E_{onset}^{red}	HOMO (eV)[c]	LUMO (eV)[d]
P1	451	490	565	2.2	2.1	0.42	-1.70	-5.2	-3.1
P2	425	487	575	2.2	2.1	0.46	-1.59	-5.3	-3.2
P3	513	518	600	2.1	1.7	0.35	-1.35	-5.2	-3.5

[a] Estimated from the optical absorption edge. [b] Estimated from HOMO - LUMO [c] HOMO = -4.8 - (E^{ox}_{onset}) (eV). [d] LUMO = -4.8 - (E^{red}_{onset}) (eV). Electrochemical properties were measured using a three-electrode cell (electrolyte: 0.1 mol/L $TBAPF_6$ in acetonitrile) with an Ag/Ag^+ reference electrode, a platinum auxiliary electrode, and a platinum-button working electrode. Reported values are referenced to Fc/Fc^+. Polymer films were drop cast from an *ortho*-dichlorobenzene (*o*DCB) solution of the polymers on to the working electrode. All cyclic voltammetry experiments were recorded at a scan rate of 50 mV/s.

Previously, we were able to evaluate the energy levels using both CV and ultraviolet photoelectron spectroscopy (UPS) and saw good correlation between both measurements. UPS provides a more accurate values for the HOMO level than CV.[49] Based on the UPS measurements switching the orientation of oxygen within benzobisoxzole from *cis* to *trans* lowered the HOMO level by 0.1 eV, and substituting the oxygen atoms in *trans*-BBO with sulfur atoms had no effect on the HOMO level. Conversely, switching the orientation within benzobisoxzole from *cis* to *trans* lowered the LUMO level by 0.1 eV, whereas replacing the oxygen atoms in *trans*-BBO with sulfur atoms raised the LUMO level by 0.1 eV. The LUMO levels of **P1** and **P2** are both 0.2 eV lower that those reported previously for the analogous quarterthiophene benzobisoxazole polymers (-2.9 eV) and the HOMO levels are both 0.1 eV higher (-5.3 and -5.4 eV).[25] However, **P3** has a significantly lower LUMO level than its quarterthiophene analog (-3.1 eV) and the HOMO level is 0.2 eV higher (-5.4 eV).[25]

5.3.3 Evaluation of Charge Carrier Mobility and Photovoltaic Properties.

The performance of all three polymers in OPVs were evaluated using $PC_{71}BM$ as the electron acceptor with a device configuration of ITO/PEDOT:PSS/polymer:$PC_{71}BM$/Ca/Al. Photovoltaic devices with this configuration were fabricated using different polymer:$PC_{71}BM$ weight ratios and are summarized in Table S1. The active layer was deposited from 21 mg/mL *o*-DCB solutions, using processing conditions selected to give a thickness of approximately 100 nm. In all cases the best performance was obtained using a 1:2.5 weight ratio of polymer to $PC_{71}BM$. The current density-voltage (*J-V*) curves of **P1**:$PC_{71}BM$, **P2**:$PC_{71}BM$, and **P3**:$PC_{71}BM$ photovoltaic devices at this weight ratio under AM 1.5 G illumination (100 mW cm^{-2}) are

shown in Figure 5-3. These devices were evaluated with and without the solvent additive, 1,8-diiodooctane (DIO). The resulting photovoltaic performances including short circuit current density (J_{SC}), open circuit voltage (V_{OC}), fill factor (FF), and PCE are shown in Table 5-3. The external quantum efficiencies (EQEs) of the solar cell devices were also examined. The EQE curves for the solar cells fabricated under the same conditions used for the J–V measurements are shown in Figure 5-S1. The trend in the EQE values is consistent with the observed performance for the cells. Overall, the devices based on **P2** gave the highest PCE at 2.78% without the use of solvent additives. The devices made from **P1** and **P3** had lower efficiencies with values of 1.75% and 1.62%, respectively. Although all of the polymers had similar V_{OC} and FF, **P2** had the highest photocurrent, and as a result, the highest PCE. This is almost a three-fold improvement over the previously reported poly(quarterthiophene benzobisoxazole).[25] Interestingly, the **P1**- and **P3**-based devices had similar performances with respective values of 1.85% and 1.62%, despite the significantly lower molecular weight of **P3**, which can negatively affect film formation and charge carrier mobility.[50, 51] The OPV performance of **P3** is comparable to that reported by Jenekhe et al. for a related benzobisthiazole polymer, poly[(4,8-bis(2-hexyldecyl)oxy)benzo[1,2-*b*:4,5-*b*']dithiophene)-2,6-diyl-alt-(2,5-bis(3-dodecylthiophen-2-yl)benzo[1,2-*d*;4,5-*d*']bisthiazole)] (PBTHDDT), which had a PCE of 1.76%, that improved to 2.96% with the use of additives.[23] We also evaluated the use of DIO as a solvent additive,[52] but only observed a nominal improvement in the PCE for **P1**, and a decrease in the performance of **P2** and **P3**. However, PBTHDDT differs from our polymer in the placement and nature of the substituents on both the thiophenes and

benzodithiophene. This suggests that additional optimization of our system could yield an even higher PCE.

The mobilities were calculated according to equation 1: The hole mobility of the polymers was examined using the space-charge-limited current (SCLC) method with a hole only device structure of ITO/PEDOT:PSS/Polymer/Al.[53] The mobilities were calculated according to the equation 1:

$$J_{SCLC} = \frac{9\varepsilon_0\varepsilon_r\mu_h V^2}{8L^3} \qquad (1)$$

where $\varepsilon_0\varepsilon_r$ is the permittivity of the polymer, μ_h is the carrier mobility, and L is the device thickness.[54] The hole mobilities were determined to be 2.19 x 10^{-5}, 2.18 x 10^{-5}, and 6.58 x 10^{-5} $cm^2V^{-1}s^{-1}$ for **P1**, **P2**, and **P3**, respectively. These values are all of the same order of magnitude indicating that the difference in the PCE of the polymers is not a function of their charge carrier mobility.

The surface roughness and phase distribution of the three polymer systems were studied by atomic force microscopy (AFM) (Figure 5-4). The AFM height images revealed that both the **P1**:$PC_{71}BM$ and **P2**:$PC_{71}BM$ blend films have large domain sizes, manifesting root-mean square surface roughness (RMS) values of 2.94 nm and 1.20 nm, respectively. Whereas, the **P3**:$PC_{71}BM$ blend film has smaller domains (RMS = 0.78 nm). The AFM phase images of **P2**:$PC_{71}BM$ film displays a refined morphology that improves the exciton dissociation efficiency and, thus, the PCE. Conversely, films of the **P1**:$PC_{71}BM$ and **P3**:$PC_{71}BM$ blend show poor intermixing between polymer and

fullerene, reducing overall efficiency. Our previous X-ray diffraction studies on poly(quarter thiophene benzobisazoles) indicate that the structural differences in the materials do not significantly impact the packing of the polymer chains.[25] Therefore, the differences in the morphology of these polymers are likely a result of differences in solubility. As Figure 5-S2-5-S4 show, the AFM surface roughness and phase images of the three polymer systems were captured at 0.5 and 2.5% DIO additives. The RMS values of the films topography (shown in Figure 5-S5) indicate that the DIO additive increases the film roughness and the polymer/fullerene phase separation as depicted in the phase images of Figure 5-S2-S4. This is true for **P1**- and **P2**-based thin films. Whereas, **P3**:PC71BM thin film that showed slight increase in the domain sizes of polymer and fullerene. The observed phase separation with DIO additive hampers the charge dissociation efficiency and, thus, the photovoltaic characteristics (Table 5-3). It is worth mentioning that The **P2**:PCBM thin films show an RMS increase from 0.91 nm for the control (no additive) to 1.75 nm and 2.54 nm for the 0.5 and 2.5% of DIO additives, respectively.

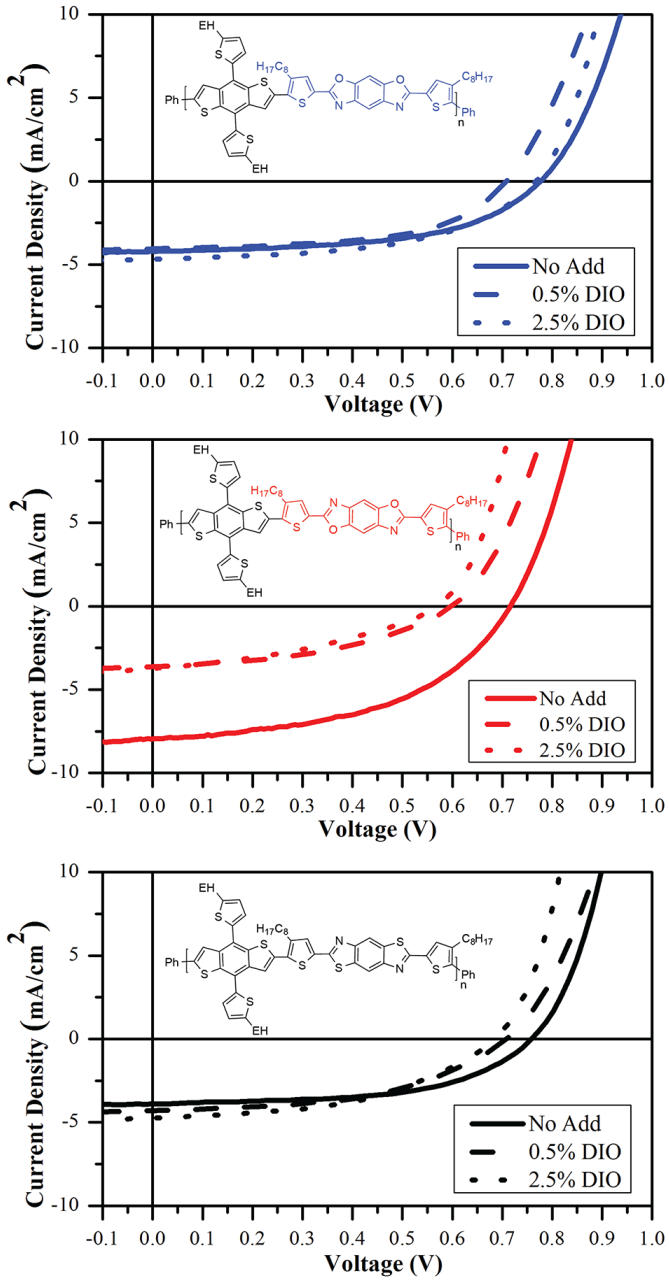

Figure 5-3. Current density-voltage *(J-V)* curves of polymer:$PC_{71}BM$, photovoltaic devices under AM 1.5 G illumination (100 mW cm^{-2}).

Table 5-3. Photovoltaic device performance of **P1 - P3** with $PC_{71}BM$.

Polymer	Additive (% DIO)	J_{SC} (mA/cm^2)	V_{OC} (V)	*FF*	PCE (%)	Max PCE (%)	R_{SH} (Ω cm^2)
P1	None	4.05±0.15	0.79±0.01	0.53±0.0	1.71±0.03	1.75	457±259
P1	0.5 %	3.99±0.05	0.70±0.00	0.56±0.0	1.57±0.04	1.61	1,656±127
P1	2.5 %	4.52±0.14	0.76±0.02	0.53±0.1	1.78±0.07	1.85	982±134
P2	None	7.81±0.18	0.72±0.01	0.49±0.0	2.74±0.05	2.78	818±209
P2	0.5 %	3.31±0.21	0.59±0.01	0.43±0.0	0.87±0.07	0.94	792±34
P2	2.5 %	3.74±0.00	0.55±0.02	0.37±0.0	0.76±0.04	0.79	708±37
P3	None	3.79±0.08	0.76±0.01	0.55±0.0	1.58±0.04	1.62	944±455
P3	0.5 %	4.26±0.08	0.69±0.02	0.51±0.2	1.50±0.00	1.50	970±40
P3	2.5 %	4.60±0.04	0.68±0.01	0.48±0.0	1.53±0.03	1.54	835±146

Photovoltaic devices with a configuration of ITO/PEDOT:PSS/Polymer:$PC_{71}BM$/Ca/Al were fabricated at a 1:2.5 weight ratio of polymer to $PC_{71}BM$ and a total solution concentration of 21 mg mL^{-1}. DIO was used as the additive (% v/v). Averages are based on 6 devices.

This strongly affects the P2:$PC_{71}BM$ intermixing, revealing average (max) PCEs of 2.54 (2.78), 0.87 (0.94) and 0.74 (0.79) % for the control, 0.5 and 2.5% DIO additives, respectively (Figure 5-S5).

Table 5-4. Hole mobility of P1-P3 hole only devices, and AFM data of polymer: $PC_{71}BM$ blends.

Polymer	μ_h ($cm^2 V^{-1} s^{-1}$)	RMS Roughness (nm)
P1	2.19×10^{-5}	2.94
P2	2.18×10^{-5}	1.20
P3	6.58×10^{-5}	0.78

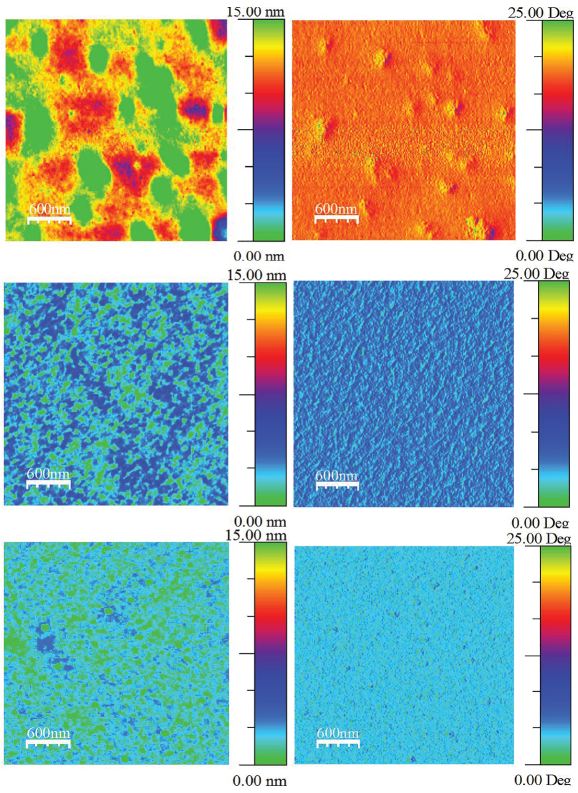

Figure 5-4. AFM height (left) and phase (right) images at 3 μm x 3 μm of devices with polymer:$PC_{71}BM$ blends at a 1:2.5 weight ratio. From top to bottom: P1:$PC_{71}BM$, P2:$PC_{71}BM$ and P3:$PC_{71}BM$.

5.4 Conclusions

Three terpolymers composed of thiophene, benzodithiophene and benzobisazoles were prepared in an effort to develop efficient materials for use in photovoltaic cells. The benzobisoxazole polymers had good solubility in various organic solvents, whereas the *trans*-benzobisthiazole polymer had limited solubility preventing the synthesis of high molecular weight polymer. All of the polymers had similar HOMO levels, but different LUMO levels and fairly wide band gaps. The *trans*-benzobisthiazole polymer, **P3**,

exhibited slightly broader and red-shifted absorption spectra relative to the other benzobisazoles in the solid state. Furthermore, this polymer also had the highest hole mobility of all three polymers. However, these properties did not translate into better performance in OPVs as the polymer based on *trans*-benzobisoxazole gave the best performance of the series at 2.78%. The poor performance of the *trans*-benzobisthiazole polymer is likely a result of the negative impact the molecular weight has on the active layer film morphology. At the same time the OPV performance of all these polymers is limited due to the wide band gap and relatively high-lying HOMO level. Given the overall ease of synthesis, benzobisazoles are still promising building blocks for the development of OPV materials. However, additional improvements in solubility, processing and electronic properties are needed. Accordingly, we are actively pursuing the synthesis of new derivatives to address the wide band gap and processability of the polymers.

5.5 Supporting Information

5.S.1 Device Fabrication and Characterization.

All devices were produced via a solution-based, spin-casting fabrication process. All polymers were mixed with $PC_{71}BM$ (SES Research) (mixed 1:2.5 (*w/w*) with a total solution concentration of 21 mg mL^{-1}) then dissolved in *o*-dichlorobenzene and stirred at 90 °C for 48 hours. ITO (20 – 25.2 Ω) coated glass slides (Delta Technologies) were cleaned by consecutive 10 minute sonications in (i) Mucasol™ detergent (dissolved in deionized water), 2x, (ii) deionized water, (iii) acetone, and then (iv) isopropanol. The

slides were then dried in an oven for at least 3 hours and cleaned with air plasma (Harrick Scientific plasma cleaner) for 10 minutes. Filtered (0.45 μm) PEDOT:PSS (Clevios P^{TM}) was spin-coated onto the prepared substrates (2000 rpm/60 sec) after first being stirred for 10 minutes at room temperature. The PEDOT:PSS films were annealed at 150 °C for 30 minutes air and transferred to an nitrogen-filled glovebox after cooling. After 48 hours of mixing, the polymer:$PC_{71}BM$ solutions were filtered (0.45 μm pore, GS-Tek) and simultaneously dropped onto the PEDOT:PSS-coated substrates and spin-cast at 1000 rpm for 60 seconds. The films were dried under vacuum overnight. Ca (20 nm) and Al (100 nm) were successively thermally evaporated through a shadow mask (area = 0.06 cm^{-2}) under vacuum of 10^{-6} mbar to complete the devices. *J-V* data was generated by illuminating the devices using an ETH quartzline lamp at 1 sun (calibrated using a crystalline silicon photodiode with a KG-5 filter). The hole mobility was extracted from the SCLC measurement using keithley 2400 source/meter in the dark under ambient condition.

5.S.2 Atomic force microscopy.

All measurements were performed on films cast as described above; electrodes were not attached to these samples. A Veeco Digital Instruments atomic force microscope was used to perform the analysis. The tapping-mode AFM was carried out using TESPA tip with scan rate of 0.5 μm sec^{-1} and scan size of 3 μm x 3 μm.

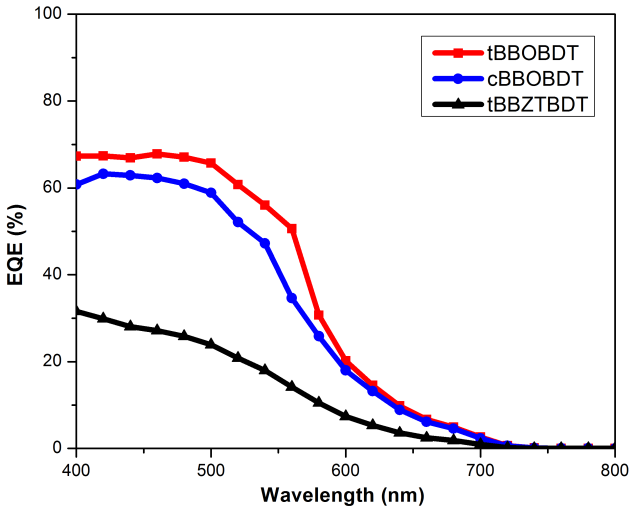

Figure 5-S1: EQE plots of P1 – P3 for photovoltaic devices with a configuration of ITO/PEDOT:PSS/Polymer:$PC_{71}BM$/Ca/Al were fabricated at a 1:2.5 weight ratio of polymer to $PC_{71}BM$ and a total solution concentration of 21mg /mL.

Table 5-S1: Photovoltaic performance of polymers P1 – P3 using different polymer:$PC_{71}BM$ blends

Polymer	Polymer:$PC_{71}BM$ Ratio	V_{OC} (V)	J_{SC} (mA cm^{-2})	FF	PCE (%)
P1	1:1.5	0.769	3.53	0.55	1.50
	1:2	0.790	3.54	0.54	1.51
	1:2.5	0.776	4.20	0.54	1.75
P2	1:1.5	0.619	4.10	0.41	1.03
	1:2	0.703	3.75	0.48	1.27
	1:2.5	0.715	7.95	0.49	2.78
P3	1:1.5	0.741	3.20	0.55	1.3
	1:2	0.735	3.58	0.56	1.50
	1:2.5	0.758	3.87	0.55	1.62

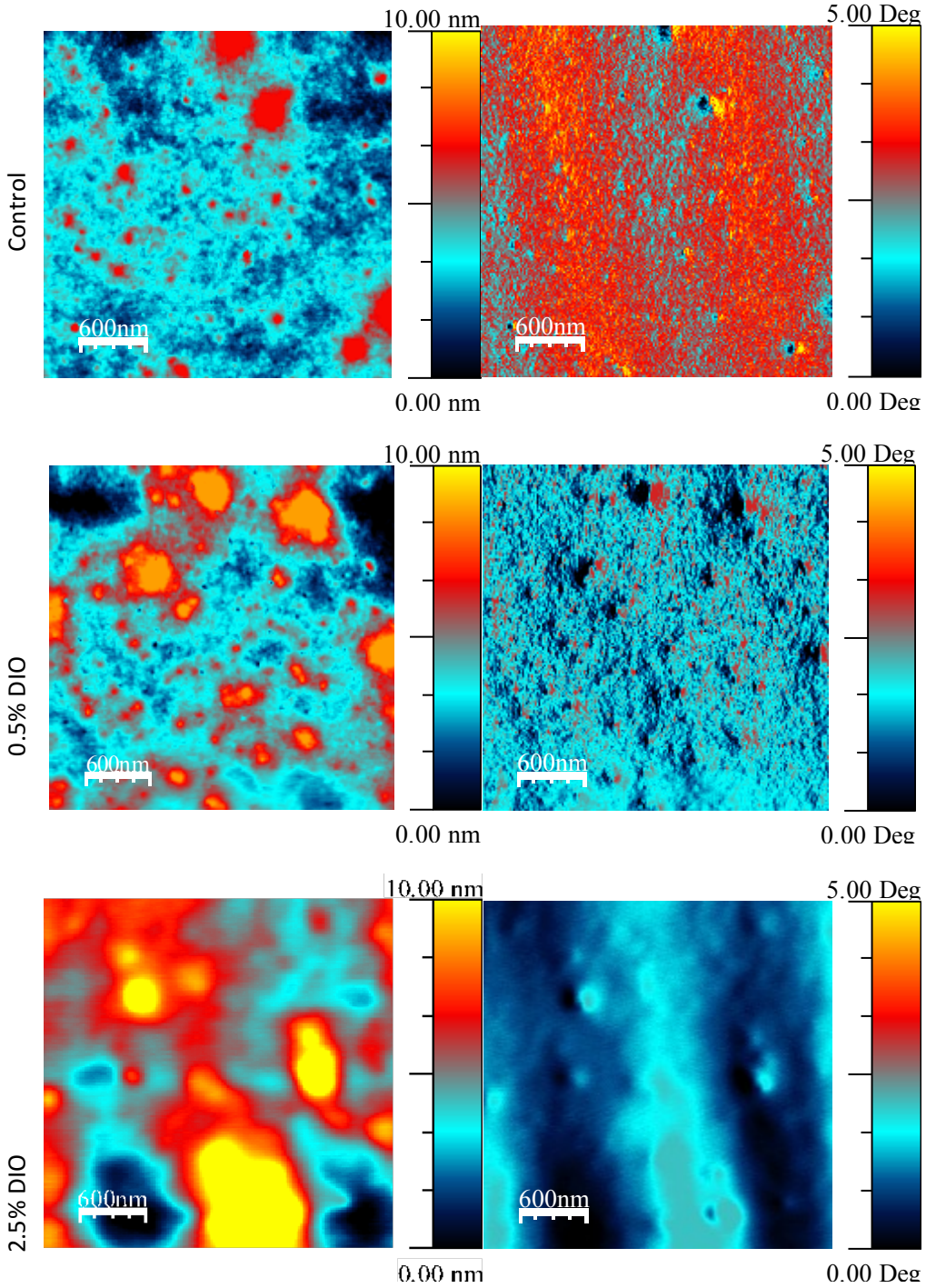

Figure 5-S2: 3 μm x 3 μm AFM images of P1:PC70BM thin films with DIO additive. (Left and right columns are the roughness and phase images, respectively)

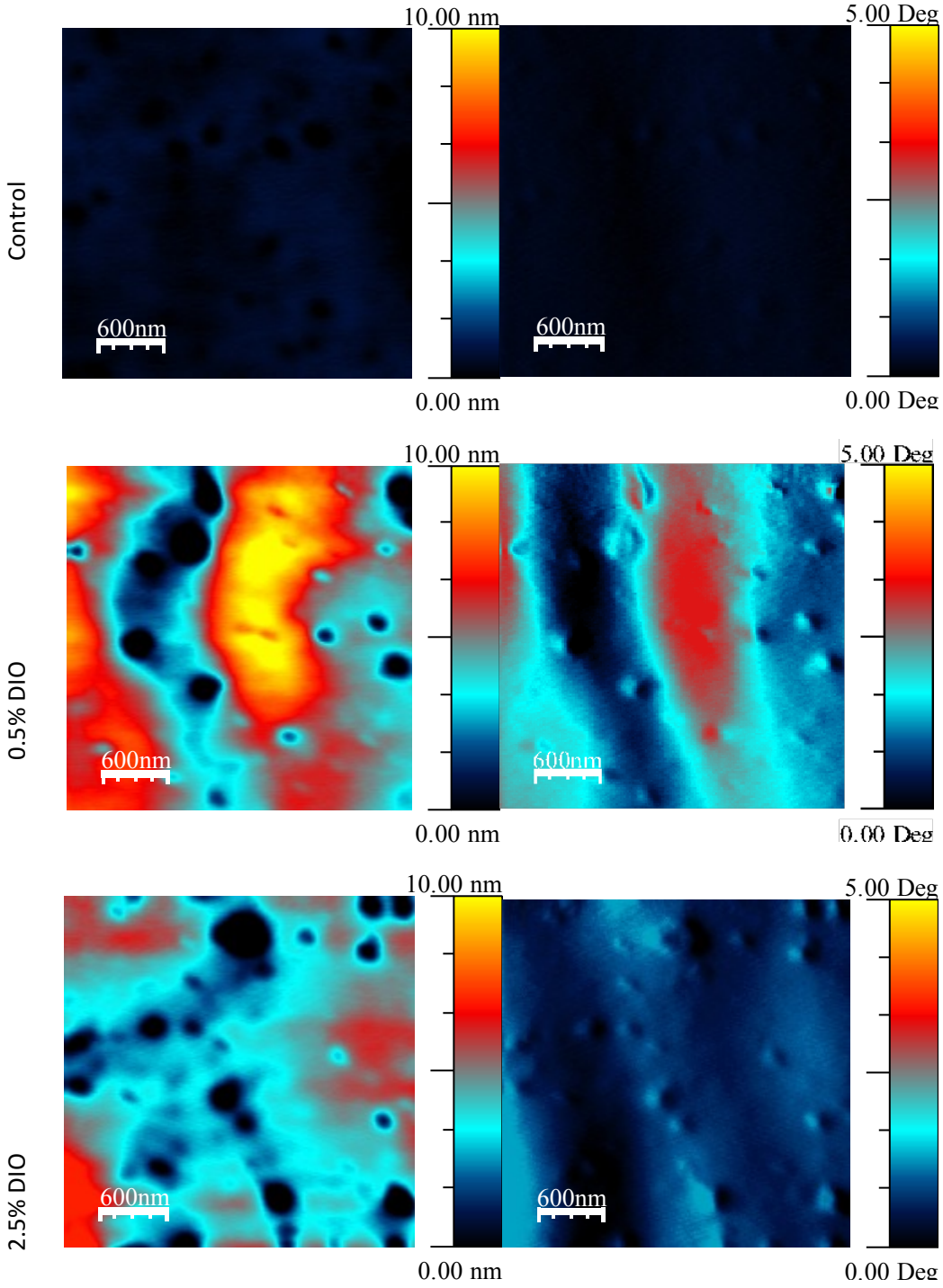

Figure 5-S3: 3 µm x 3 µm AFM images of P2:$PC_{70}BM$ thin films with DIO additive. (Left and right columns are the roughness and phase images, respectively)

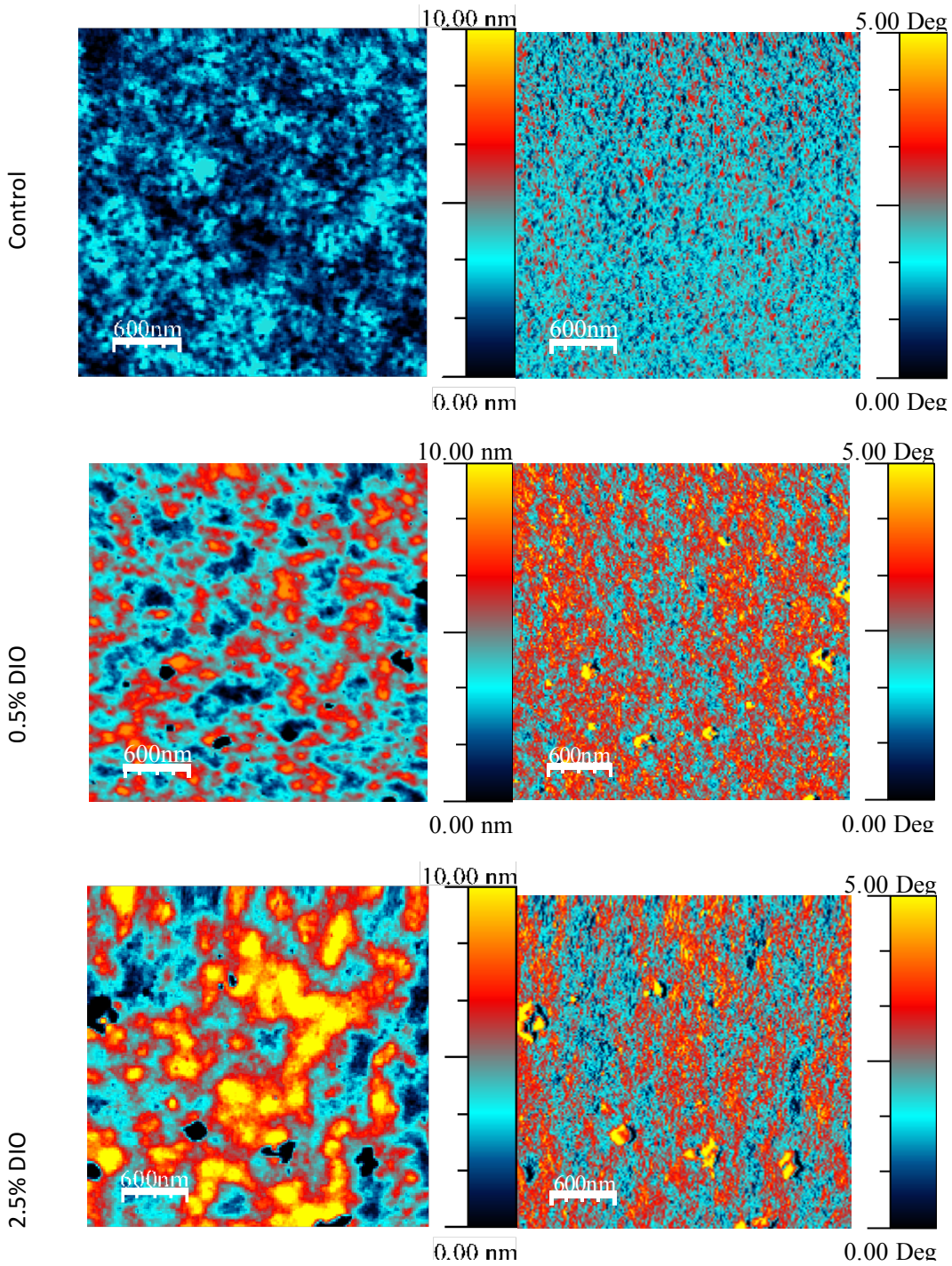

Figure 5-S4: 3 μm x 3 μm AFM images of P3:$PC_{70}BM$ thin films with DIO additive. (Left and right columns are the roughness and phase images, respectively)

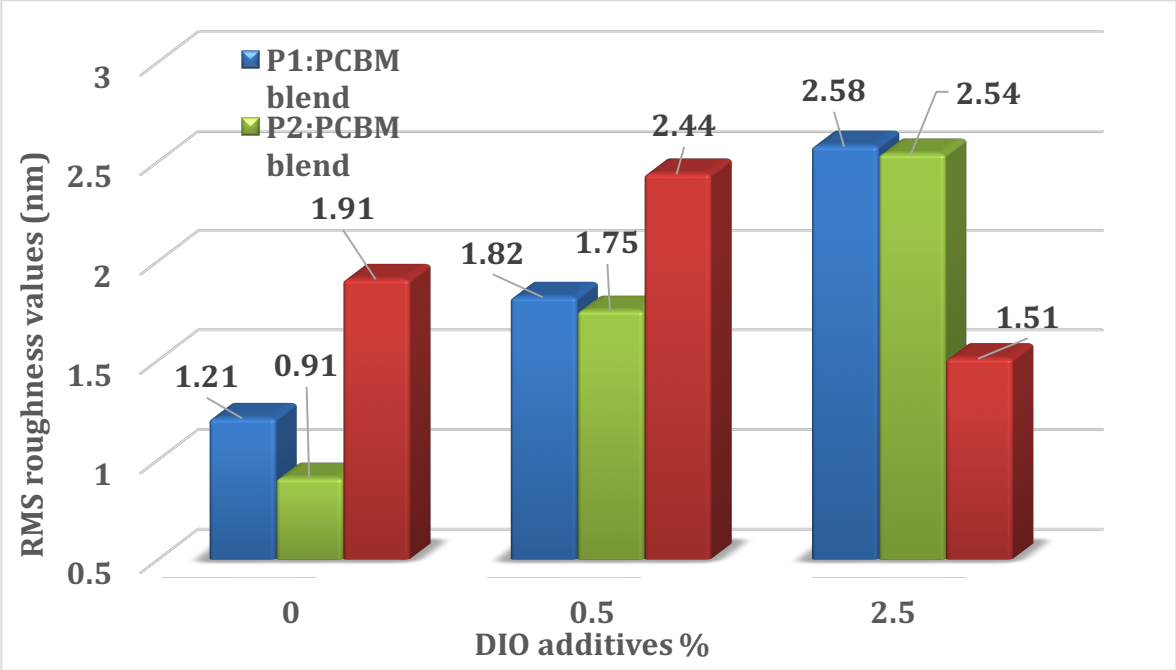

Figure 5-S5: Root-mean square values extracted from the AFM roughness images of the three investigated polymer:$PC_{71}BM$ thin films.

Sample		3 µm x 3 µm
		RMS Roughness (max height) (nm)
P1	Control	1.21 (6.76)
	0.5% DIO	1.82 (8.77)
	2.5% DIO	2.58 (11.92)
P2	Control	0.91 (3.82)
	0.5% DIO	1.75 (8.57)
	2.5% DIO	2.54 (11.23)
P3	Control	1.91 (8.19)
	0.5% DIO	2.44 (10.58)
	2.5% DIO	1.51 (7.07)

5.6 REFERENCES

1. Yu, G.; Gao, J.; Hummelen, J. C.; Wudl, F.; Heeger, A. J., *Science* **1995,** *270* (5243), 1789-1791.
2. Zhou, H.; Yang, L.; You, W., *Macromolecules* **2012,** *45* (2), 607-632.
3. van Mullekom, H. A. M.; Vekemans, J. A. J. M.; Havinga, E. E.; Meijer, E. W., *Mater. Sci. Eng., R* **2001,** *32* (1), 1-40.
4. Havinga, E. E.; ten Hoeve, W.; Wynberg, H., *Polymer Bulletin* **1992,** *29* (1), 119-126.
5. Beaujuge, P. M.; Amb, C. M.; Reynolds, J. R., *Acc. Chem. Res.* **2010,** *43* (11), 1396-1407.
6. Amb, C. M.; Chen, S.; Graham, K. R.; Subbiah, J.; Small, C. E.; So, F.; Reynolds, J. R., *J. Am. Chem. Soc.* **2011,** *133* (26), 10062-10065.
7. Facchetti, A., *Chem. Mater.* **2011,** *23* (3), 733-758.
8. Wolfe, J. F.; Arnold, F. E., *Macromolecules* **1981,** *14*, 909-915.
9. Wolfe, J. F.; Loo, B. H.; Arnold, F. E., *Macromolecules* **1981,** *14*, 915-920.
10. Choe, E. W.; Kim, S. N., *Macromolecules* **1981,** *14*, 920-924.
11. Jenekhe, S. A.; Osaheni, J. A.; Meth, J. S.; Vanherzeele, H., *Chem. Mater.* **1992,** *4* (3), 683-687.
12. Osaheni, J. A.; Jenekhe, S. A., *Macromolecules* **1993,** *26* (17), 4726-8.
13. Intemann, J.; Mike, J.; Cai, M.; Bose, S.; Xiao, T.; Mauldin, T.; Roggers, R.; Shinar, J.; Shinar, R.; Jeffries-EL, M., *Macromolecules* **2011,** *44* (2), 248-255.
14. Intemann, J. J.; Mike, J. F.; Cai, M.; Barnes, C. A.; Xiao, T.; Roggers, R. A.; Shinar, J.; Shinar, R.; Jeffries-EL, M., *J. Polym. Sci., Part A* **2013,** *51* (4), 916-923.
15. Intemann, J. J.; Hellerich, E. S.; Tlach, B. C.; Ewan, M. D.; Barnes, C. A.; Bhuwalka, A.; Cai, M.; Shinar, J.; Shinar, R.; Jeffries-El, M., *Macromolecules* **2012,** *45* (17), 6888-6897.
16. Hellerich, E. S.; Intemann, J. J.; Cai, M.; Liu, R.; Ewan, M. D.; Tlach, B. C.; Jeffries-EL, M.; Shinar, R.; Shinar, J., *J. Mater. Chem. C* **2013,** *1* (34), 5191-5199.
17. Mike, J. F.; Intemann, J. J.; Cai, M.; Xiao, T.; Shinar, R.; Shinar, J.; Jeffries-EL, M., *Polym. Chem.* **2011,** *2* (10), 2299-2305.
18. Alam, M. M.; Jenekhe, S. A., *Chem. Mater.* **2002,** *14* (11), 4775-4780.
19. Osaka, I.; Takimiya, K.; McCullough, R. D., *Adv. Mater.* **2010,** *22* (44), 4993-4997.
20. Ahmed, E.; Briseno, A. L.; Xia, Y.; Jenekhe, S. A., *J. Am. Chem. Soc.* **2008,** *130* (4), 1118-1119.
21. Ahmed, E.; Kim, F. S.; Xin, H.; Jenekhe, S. A., *Macromolecules* **2009,** *42* (22), 8615-8618.
22. Pang, H.; Vilela, F.; Skabara, P. J.; McDouall, J. J. W.; Crouch, D. J.; Anthopoulos, T. D.; Bradley, D. D. C.; de Leeuw, D. M.; Horton, P. N.; Hursthouse, M. B., *Adv. Mater.* **2007,** *19* (24), 4438-4442.
23. Ahmed, E.; Subramaniyan, S.; Kim, F. S.; Xin, H.; Jenekhe, S. A., *Macromolecules* **2011,** *44* (18), 7207-7219.
24. Patil, A. V.; Park, H.; Lee, E. W.; Lee, S.-H., *Synth. Met.* **2010,** *160* (19-20), 2128-2134.
25. Bhuwalka, A.; Mike, J. F.; He, M.; Intemann, J. J.; Nelson, T.; Ewan, M. D.; Roggers, R. A.; Lin, Z.; Jeffries-El, M., *Macromolecules* **2011,** *44* (24), 9611-9617.
26. Subramaniyan, S.; Kim, F. S.; Ren, G.; Li, H.; Jenekhe, S. A., *Macromolecules* **2012,** *45* (22), 9029-9037.
27. Saeki, A.; Tsuji, M.; Yoshikawa, S.; Gopal, A.; Seki, S., *J. Mater. Chem. A* **2014,** *2* (17), 6075-6080.
28. Tsuji, M.; Saeki, A.; Koizumi, Y.; Matsuyama, N.; Vijayakumar, C.; Seki, S., *Adv. Funct. Mater.* **2014,** *24* (1), 28-36.

29. Inbasekaran, M.; Strom, R., *OPPI Briefs* **1994,** *23*, 447-450.
30. Laquindanum, J. G.; Katz, H. E.; Lovinger, A. J.; Dodabalapur, A., *Adv. Mater.* **1997,** *9* (1), 36-39.
31. Hou, J.; Park, M.-H.; Zhang, S.; Yao, Y.; Chen, L.-M.; Li, J.-H.; Yang, Y., *Macromolecules* **2008,** *41* (16), 6012-6018.
32. Sista, P.; Biewer, M. C.; Stefan, M. C., *Macromol. Rapid Commun.* **2012,** *33* (1), 9-20.
33. Liang, Y.; Xu, Z.; Xia, J.; Tsai, S.-T.; Wu, Y.; Li, G.; Ray, C.; Yu, L., *Adv. Mater.* **2010,** *22* (20), E135-E138.
34. Najari, A.; Beaupré, S.; Berrouard, P.; Zou, Y.; Pouliot, J.-R.; Lepage-Pérusse, C.; Leclerc, M., *Adv. Funct. Mater.* **2011,** *21* (4), 718-728.
35. Li, K.; Li, Z.; Feng, K.; Xu, X.; Wang, L.; Peng, Q., *J. Am. Chem. Soc.* **2013,** *135* (36), 13549-13557.
36. Dou, L.; You, J.; Yang, J.; Chen, C.-C.; He, Y.; Murase, S.; Moriarty, T.; Emery, K.; Li, G.; Yang, Y., *Nat Photon* **2012,** *6* (3), 180-185.
37. Liang, Y.; Feng, D.; Wu, Y.; Tsai, S.-T.; Li, G.; Ray, C.; Yu, L., *Journal of the American Chemical Society* **2009,** *131* (22), 7792-7799.
38. Chen, H.-C.; Chen, Y.-H.; Liu, C.-C.; Chien, Y.-C.; Chou, S.-W.; Chou, P.-T., *Chem. Mater.* **2012,** *24* (24), 4766-4772.
39. He, Z.; Zhong, C.; Su, S.; Xu, M.; Wu, H.; Cao, Y., *Nat Photon* **2012,** *6* (9), 591-595.
40. Zhang, S.; Ye, L.; Zhao, W.; Liu, D.; Yao, H.; Hou, J., *Macromolecules* **2014,** *47* (14), 4653-4659.
41. Huo, L.; Hou, J.; Zhang, S.; Chen, H.-Y.; Yang, Y., *Angew. Chem., Int. Ed.* **2010,** *49* (8), 1500-1503.
42. Ye, L.; Zhang, S.; Huo, L.; Zhang, M.; Hou, J., *Acc. Chem. Res.* **2014,** *47* (5), 1595-1603.
43. Bhuwalka, A.; Ewan, M. D.; Mike, J. F.; Elshobaki, M.; Kobilka, B.; Chaudhary, S.; Jeffries-El, M., *J. Polym. Sci., Part A* **2015,** *53* (13), 1533-1540.
44. Yuan, J.; Zhai, Z.; Dong, H.; Li, J.; Jiang, Z.; Li, Y.; Ma, W., *Adv. Funct. Mater.* **2013,** *23* (7), 885-892.
45. Sanchez, R. S.; Zhuravlev, F. A., *J. Am. Chem. Soc.* **2007,** *129* (18), 5824-5825.
46. Kokubo, H.; Sato, T.; Yamamoto, T., *Macromolecules* **2006,** *39* (11), 3959-3963.
47. Cardona, C. M.; Li, W.; Kaifer, A. E.; Stockdale, D.; Bazan, G. C., *Adv. Mater.* **2011,** *23* (20), 2367-2371.
48. Thompson, B. C.; Kim, Y.-G.; Reynolds, J. R., *Macromolecules* **2005,** *38* (13), 5359-5362.
49. Salaneck, W. R., *Journal of Electron Spectroscopy and related Phenomena* **2009,** *174* (1-3), 3-9.
50. Kline, R. J.; McGehee, M. D.; Kadnikova, E. N.; Liu, J.; Frechet, J. M. J.; Toney, M. F., *Macromolecules* **2005,** *38* (8), 3312-3319.
51. Zhang, R.; Li, B.; Iovu, M. C.; Jeffries-El, M.; Sauve, G.; Cooper, J.; Jia, S.; Tristram-Nagle, S.; Smilgies, D. M.; Lambeth, D. N.; McCullough, R. D.; Kowalewski, T., *J. Am. Chem. Soc.* **2006,** *128* (11), 3480-3481.
52. Lee, J. K.; Ma, W. L.; Brabec, C. J.; Yuen, J.; Moon, J. S.; Kim, J. Y.; Lee, K.; Bazan, G. C.; Heeger, A. J., *Journal of the American Chemical Society* **2008,** *130* (11), 3619-3623.
53. Mihailetchi, V. D.; Wildeman, J.; Blom, P. W. M., *Phys. Rev. Lett.* **2005,** *94* (12), 126602.
54. Shrotriya, V.; Yao, Y.; Li, G.; Yang, Y., *Appl. Phys. Lett.* **2006,** *89* (6), 063505-3.

CHAPTER 6

CONCLUSIONS

6.1 Dissertation Conclusions

We were able to incorporate benzobisoxazoles into D-A polymer organic cells. While were able to obtain modest power conversion efficiencies and great improvements in solar cell performances over previous materials, there are two possible ways we can further improve the performance of BBO-based polymers in organic cells.

6.2 Ongoing And Future Research

6.2.1 BBOs in weak donor – strong acceptor copolymers

Currently, our use of BBOs has been limited to acceptor moieties in D-A copolymers. In the literature the BBO analogue, BBZT, has been able to achieve maximum power conversion efficiencies of 3.83% in organic solar cells. BBO-based copolymers, the film state, usually have absorption maxima that are less than 560 nm. This, coupled with modeled HOMO/LUMO levels, strongly suggests that BBO is a weak acceptor. There have been reports in the literature that use BBZT as a weak donor in weak donor – strong acceptor copolymers for organic solar cells. This design strategy is expected to yield both a low bandgap and a deep HOMO level. DFT calculations have shown than when BBZT-type moieties are copolymerized with stronger acceptors, the LUMO of the resulting copolymer is localized on the stronger accepting units. It is by this mechanism, that BBZT is able to act as a weak donor[1]. Seki *et al.* have reported BBZT copolymers that have attained PCEs of 6.5% when copolymerized with the

electron acceptor thienyl-benzothiadiazole[2, 3]. In this same vein, this author proposes a series of copolymers based on t-BBO as a week donor (**Figure 6-1**).

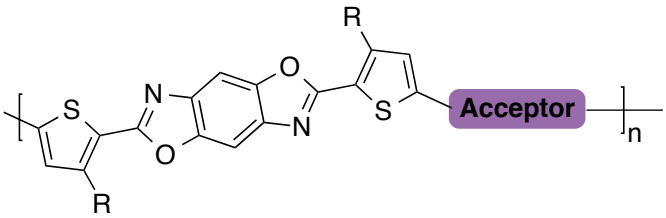

Figure 6-1. Proposed t-BBO polymer series

The best choice of acceptor units is benzothiadiazole (**1**). Next in the series is fluorinated benzothiadiazole (**2**), which has been shown to be a stronger acceptor than its predecessor[4-7]. The third proposed acceptor, alkyl-5*H*-[1,2,5]thiadiazolo[3,4-*f*]isoindole-5,7(6*H*)-dione (**3**) has been far less studied in the literature as an electron acceptor. However, it is expected to have better electron accepting properties because of its lower LUMO[8-10], relative to (**2**). It can also be functionalized with alkyl chains, which limits the necessity for alkyl thiophene groups for solubility. The next acceptors (**4-6**) enable the investigation of the selenium analogs of acceptors (**1-3**) and would be a two-fold experiment to ascertain the heteroatom effect in this polymer series.

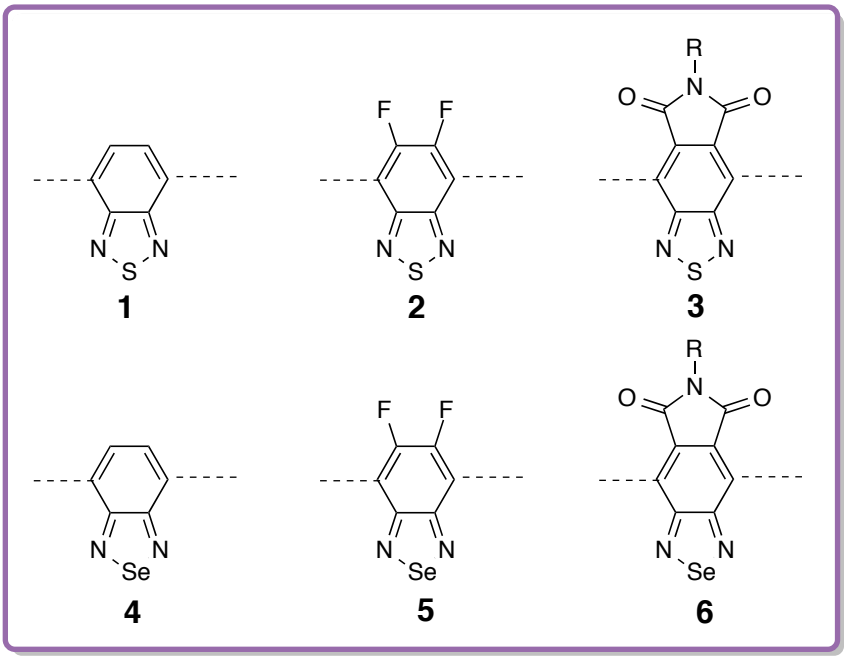

Figure 6-2. Proposed acceptors for D-A copolymers

6.1.2 A BBO-based hole transporting layer

If *t*BBO is implemented as a weak donor in weak donor – strong acceptor solar cells, a good strategy to further improve its performance is to incorporate BBO as the core in an HTL. If BBO is used as the core in the backbone of the molecule, then it is expected that there will be a more optimal alignment of the energy levels of the solar cell components. There would be a better alignment of the donor, n-type material and the hole transport layer. This should increase ohmic contact within the solar cell and make charge transport more efficient.

The active layer components are usually spincast from common organic solvents. Therefore, the hole transport layer, if solution processed, would have to be soluble in orthogonal solvents. A common way to achieve this is through the formation of polyelectrolytes[11, 12].

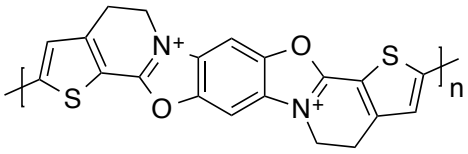

Figure 6-3. Molecular structure of proposed t-BBO-based polyelectrolyte

Figure 6-3 shows the molecular structure for a proposed polyelectrolyte based on the BBO core. The synthetic route start with the CH activation reaction of benzobisoxazole with (2-(2-bromothiophen-3-yl)ethoxy)(*tert*-butyl)dimethylsilane (Scheme 6-1). There would be just three reactions remaining to achieve the final product shown in Figure 6-3.

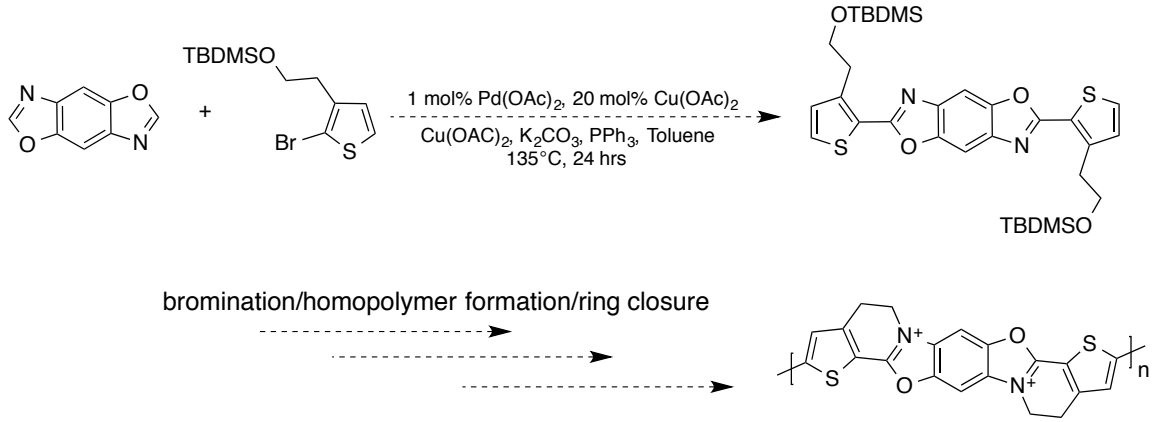

Scheme 6-1. Synthetic scheme to get to BBO polyelectrolyte product

6.3 Acknowledgements

I would like to thank my family for all of their support and encouragement throughout all of my endeavors: my parents for their continued support and guidance, my siblings for their unwavering faith and my husband, Dr. Christopher Knorowski, for his support, assistance and motivation. I would also like to thank my extended family and friends for their encouragement.

My time at Iowa State University would not have been possible without my advisor, Dr. Malika Jeffries-EL. I would like to thank her for her incredible encouragement and support as well his guidance into the fascinating and complex world of organic photovoltaics. I would also like to thank my secondary advisor, Dr. Sumit Chaudhary for always being available to assist when possible. I would like to thank the rest of my thesis committee members, Dr. Javier Vela, Dr. Arthur Winter and Dr. Joseph Shinar for their time and advice.

No tenure in the Jeffries-EL lab is achievable without the assistance and guidance of labmates. As such, I would like to thank the past members: Dr, Jared F. Mike, Dr. Jeremy Intemann, Dr. Brandon M. Kobilka, Dr. Brian C. Tlach and Dr. Achala Bhuwalka for all their assistance and tutelage. I would also like to thank the current group members: Ramiro Chavez, Evan Muller, Alfred Burney-Allen and Amy Brown for their support and encouragement in these past, difficult months.

I would like to thank Dr. John Carr, Dr. Yuqing Chen and Dr. Moneim Elshobaki from the Chaudhary research group for all their guidance with solar cell fabrication. I would also like to thank Mr. Max Noack at the Microelectronics Research Center at Iowa State University for his dedication to making sure that our glove boxes and equipment were always working. Additionally I would like to thank Dr. Vlad Duzhko from the University of Massachusetts, Amherst for assisting my with device fabrication at his facility. Lastly, I would like to thank the Institute for Physical Research and Technology at Iowa State University for providing the funds for the Catron Fellowship, which has funded my graduate education for the past three years.

6.4 REFERENCES

1. Tsuji, M.; Saeki, A.; Koizumi, Y.; Matsuyama, N.; Vijayakumar, C.; Seki, S., *Advanced Functional Materials* **2014,** *24* (1), 28-36.
2. Saeki, A.; Tsuji, M.; Yoshikawa, S.; Gopal, A.; Seki, S., *Journal of Materials Chemistry A* **2014,** *2* (17), 6075-6080.
3. Gopal, A.; Saeki, A.; Ide, M.; Seki, S., *ACS Sustainable Chemistry & Engineering* **2014,** *2* (11), 2613-2622.
4. Zhou, H.; Yang, L.; Stuart, A. C.; Price, S. C.; Liu, S.; You, W., *Angewandte Chemie* **2011,** *123* (13), 3051-3054.
5. Schroeder, B. C.; Ashraf, R. S.; Thomas, S.; White, A. J. P.; Biniek, L.; Nielsen, C. B.; Zhang, W.; Huang, Z.; Tuladhar, P. S.; Watkins, S. E., *Chemical Communications* **2012,** *48* (62), 7699-7701.
6. Bronstein, H.; Frost, J. M.; Hadipour, A.; Kim, Y.; Nielsen, C. B.; Ashraf, R. S.; Rand, B. P.; Watkins, S.; McCulloch, I., *Chemistry of Materials* **2013,** *25* (3), 277-285.
7. Love, J. A.; Nagao, I.; Huang, Y.; Kuik, M.; Gupta, V.; Takacs, C. J.; Coughlin, J. E.; Qi, L.; van der Poll, T. S.; Kramer, E. J., *Journal of the American Chemical Society* **2014,** *136* (9), 3597-3606.
8. Nielsen, C. B.; Ashraf, R. S.; Treat, N. D.; Schroeder, B. C.; Donaghey, J. E.; White, A. J. P.; Stingelin, N.; McCulloch, I., *Advanced Materials* **2015,** *27* (5), 948-953.
9. Li, H.; Koh, T. M.; Hagfeldt, A.; Grätzel, M.; Mhaisalkar, S. G.; Grimsdale, A. C., *Chemical Communications* **2013,** *49* (24), 2409-2411.
10. Wang, L.; Cai, D.; Zheng, Q.; Tang, C.; Chen, S.-C.; Yin, Z., *ACS Macro Letters* **2013,** *2* (7), 605-608.
11. Li, C.-Y.; Wen, T.-C.; Guo, T.-F., *Journal of Materials Chemistry* **2008,** *18* (37), 4478-4482.
12. Zhou, H.; Zhang, Y.; Mai, C. K.; Collins, S. D.; Nguyen, T. Q.; Bazan, G. C.; Heeger, A. J., *Advanced Materials* **2014,** *26* (5), 780-785.

APPENDIX

LIST OF ACRONYMS AND DESCRIPTIONS

Acronym	Description
2D	Two-Dimensional
AFM	Atomic Force Microscopy
BBO	Benzobisoxazole
BDF	Benzo[1,2-b:4,5-b']difuran
BDT	Benzo[1,2-b:4,5-b']dithiophene
BHJ	Bulk-Heterojunction
BLA	Bond Length Alternation
*c*BBO	benzo[1,2-d;5,4-d']bisoxazole
CN	1-Chloronapthalene
CP	Conjugated Polymer
CV	Cyclic Voltammerty
D-A	Donor-Acceptor
DIO	1,8-Diiodooctane
DP	Degree of Polymerization
DPP	Diketopyrrolepyrrole
DPV	Differential Pulse Voltammetry
DSC	Differential Scanning Calorimetry
DTS	Dithieno-[2,3-b:2',3'-d]silole
E_g	Band Gap

Acronym	Description
EA	Electron Affinity
EQE	External Quantum Efficiency
ESI	Electron-Spray Ionization
FF	Fill Factor
GPC	Gel Permeation Chromatography
HMW	High Molecular Weight
HOMO	Highest Occupied Molecular Orbital
HWE	Horner-Wadsworth-Emmons
HRMS	High Resolution Mass Spectrometry
ICT	Intramolecular charge transfer
ITO	Indium Tin Oxide
IP	Ionization Potential
J_{sc}	Short Circuit Current Density
LMW	Low Molecular Weight
LUMO	Lowest Unoccupied Molecular Orbital
MMW	Medium Molecular Weight
M_n	Number-Averaged Molecular Weight
MO	Molecular Orbital
M_w	Weight-Averaged Molecular Weight
NDT	Naphtho[1,2-b:5,6-b']dithiophene
NDF	Naphtho[1,2-b:5,6-b']difuran

NMR	Nuclear Magnetic Resonance
Acronym	Description
o-DCB	ortho-Dichlorobenzene
OFET	Organic Field-Effect Transistor
OLED	Organic Light-Emitting Diode
OPV	Organic Photovoltaic Cell
PA	Polyacetylene
PBO	Polybenzobisoxazole
P3AT	poly(3alkylthiophene)
P3HT	poly(3-hexylthiophene)
$PC_{61}BM$	[6,6]-Phenyl-C61-butyric acid methyl ester
$PC_{71}BM$	[6,6]-Phenyl-C71-butyric acid methyl ester
PCE	Power Conversion Efficiency
PDI	Poly Dispersity Index
PEDOT:PSS	Poly(3,4-ethylenedioxythiophene) poly(styrenesulfonate)
PITN	Polyisothianapthene
PPA	Polyphosphoric Acid
PPP	Poly(para-phenylenevinylene)
PPV	Poly(phenylenevinylene)
PT	Pyridalthiadiazole
PV	Photovoltaic
PVC	Photovoltaic Cell
SCLC	Space-Charge-Limited Current

Acronym	Description
SI	Supplemental Information
*t*BBO	benzo[1,2-d;4,5-d']bisoxazole
*t*BBZT	benzo[1,2-d;4,5-d']bisthiazole
T_d	Thermal Decomposition Temperature
T_g	Glass Transition Temperature
TDPP	3,6-di(2-thienyl)-1,4-diketopyrrolo[3,4-c]pyrrole
TFA	Trifluoroacetic acid
THF	Tetrahydrofuran
TGA	Thermal Gravimetric Analysis
TMS	Trimethylsilyl
TP	thiazolo[5,4-c]pyridine
TW	Terawatts
UPS	Ultraviolet Photoelectron Spectroscopy
Voc	Open Circuit Voltage
Wt%	Weight Percent
XRD	X-Ray Diffraction